Recommended Design Specifications for Live Load Distribution to Buried Structures

DETAILS

75 pages | | PAPERBACK

ISBN 978-0-309-11822-4 | DOI 10.17226/14377

AUTHORS

Charles R Nelson; Timothy J McGrath; Yasuo Kitane; Gang Li; D Lee Petersen; Transportation Research Board

NATIONAL COOPERATIVE HIGHWAY RESEARCH PROGRAM

NCHRP REPORT 647

Recommended Design Specifications for Live Load Distribution to Buried Structures

D. Lee Petersen
Charles R. Nelson
Gang Li
CNA Consulting Engineers
Minneapolis, MN

Timothy J. McGrath
Yasuo Kitane
Simpson Gumpertz & Heger Inc.
Waltham, MA

Subscriber Categories
Highways • Bridges and Other Structures

Research sponsored by the American Association of State Highway and Transportation Officials
in cooperation with the Federal Highway Administration

TRANSPORTATION RESEARCH BOARD

WASHINGTON, D.C.
2010
www.TRB.org

NATIONAL COOPERATIVE HIGHWAY RESEARCH PROGRAM

Systematic, well-designed research provides the most effective approach to the solution of many problems facing highway administrators and engineers. Often, highway problems are of local interest and can best be studied by highway departments individually or in cooperation with their state universities and others. However, the accelerating growth of highway transportation develops increasingly complex problems of wide interest to highway authorities. These problems are best studied through a coordinated program of cooperative research.

In recognition of these needs, the highway administrators of the American Association of State Highway and Transportation Officials initiated in 1962 an objective national highway research program employing modern scientific techniques. This program is supported on a continuing basis by funds from participating member states of the Association and it receives the full cooperation and support of the Federal Highway Administration, United States Department of Transportation.

The Transportation Research Board of the National Academies was requested by the Association to administer the research program because of the Board's recognized objectivity and understanding of modern research practices. The Board is uniquely suited for this purpose as it maintains an extensive committee structure from which authorities on any highway transportation subject may be drawn; it possesses avenues of communications and cooperation with federal, state and local governmental agencies, universities, and industry; its relationship to the National Research Council is an insurance of objectivity; it maintains a full-time research correlation staff of specialists in highway transportation matters to bring the findings of research directly to those who are in a position to use them.

The program is developed on the basis of research needs identified by chief administrators of the highway and transportation departments and by committees of AASHTO. Each year, specific areas of research needs to be included in the program are proposed to the National Research Council and the Board by the American Association of State Highway and Transportation Officials. Research projects to fulfill these needs are defined by the Board, and qualified research agencies are selected from those that have submitted proposals. Administration and surveillance of research contracts are the responsibilities of the National Research Council and the Transportation Research Board.

The needs for highway research are many, and the National Cooperative Highway Research Program can make significant contributions to the solution of highway transportation problems of mutual concern to many responsible groups. The program, however, is intended to complement rather than to substitute for or duplicate other highway research programs.

NCHRP REPORT 647

Project 15-29
ISSN 0077-5614
ISBN 978-0-309-11822-4
Library of Congress Control Number 2010922165

COPYRIGHT INFORMATION

NOTICE

The project that is the subject of this report was a part of the National Cooperative Highway Research Program conducted by the Transportation Research Board with the approval of the Governing Board of the National Research Council. Such approval reflects the Governing Board's judgment that the program concerned is of national importance and appropriate with respect to both the purposes and resources of the National Research Council.

The members of the technical committee selected to monitor this project and to review this report were chosen for recognized scholarly competence and with due consideration for the balance of disciplines appropriate to the project. The opinions and conclusions expressed or implied are those of the research agency that performed the research, and, while they have been accepted as appropriate by the technical committee, they are not necessarily those of the Transportation Research Board, the National Research Council, the American Association of State Highway and Transportation Officials, or the Federal Highway Administration, U.S. Department of Transportation.

Each report is reviewed and accepted for publication by the technical committee according to procedures established and monitored by the Transportation Research Board Executive Committee and the Governing Board of the National Research Council.

The Transportation Research Board of the National Academies, the National Research Council, the Federal Highway Administration, the American Association of State Highway and Transportation Officials, and the individual states participating in the National Cooperative Highway Research Program do not endorse products or manufacturers. Trade or manufacturers' names appear herein solely because they are considered essential to the object of this report.

Published reports of the

NATIONAL COOPERATIVE HIGHWAY RESEARCH PROGRAM

are available from:

Transportation Research Board
Business Office
500 Fifth Street, NW
Washington, DC 20001

and can be ordered through the Internet at:

http://www.national-academies.org/trb/bookstore

Printed in the United States of America

THE NATIONAL ACADEMIES

Advisers to the Nation on Science, Engineering, and Medicine

The **National Academy of Sciences** is a private, nonprofit, self-perpetuating society of distinguished scholars engaged in scientific and engineering research, dedicated to the furtherance of science and technology and to their use for the general welfare. On the authority of the charter granted to it by the Congress in 1863, the Academy has a mandate that requires it to advise the federal government on scientific and technical matters. Dr. Ralph J. Cicerone is president of the National Academy of Sciences.

The **National Academy of Engineering** was established in 1964, under the charter of the National Academy of Sciences, as a parallel organization of outstanding engineers. It is autonomous in its administration and in the selection of its members, sharing with the National Academy of Sciences the responsibility for advising the federal government. The National Academy of Engineering also sponsors engineering programs aimed at meeting national needs, encourages education and research, and recognizes the superior achievements of engineers. Dr. Charles M. Vest is president of the National Academy of Engineering.

The **Institute of Medicine** was established in 1970 by the National Academy of Sciences to secure the services of eminent members of appropriate professions in the examination of policy matters pertaining to the health of the public. The Institute acts under the responsibility given to the National Academy of Sciences by its congressional charter to be an adviser to the federal government and, on its own initiative, to identify issues of medical care, research, and education. Dr. Harvey V. Fineberg is president of the Institute of Medicine.

The **National Research Council** was organized by the National Academy of Sciences in 1916 to associate the broad community of science and technology with the Academy's purposes of furthering knowledge and advising the federal government. Functioning in accordance with general policies determined by the Academy, the Council has become the principal operating agency of both the National Academy of Sciences and the National Academy of Engineering in providing services to the government, the public, and the scientific and engineering communities. The Council is administered jointly by both the Academies and the Institute of Medicine. Dr. Ralph J. Cicerone and Dr. Charles M. Vest are chair and vice chair, respectively, of the National Research Council.

The **Transportation Research Board** is one of six major divisions of the National Research Council. The mission of the Transportation Research Board is to provide leadership in transportation innovation and progress through research and information exchange, conducted within a setting that is objective, interdisciplinary, and multimodal. The Board's varied activities annually engage about 7,000 engineers, scientists, and other transportation researchers and practitioners from the public and private sectors and academia, all of whom contribute their expertise in the public interest. The program is supported by state transportation departments, federal agencies including the component administrations of the U.S. Department of Transportation, and other organizations and individuals interested in the development of transportation. **www.TRB.org**

www.national-academies.org

COOPERATIVE RESEARCH PROGRAMS

CRP STAFF FOR NCHRP REPORT 647

Christopher W. Jenks, *Director, Cooperative Research Programs*
Crawford F. Jencks, *Deputy Director, Cooperative Research Programs*
David B. Beal, *Senior Program Officer, Retired*
Waseem Dekelbab, *Senior Program Officer*
Danna Powell, *Senior Program Assistant*
Eileen P. Delaney, *Director of Publications*
Hilary Freer, *Senior Editor*

NCHRP PROJECT 15-29 PANEL
Field of Design—Area of General Design

Brian G. Thompson, *Pennsylvania DOT, Harrisburg, PA* (Chair)
Scott A. Anderson, *Federal Highway Administration, Lakewood, CO*
Harry A. Capers, Jr., *Arora and Associates, P.C., Lawrenceville, NJ*
Susan E. Hida, *California DOT, Sacramento, CA*
Michael G. Katona, *Washington State University, Gig Harbor, WA*
Roman J. Selig, III, *Hanson Pipe & Precast, Birmingham, AL*
Amjad Waheed, *Ohio DOT, Columbus, OH*
James L. Withiam, *Ground Technology, Inc., Monroeville, PA*
Firas I. Sheikh Ibrahim, *FHWA Liaison*
Stephen F. Maher, *TRB Liaison*

FOREWORD

By Waseem Dekelbab
Staff Officer
Transportation Research Board

This report provides recommendations to revise the AASHTO LRFD Bridge Design Specifications relating to the distribution of live load to buried structures. The report details the development of simplified design equations (SDEs) for structural response based on three-dimensional (3D) analysis of 830 buried culverts. In addition, the report provides guidelines for conducting 2D and 3D modeling for design situations with conditions not covered by the SDEs. The material in this report will be of immediate interest to roadway and bridge designers.

Much analytical and experimental work has been conducted to investigate the distribution of surface loads through earth fills. The classic Boussinesq (1885) solution, and simple assumptions such as spreading a surface load over an area that is a linear function of depth, remain perhaps the most widely used calculation procedures. The approximate method for estimating the distribution of vehicular live loads through earth fill in the AASHTO Standard Specifications has, over many years, produced designs that have performed acceptably. The AASHTO LRFD Bridge Design Specifications use a different approximation method that significantly increases live load pressures on buried structures compared with the Standard Specifications. When combined with the increased dynamic load allowance prescribed in the LRFD Specifications, this increase is even greater. In addition, the basis of the approximation methods in both codes is neither well documented nor understood.

The objective of this project was to develop (1) recommended revisions to the AASHTO LRFD Bridge Design Specifications relating to the distribution of live load to buried structures and (2) refined methods for analyzing the distribution of live load to buried structures, including selection of an appropriate soil models.

This research was managed by Charles R. Nelson and Lee Petersen, CNA Consulting Engineers, in Minneapolis, Minnesota, with the assistance of Timothy J. McGrath, Simpson Gumpertz & Heger, Inc., in Waltham, Massachusetts. The report fully documents the research leading to the recommended design specifications for live load distribution to buried structures.

Appendixes A through E from the research agency's final report are not published herein but are available on the TRB website. These appendixes are as follows:

- Appendix A—3-D Numerical Analysis of Live Load Distribution: Soil Constitutive Models, Load Factoring and Comparison with Field Measurements
- Appendix B—3-D Numerical Analysis of Live Load Distribution: Model Details and Results

- Appendix C—Recommended Revision to AASHTO LRFD Bridge Design Specifications
- Appendix D.1—Parametric Study MathCAD Calculation Sheets
- Appendix D.2—Tabular Listings of Parametric Study Results
- Appendix E—Refined Analysis Guidelines

CONTENTS

SUMMARY

Recommended Design Specifications for Live Load Distribution to Buried Structures

NCHRP Project 15-29, "Design Specifications for Live Load Distribution to Buried Structures," investigated how surface live loads distribute through the soil and load various culvert structures. AASHTO Standard and LRFD Specifications differ in how live loads are spread through fill onto culvert structures. AASHTO Standard Specifications apply surface point loads and spread loads at the rate of 1.75 times the culvert depth. The LRFD Specifications apply live load through a tire footprint of 10 in. by 20 in. at the surface but attenuate with a lower coefficient (1.00 or 1.15 as a function of soil type) as the depth of fill increases.

This research investigated how live loads spread with depth, as a function of soil and culvert type, using three-dimensional (3D) numerical modeling. The numerical investigation included selection of appropriate software and soil models, verification of model predictions, and 3D analysis of 830 buried culverts. Modeling was conducted for the following six culvert types:

- Concrete arch,
- Concrete pipe,
- Concrete box,
- Corrugated metal pipe,
- Corrugated metal arch, and
- High-density polyethylene (HDPE) profile wall pipe.

This modeling provided a basis for developing simplified design equations (SDEs) for structural response.

Numerical modeling conducted to evaluate model characteristics, software, and soil constitutive models indicated that a linearly elastic, perfectly plastic model with a Mohr-Coulomb failure criterion provided the best mix of capturing (1) the important aspects of soil behavior in transmitting live loads to structures and (2) offering simplicity in modeling. In implementing this soil model, the elastic soil properties were based on depth of fill. Parameters for the soil model were based on the Selig (1988 and 1990) properties. The proposed properties are conservative relative to field data.

Culverts composed of solid material and regular geometry may be represented by isotropic structural elements, meaning that bending and membrane properties are the same in all directions. This category includes concrete boxes, concrete pipe, smooth steel pipe, and smooth thermoplastic pipe. Both thermoplastic and metal culvert products use cross-sectional shapes that are orthotropic, meaning the structural properties vary by direction. These culvert shapes typically have much higher circumferential bending stiffness than longitudinal bending stiffness. In addition, the circumferential membrane stiffness is higher than the longitudinal membrane stiffness. In order to model these culverts accurately, 3D orthotropic

structural elements that permit specification of different stiffnesses for bending and membrane behavior are required.

Modeling results show that live load spread depends on depth, soil characteristics, and culvert characteristics. Pavements substantially reduce soil stress and structure forces, so the unpaved case controls. The distribution of vertical stresses on the plane at the crown of buried culverts varies substantially depending on the soil properties, culvert characteristics and depth. A spreading constant of 1.75 does not adequately represent the modeling results; a spreading constant of 1.15 is slightly unconservative at shallow depths, is adequate for 24-in culverts at most depths, and conservative for larger culverts.

Regarding bending moments in the structures, the crown bending moment has the greatest absolute magnitude in response to live loads. The peak negative bending moment is typically at the springline or above, as high as 60 degrees above the springline for large-diameter culverts near the surface. Peak thrusts may occur anywhere from the culvert crown to the springline. Shallow burial tends to produce peak thrusts near the crown and deeper burial tends to shift the peak thrust closer to the springline. Invert thrusts typically are small and may be either slightly negative or slightly positive.

Proposed revisions to the 4th edition of the AASHTO Design Specifications were developed using the following methodology. First, the limit states and current design methodologies were evaluated and compared for all culvert types included in the AASHTO specifications. Next, numerical values of the limit states from the numerical modeling were compared with the values resulting from the Standard and LRFD Specifications. Finally, proposed SDEs were developed that provided better correlation with modeling results.

For all culvert types, the proposed SDEs included a culvert span-related term in the calculation of the load spread parallel to the culvert axis (perpendicular to the direction of vehicle travel). The following proposed SDE for concrete box culverts illustrates the change. The first equation determines the depth at which adjacent wheels on an axle, or wheels on adjacent axles, interact:

$$H_{\text{int}} = \frac{s_w - \frac{w_t}{12} - \frac{0.06 D_i}{12}}{LLDF_l} \tag{1}$$

where

H_{int} is the wheel interaction depth, ft
s_w is the wheel spacing, 6 ft
w_t is the tire patch width, 20 in.
$LLDF_l$ is the live load distribution factor, typically 1.15
D_i is the inside span of the culvert, in.

The area loaded by the wheel load may be estimated by

$$\text{For } H < H_{\text{int}} \qquad A_{LL} = \left(\frac{w_t}{12} + LLDF_l \cdot H + 0.06 \cdot D_i/12\right) \cdot \left(\frac{l_t}{12} + LLDF_l \cdot H\right) \tag{2}$$

$$\text{For } H \geq H_{\text{int}} \qquad A_{LL} = \left(\frac{w_t}{12} + s_w + LLDF_l \cdot H + 0.06 \cdot D_i/12\right) \cdot \left(\frac{l_t}{12} + LLDF_l \cdot H\right) \tag{3}$$

where

H is the culvert depth, ft
l_t is the tire patch length, 10 in.

Figure S-1 compares the variation of live load with depth for concrete boxes, for the Standard, LRFD, and proposed SDE. The SDE distribution starts out wider than LRFD, but increases width with depth at the same rate.

Recommended changes to the AASHTO LRFD Design Specifications are presented in Chapter 3 and Appendix C. The recommended changes are limited to Specification Section 3, where the live load magnitude is specified, and Section 12, where structural responses are calculated. Table 3-1 in Chapter 3 summarizes the changes to each section for the six culvert types.

In order to understand the effect of the proposed SDEs on culvert designs, the critical structural responses were calculated and compared (for Standard, LRFD and proposed design equations) for the following 248 culvert, depth, span, and soil combinations:

- Concrete box—6 cases;
- Concrete pipe—100 cases;
- Corrugated metal pipe—42 cases;
- Thermoplastic (profile wall)—80 cases;
- Metal arch—6 cases; and
- Concrete arch—8 cases.

The findings of the parametric study are discussed below in the context of the overall design and reliability margin.

The research team conducted extensive 3D modeling of the transfer of surface live loads to buried culverts. From the results, the research team has proposed SDEs that permit culvert design without modeling. However, many design situations are not addressed by the SDEs. In these situations, two-dimensional (2D) and 3D modeling may be necessary for design.

Guidelines were developed for conducting 2D and 3D modeling. The 2D guidelines provide a means for selecting the surface load intensity to be applied to a 2D elastic model, the most commonly used modeling technique. 2D computer models have an inherent limitation

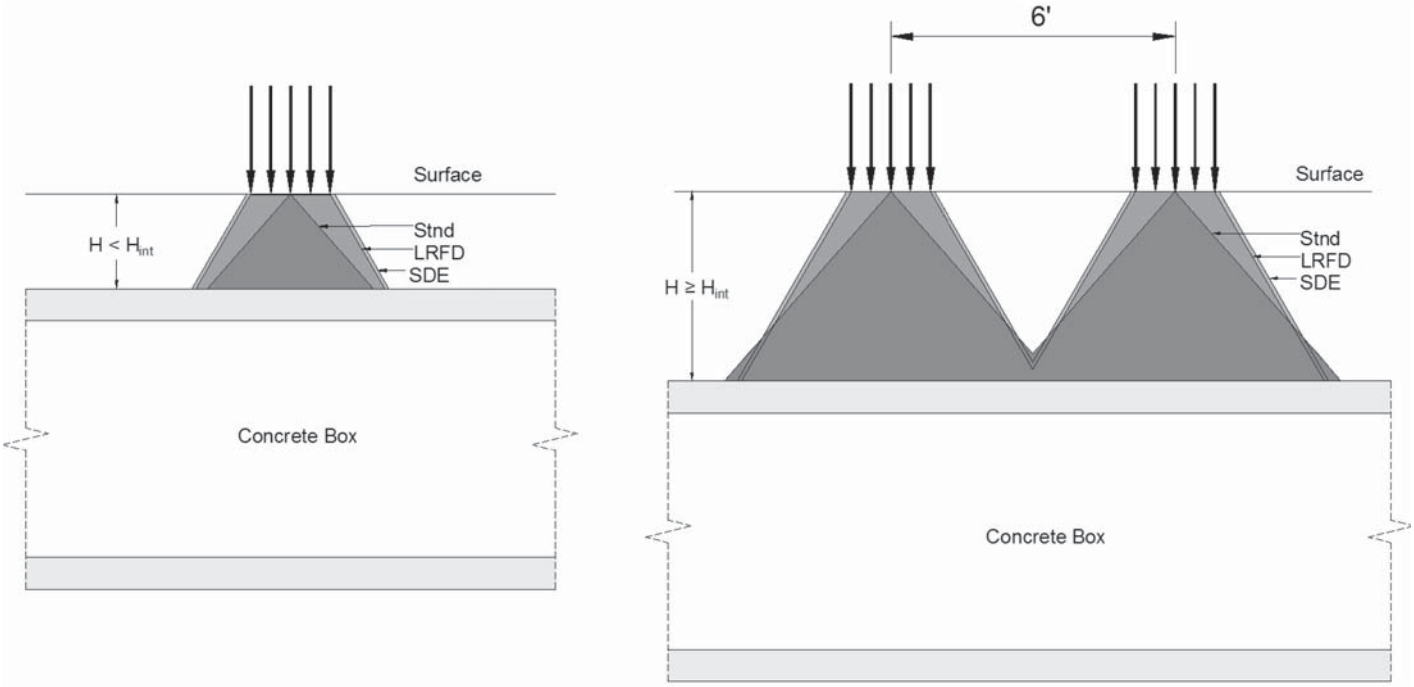

Figure S-1. Live load variation with depth for concrete box culverts (SDE refers to the proposed simplified design equations).

when computing the effect of surface live loads. Because the models are 2D, the load spreading that occurs in the longitudinal direction, parallel to the axis of the culvert, cannot be correctly computed. The model represents a vertical slice through the real-world, 3D geometry. Parameters for peak thrust and crown moment are sufficiently different that separate analyses should be conducted for each. 2D response ratios for concrete boxes, concrete arches, and corrugated metal arches were too variable to be captured adequately by these guidelines.

The 3D guidelines address software, live load application, representing the pavement, representing the soil, model dimensions, element size, symmetry and boundary conditions, representing culvert structures, and the soil-culvert interface. Details may be found in Section 2.5.2.

The overall design and reliability margin of the proposed SDEs was assessed by computing statistics about the ratio of SDE design force to Standard design force, and the ratio of SDE to LRFD design forces.

The maximum, minimum, and average design force ratios are shown in Figure S-2. In the figure, the square represents the average ratio, and the ends of the vertical bars represent the minimum and maximum ratios. For most design forces, the average ratio of SDE to LRFD is between about 0.9 and 1.1. Exceptions to these limits are the reinforced concrete pipe (RCP) crown moment at 0.888, the corrugated metal arch (CMA) peak thrust at 1.460, and the reinforced concrete arch (RCA) peak moment at 0.882.

The range of design force ratios is generally larger for the SDE/Standard ratio. This reflects that the SDEs, like the LRFD design methods, spread the loads from a finite-size wheel patch (typically 20 in. by 10 in.), rather than a point load.

Figure S-2 illustrates that, except for a few structure forces, the proposed SDEs do not significantly affect the design margin or reliability on average. However, the relatively large spread in the ratios does mean that for some combinations of soil type, diameter, and depth the SDEs are significantly different than the LRFD design forces.

Where there is a significant variation between the proposed SDEs and current practice, the differences are not random—the SDEs model behavior not captured in the current standards.

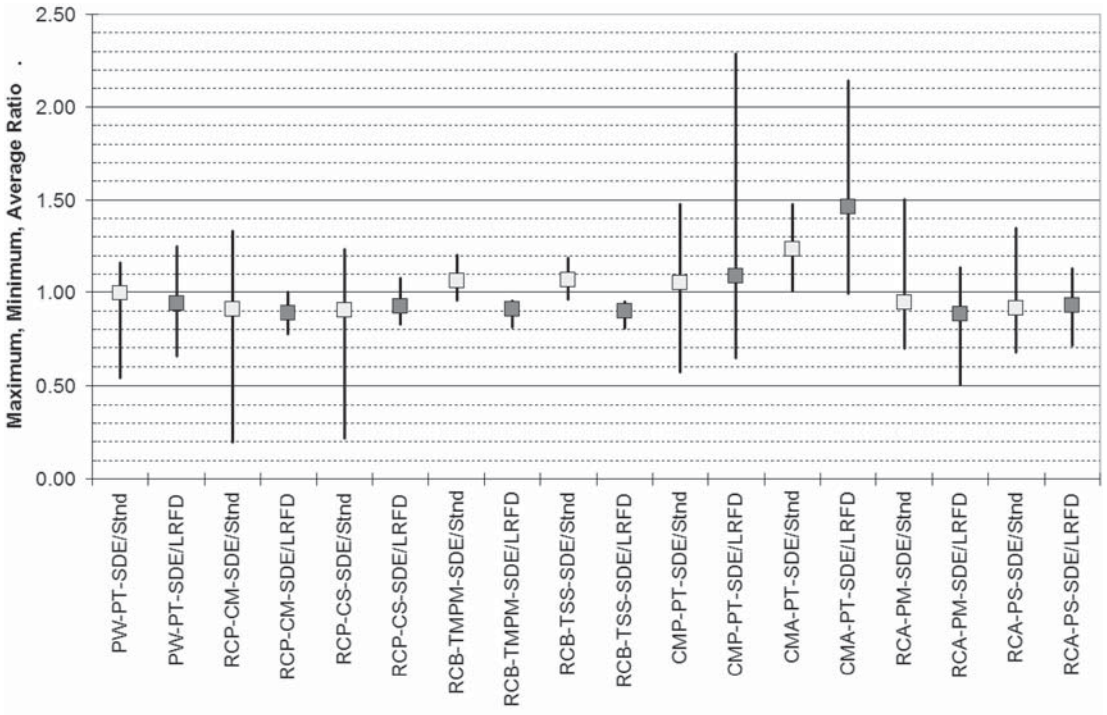

Figure S-2. Maximum, minimum and average design force ratio.

For example, in corrugated metal pipe, the ratio gets larger as depth of fill decreases. As noted earlier, this is the result of the high thrust occurring in the crown of these culverts, which occurs because of the low bending stiffness and high axial stiffness.

Based on this research, the current AASHTO load spreading method provides a neutral or conservative approach for all culvert types, except corrugated metal arches. The proposed SDEs are a better fit to the modeling results produced in this study and are generally less conservative than the current AASHTO load-spreading method.

For most reinforced concrete pipe diameters and depths considered, the SDEs generally predict much lower crown moments than the Standard method and moderately lower crown moments that the LRFD method. However, the SDEs are still quite conservative relative to the American Concrete Pipe Association (ACPA) Handbook methods that have been used without issue for a substantial number of years.

The research team believes that the proposed SDEs reflect an improvement in the distribution of live load with depth and better culvert designs.

CHAPTER 1

Introduction and Research Approach

Much analytical and experimental work has been conducted to investigate the distribution of surface loads through earth fills. The classical Boussinesq (1885) solution and simple assumptions such as spreading a surface load over an area that is a linear function of depth are perhaps the most widely used calculation procedures. Poulos and Davis (1974) summarize several elastic solutions for this problem, mostly considering different configurations of surface loads. However, little definitive work has been completed regarding the distribution of live loads through fills when a structure is embedded in the ground, because the problem remains too complex to complete closed form solutions for the wide range of the variables that must be considered. Experimental work (McGrath, et al., 2002, and other studies) has shown that the presence of a structure increases the effective spread of a live load substantially.

Probably two key mechanisms are involved in distributing live loads to buried structures:

- The stiffness of buried structures allows distribution of the live load within the structure. For example, live load in a box culvert slab can be distributed over a width of about 4 ft due solely to the structural stiffness of the slab (McGrath, et al., 2005). This behavior is well documented.
- The shear stiffness of soil spreads load over greater areas when flexible structures deform under live loads. Although not quantified through research, this mechanism is believed to explain why live load distribution on flexible structures is similar in width to that in rigid culverts, even though flexible culverts often do not have sufficient internal stiffness to accomplish the spreading.

For design, the AASHTO Standard and LRFD Specifications have two major differences relative to the treatment of live loads spreading through fills:

- The Standard Specifications apply live loads as a point load at the surface, increasing with depth to a square with sides equal to 1.75 times the depth of cover. The LRFD specifications apply live load through a tire footprint of 10 in. by 20 in. at the surface but attenuate with a lower coefficient (1.00 or 1.15 as a function of soil type) as the depth of fill increases.
- The Standard Specifications increase loads for impact effects by 30% for zero depth of cover, decaying to 0% for 3 ft of cover; the LRFD specifications increase loads for impact effects by 33% for zero depth of cover, but the effect does not drop to 0% until the depth of cover is 8 ft. At depths of about 2 to 4 ft, the LRFD Specifications result in loads about 15 to 20% higher than the Standard Specifications.

Because of the two key mechanisms described above, investigating the differences between the Standard and LRFD Specifications required a comprehensive program of three-dimensional (3D) numerical analyses of buried culverts. In order to be reliable, the analyses had to be conducted using an appropriate soil model and structural analysis software capable of incorporating several types of soil, several types of structures, and appropriate soil structure interfaces. The research approach adopted for the project involved several sequential steps of literature review, model development, model testing, extensive modeling, analysis and synthesis of model results, and development of simplified design equations (SDEs). The resulting SDEs were exercised to demonstrate their effect on culvert forces. Included in the research was development of guidelines for two-dimensional (2D) and 3D modeling for those designers interested in more refined analysis. The research results were incorporated into the recommended AASHTO LRFD design specifications. The specifics of the research approach are described in the following paragraphs.

1.1 Review and Evaluation of Relevant Experience

The foundation of the research was a review and evaluation of relevant field and modeling experience. The research team reviewed and evaluated relevant practice, performance data, research findings, and other information from domestic and international research, on the basis of applicability, conclusiveness of findings, and usefulness for the development of LRFD specifications for live load distribution to buried structures. Specific areas of interest were as follows:

- Data from tests required to validate the computer modeling conducted later in the project. Of greatest interest were reports and papers where the structure, the backfill, and the load vehicle and loading procedures were well documented.
- Candidate soil models were investigated to identify those models suitable for analysis of the live load problem.
- Appropriate software for conducting the 3D analyses necessary to investigate the transfer of live loads from the surface to the buried structures was identified.

1.2 Soil Constitutive Models and Software

Next, the research team selected and tested soil models having the following characteristics:

- Stress-dependent stiffness. The model must stiffen as confining stresses increase and soften as the deviator stress increases.
- Strength. Under many live load conditions, soil failure can occur under the vehicle wheels and at the structure-soil interface; this failure probably affects the load transferred into the structure.
- 3D behavior. Live load distribution through fills is a 3D problem.

The research team next developed the following criteria for assessing the suitability of specific modeling software:

- Soil-structure interaction. This capability was essential, because it is the principal focus of this project.
- Sequential model development. This capability, to "build" models in a manner compatible with real-world construction sequences, was essential.
- Structure/soil interface modeling. The software had to have a general capability to model the contact between the buried structure and the soil.
- 2D and 3D—A single source for both 2D and 3D software was important, but not essential.
- Structural analysis capabilities. Most candidate software could not model culverts with orthotropic structural response (i.e., corrugated metal pipe and profile wall thermoplastic culverts). The ability to do so was essential.
- Built-in soil models with non-linear material capabilities. This was essential because prior experience indicated that linear soil material behavior is inadequate to model buried structure problems.
- User-friendliness/learning curve. This was moderately important for software not currently in use at the organizations performing the research.
- Efficiency of computations. This criterion was important, but slow software can be overcome with additional computer hardware and software.
- Output capabilities. This criterion was moderately important.

After considering these initial criteria, the research team selected FLAC3D (Itasca, 2005). FLAC3D has a graphical user interface and a command-line or datafile-driven interface. The command-line/datafile-driven interface is readily amenable to parametric studies. In addition, much pre- and post-processing can be further automated using the built-in programming language. Using the built-in language, the research team automated all major model development steps, based on relatively few input parameters (e.g., depth, diameter, structure type, and soil type).

1.3 2D and 3D Modeling

After selecting and testing both soil constitutive models and software, the research team conducted more than 800 3D analyses of buried culverts. Nine culvert structures were modeled:

- Concrete arch,
- Concrete pipe,
- Concrete box,
- Corrugated metal pipe (CMP),
- Corrugated metal arch (CMA),
- Fiberglass-reinforced plastic pipe,
- High-density polyethylene (HDPE) profile wall pipe,
- Polyvinyl chloride (PVC) pipe, and
- Smooth metal pipe.

The solid cross-section culverts were all modeled as isotropic structures, and the corrugated metal pipe, corrugated metal arch, and HDPE profile wall pipe were modeled as orthotropic structures. Depths ranged from 1 to 12 ft, spans ranged from 1 to 30 ft, and four soil types were considered.

Three model states were saved for each analysis conducted: State 1 was the soil mass in equilibrium, with no culvert or live

load; State 2 (dead load) was the soil mass plus the culvert, in equilibrium; State 3 (dead load plus live load) was State 2 plus application of the live load pressure. Unless noted otherwise, all numerical results presented in tables and graphs in this report are for State 3 minus State 2 (i.e., dead plus live load minus dead load). All graphical output from FLAC3D is for States 1, 2, or 3 (but not, for example, State 3 minus State 2).

The built-in programming language of FLAC3D was used to extract selected results, typically thrust and moment in the structure, and normal and shear forces on the structure, on a plane under the live load. The results for all structure/depth/span/soil combinations were imported into a spreadsheet for quality control review, analysis, and presentation.

1.4 Development of SDEs

The existing Standard and LRFD methods for simplified design were reviewed and summarized. Then, proposed SDEs were developed based on the culvert structure forces predicted by the structural analyses.

Box section forces were evaluated first, because box sections have flat top slabs which afford an opportunity to evaluate not only the design forces but the vertical soil stresses on the top slab. Normal pressures on round or elliptical culverts are typically more difficult to interpret. The findings from box sections were then used to investigate the other culverts.

For all culvert types, design equation development focused on modifications to how the surface live loads spread with depth in the direction parallel to the culvert (perpendicular to the direction of vehicle travel).

1.5 Investigation of Effect of SDEs on Culvert Forces

A critical metric in assessing the SDEs was the effect on critical culvert forces (and hence the culvert design). Knowing if the proposed design equations affect culvert forces significantly was important. The research team calculated and compared the critical structural responses (for Standard, LRFD, and proposed design equations) for the following 242 culvert, depth, span, and soil combinations:

- Concrete box—6 cases
- Concrete pipe—100 cases
- Corrugated metal pipe—42 cases
- Thermoplastic (profile wall)—80 cases
- Metal arch—6 cases
- Concrete arch—8 cases

Graphs directly comparing the structural responses generated under the AASHTO Standard Specification, the AASHTO LRFD Specification, and the proposed SDEs were prepared. (Appendix D.1 contains MathCAD templates illustrating Standard, LRFD, and Proposed calculations for all structure types; Appendix D.2 lists the results.)

1.6 Refined Analysis Guidelines

In cases where the SDEs are not applicable, refined analysis methods (e.g., 2D and 3D structural analysis) will be necessary. This research provided significant insight into the 3D modeling of buried culverts. The experience gained from this research may be helpful in selecting soil constitutive models, software, loading conditions, model sizes, element sizes, soil-structure interfaces, and other features.

Although the spread of live load with depth is inherently a 3D problem, many designers do not have access to 3D modeling software or expertise. In these situations, it may be useful to have guidelines for the pseudo live loads to apply to 2D models to achieve appropriate results. A series of 2D-3D companion models were run for the same physical problem. The results were used to develop empirical equations for estimating the 2D live load to apply.

CHAPTER 2

Findings

2.1 Review and Evaluation of Relevant Experience

2.1.1 Soil Constitutive Models

Numerous soil constitutive models have been developed and are available for finite-element analysis. Lade (2005) summarized widely available soil constitutive models. Each model has different capabilities and requires different experimental data for calibration.

Predicting the response of buried structures to surface live loads in a finite-element analysis requires a soil constitutive model that captures culvert-soil interaction accurately. Research has been conducted with linear-elastic soil models (e.g., Moore and Brachman, 1994, and Fernando and Carter, 1998) with nonlinear models, including nonlinear elastic models, perfectly plastic models, and plastic models with hardening (e.g., Pang, 1999). For typical culvert analysis, which has been historically conducted in two dimensions, stress-dependent stiffness and shear failure have been found to be important characteristics of suitable soil models. The Duncan-Selig hyperbolic model (Duncan et al., 1980, and Selig, 1988) has such features and has been implemented in the finite-element programs CANDE (Musser, 1989) and SPIDA (Heger et al., 1985) to analyze soil-structure interaction problems for culverts. Soil properties based on these models have been used to develop current AASHTO specifications for reinforced concrete and thermoplastic pipe. The Duncan-Selig model consists of the hyperbolic Young's modulus model developed by Duncan et al. (1980) and the hyperbolic bulk modulus developed by Selig (1988). As discussed below, the soil properties used with this model were developed by Selig (1988).

CANDE, developed by the FHWA, has been widely used to design culverts, but operates only in two dimensions. For ease of computation and to allow comparison with CANDE, the research team conducted preliminary analyses in two dimensions and then extended these models to three dimensions for a complete investigation of actual live load distribution.

3D modeling is computationally intensive, so it is important to select the computationally simplest soil model that can accurately capture culvert-soil interaction resulting from live load. The research team selected three soil models with varying levels of sophistication for preliminary assessment:

- Linear-elastic (representing the simplest possible model),
- Mohr-Coulomb (linear-elastic model with post-failure plasticity), and
- Hardening-soil (stress dependence plus plasticity, similar to Duncan-Selig).

2.1.2 Model Verification with Field Tests

Initial investigation of culvert responses to live loads from 2D analyses with linear-elastic, Mohr-Coulomb, and hardening-soil models showed that responses from the Mohr-Coulomb and hardening-soil models were very close to each other whereas responses from the linear-elastic model were significantly different from other models (see Appendix A for the detailed treatment). As a result, the Mohr-Coulomb model was selected for use in the 3D analysis of field tests. Subsequent Panel comments suggested comparison of the Mohr-Coulomb and hardening-soil models in the 3D analysis as a confirmation of selection of an appropriate soil model. To compare culvert responses from these two soil models, 3D analyses were performed of a long-span metal arch from NCHRP Project 12-45 (McGrath et al., 2002) and HDPE pipe from the Minnesota DOT (MNDOT) study (McGrath et al., 2005).

Method of Approach

Soil-structure interaction analysis of culverts subjected to the surface live load is performed using Plaxis 3D Tunnel,

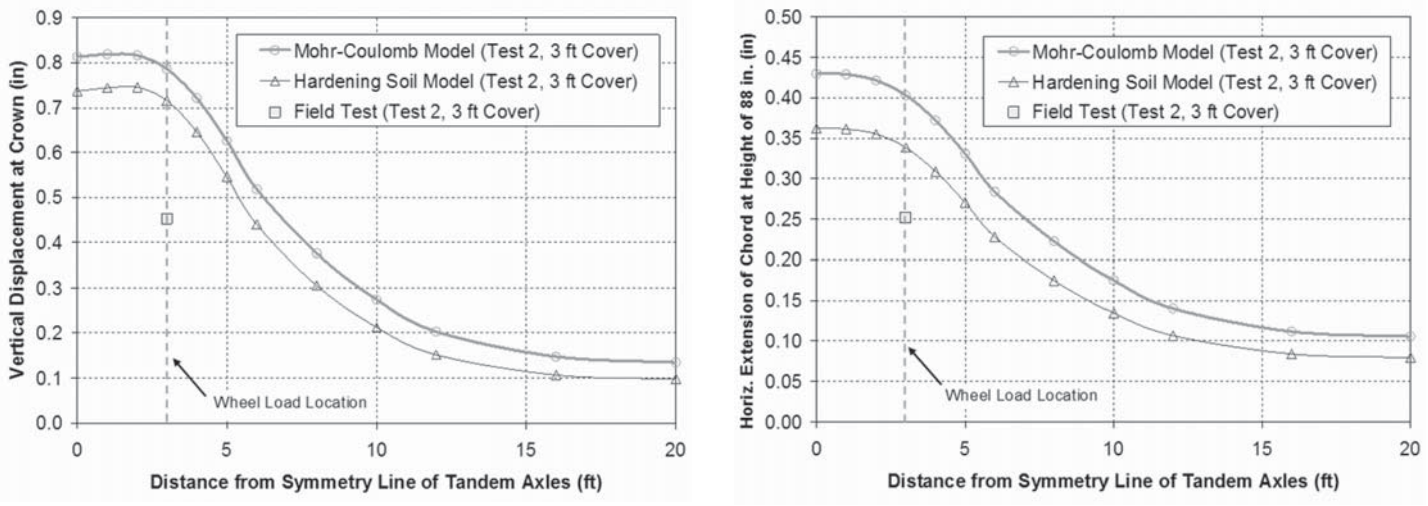

(a) Vertical crown (b) Horizontal chord

Figure 2-1. Comparison of displacements between cases with Mohr-Coulomb and hardening-soil models (metal arch, Test 2, 3 ft cover).

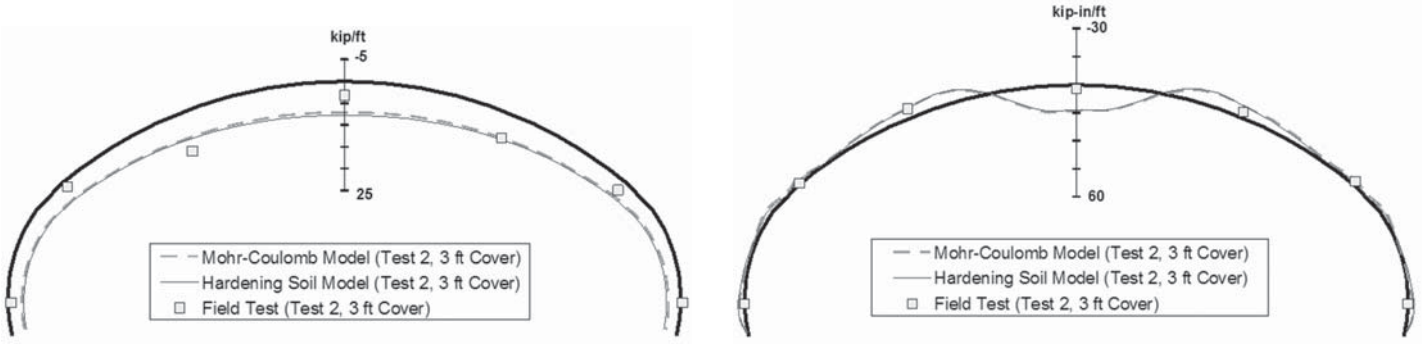

(a) Thrust (b) Moment

Figure 2-2. Comparison of thrusts and moments under wheel between cases with Mohr-Coulomb and hardening-soil models (metal arch, Test 2, 3 ft cover).

Version 2[1] (Brinkgreve and Broere, 2004). Two structural models were selected as described above: (1) a long-span metal arch, Test 2, 3-ft cover (*NCHRP Report 473*); and (2) an HDPE pipe, Pipe Run 7, A-2 backfill, 2.8-ft cover (MNDOT study). These structures were analyzed with both Mohr-Coulomb and hardening-soil models, and structural responses were compared. In the metal arch model, backfill was assumed to have properties of SW85, and the soil above the crown of the arch was assumed to have properties of SW95. With the HDPE pipe model, backfill was assumed to have properties of ML95. The interface strength was assumed to be 50% of the strength of surrounding soil. Structures, finite-element models, live load tests, and material properties were described in detail in the literature (McGrath et al., 2002, and McGrath et al., 2005). The results of the comparison of predictions from computer models with data from actual field tests was often poor; extenuating circumstances are discussed in Section 2.1.3.

[1]Plaxis 3D Tunnel is a finite-element package focused on the analysis of structures in soil and rock materials. Special features include non-linear, time-dependent, and anisotropic behavior of the earth materials, multiphase problems, and soil-structure interaction.

Results

Metal Arch in Test 2 with 3 ft Cover. Figure 2-1 compares vertical crown displacements and horizontal chord extensions along the culvert for the two cases of the metal arch analysis: the case with the Mohr-Coulomb model and the case with the hardening-soil model. Figure 2-2 compares thrusts and moments under the wheel load for the two cases. These figures also show displacements and forces measured in the field tests. Measured thrusts and moments are average values of measurements under the left and right wheels. Tables 2-1 through 2-3 also compare displacements and forces of the two cases. Differences in moments and thrusts of the two soil models were insignificant. Displacements were slightly smaller with the hardening-soil model than the Mohr-Coulomb model: by 9%

Table 2-1. Summary of displacements under wheel (metal arch, Test 2, 3 ft cover).

Vertical or Horizontal	Field Test (in.)	Plaxis 3D (in.)		Ratio: Plaxis 3D / Field Test	
		Mohr-Coulomb	Hardening-Soil	Mohr-Coulomb	Hardening-Soil
Vertical crown displacement	0.45	0.79	0.72	1.74	1.58
Horizontal chord extension	0.25	0.40	0.34	1.60	1.34

Table 2-2. Summary of thrusts under wheel (metal arch, Test 2, 3 ft cover).

Location	Field Test (kip/ft)	Plaxis 3D (kip/ft)		Ratio: Plaxis 3D/Field Test	
		Mohr-Coulomb	Hardening-Soil	Mohr-Coulomb	Hardening-Soil
NS	0.69	3.12	3.54	4.54	5.15
NC	1.42	4.41	4.70	3.10	3.31
NH	9.07	5.92	6.27	0.65	0.69
CR	3.08	7.05	7.75	2.29	2.51
SH	5.84	5.80	6.18	0.99	1.06
SC	2.46	4.08	4.46	1.66	1.81
SS	-0.34	2.75	3.25	-7.98	-9.44

NS = north springline; NC = north chord point at intersection of top plates and side plates; NH = north haunch, about halfway between NC and CR; CR = crown; SS = south springline; SC = south chord point at intersection of top plates and side plates; SH = south haunch, about halfway between SC and CR

Table 2-3. Summary of moments under wheel (metal arch, Test 2, 3 ft cover).

Location	Field Test (kip/ft)	Plaxis 3D (kip/ft)		Ratio: Plaxis 3D/Field Test	
		Mohr-Coulomb	Hardening-Soil	Mohr-Coulomb	Hardening-Soil
NS	-0.03	-3.14	-3.61	94.73	108.90
NC	-0.38	-2.75	-2.13	7.27	5.63
NH	-5.24	-5.25	-5.42	1.10	1.03
CR	2.04	13.71	13.38	6.74	6.57
SH	-3.28	-6.43	-6.26	1.96	1.91
SC	-1.97	-2.62	-1.78	1.33	0.91
SS	0.07	-2.66	-3.31	-35.61	-44.31

See notes on Table 2 for definition of Location acronyms.

for the vertical crown displacement and by 16% for the horizontal displacement. Therefore, displacement results were closer to the field measurements with the hardening-soil model than with the Mohr-Coulomb soil model in this case.

HDPE Pipe with A2 Backfill and 2.8-ft Cover. For the HDPE pipe study, evaluating the Plaxis model predictions for the Mohr-Coulomb and hardening-soil models against the field data was accomplished by comparing deflections, and evaluating the force predictions. Figures 2-3 and 2-4 compare vertical crown displacements horizontal diameter extensions along the culvert for the two cases of HDPE pipe analysis: the case with the Mohr-Coulomb model and the case with the hardening-soil model. These figures also show displacements measured in the field tests. In the figures, P3 indicates a single axle centered over the pipe, P4 indicates tandem axles located symmetrically over the pipe, "heavy" indicates 24,000 lb axles and "light" indicates 18,000 lb axles. The dates of the tests (i.e., when the data were collected) are also provided. For example, Oct '00 represents nearly the first loading after construction, May '01 represents a time shortly after the winter frost had melted and the ground was soft, and Aug '02 represents data after numerous loading cycles at a dry time of the year. Figures 2-5 and 2-6 compare thrusts moments under the wheel load for the two cases. Tables 2-4 and 2-5 compare field displacements with the Plaxis model displacements, while Table 2-6 compares forces for the two cases.

Calculated displacements were larger with the hardening-soil model than with the Mohr-Coulomb model: by about 30% for the vertical crown displacement and by about 55%

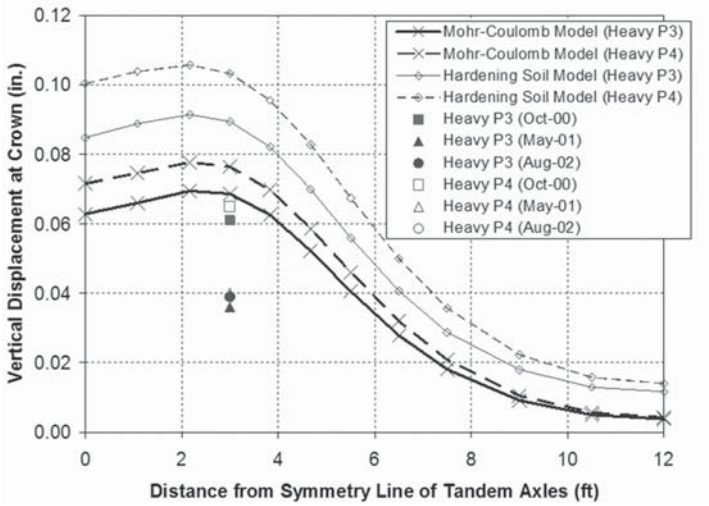

(a) Heavy truck

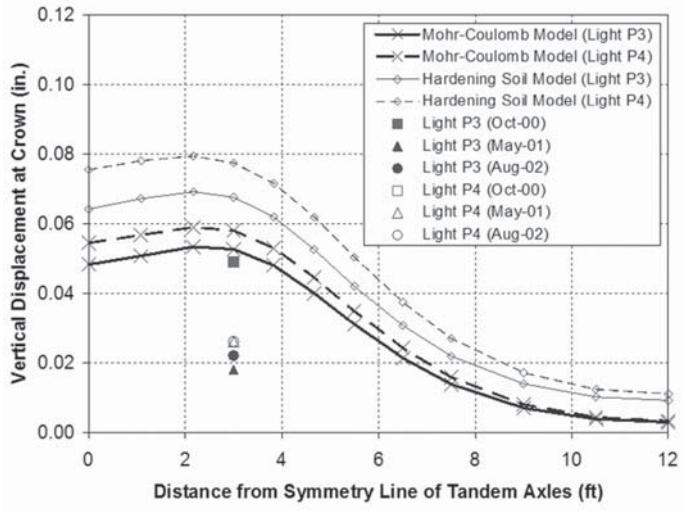

(b) Light truck

Figure 2-3. Comparison of crown vertical displacements between cases with Mohr-Coulomb and hardening-soil models (HDPE pipe, A-2 soil, 2.8 ft cover).

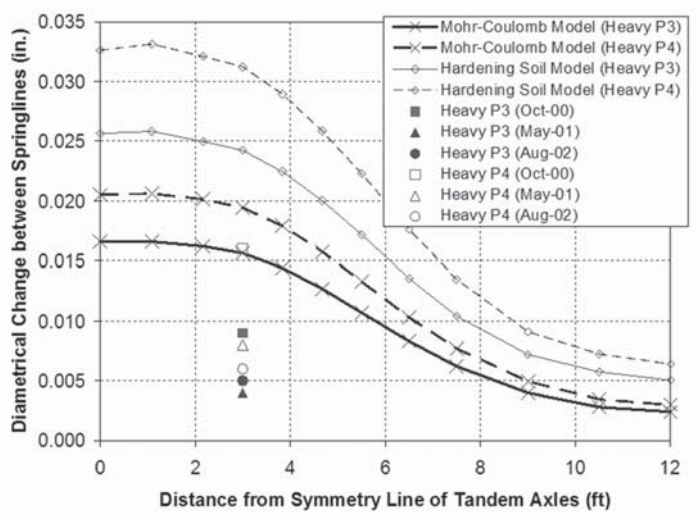

(a) Heavy truck

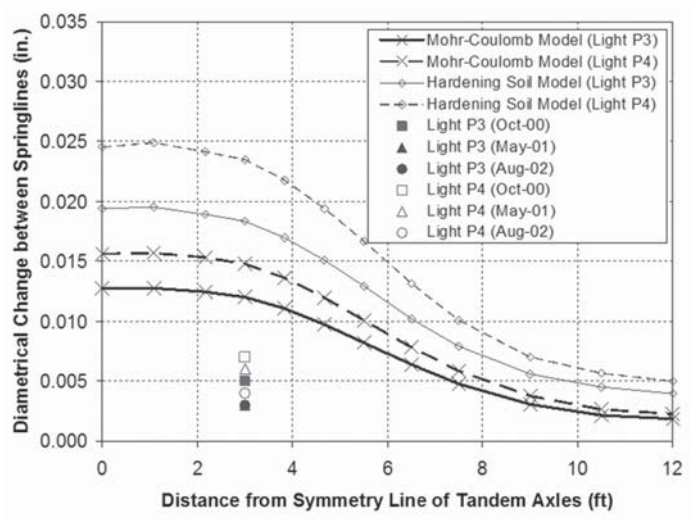

(b) Light truck

Figure 2-4. Comparison of horizontal diameter changes between cases with Mohr-Coulomb and hardening-soil models (HDPE pipe, A-2 soil, 2.8 ft cover).

for the horizontal displacement. Therefore, displacement results from the Mohr-Coulomb model were closer to the measured displacements in the field tests in this particular case. Because of the larger displacements, moments and thrusts were also larger with the hardening-soil model. Thrusts from the hardening-soil model were up to 20% higher than those from the Mohr-Coulomb model, and moments were up to 44% higher. Softer soil responses obtained for the hardening-soil model can be explained by the lower stiffness of the hardening-soil model when compared with that of the Duncan-Selig model. By selecting higher stiffness values for hardening-soil properties of ML95, force results can be brought closer to those of the Mohr-Coulomb model.

2.1.3 Discussion

During development and testing of computer models, soil models, and modeling methodology (described in Appendix A) the research team learned that soil-structure interaction analysis of buried culverts subjected to live loads with the linear-elastic soil model could produce significantly different structural response than those with the Mohr-Coulomb soil model

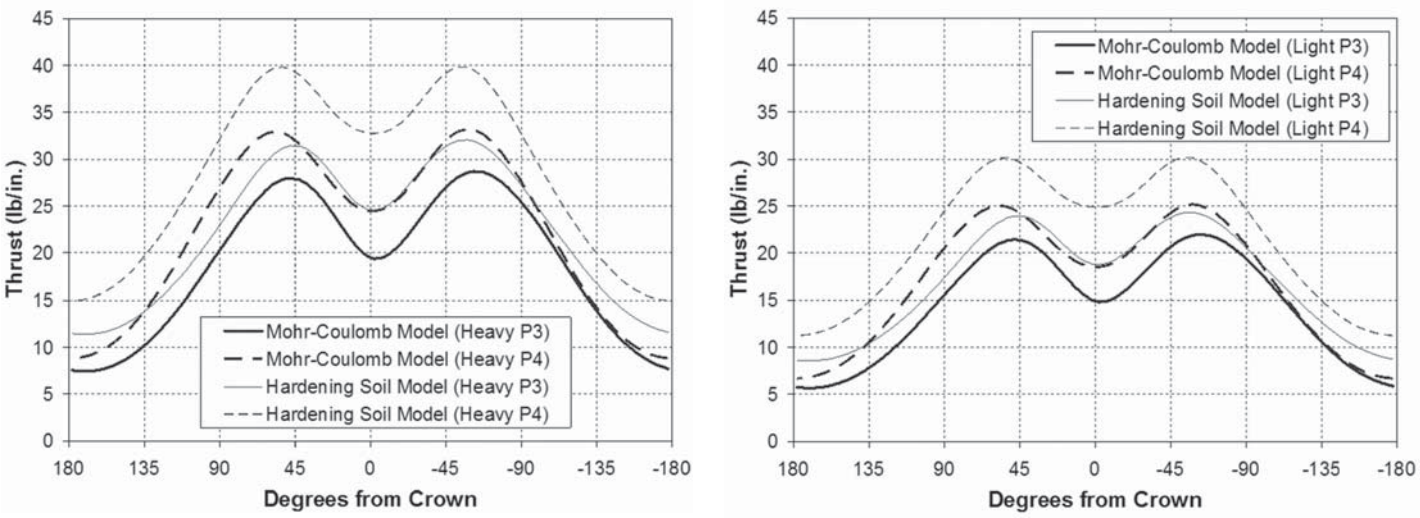

(a) Heavy truck (b) Light truck

Figure 2-5. Comparison of thrusts between cases with Mohr-Coulomb and hardening-soil models (HDPE pipe, A-2 soil, 2.8 ft cover).

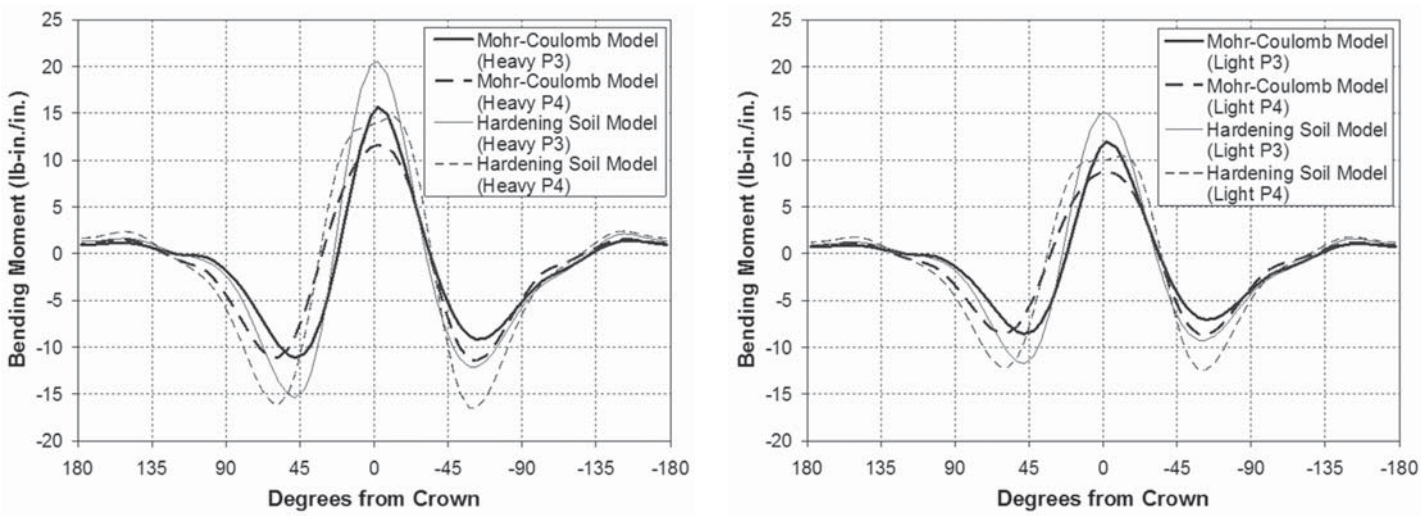

(a) Heavy truck (b) Light truck

Figure 2-6. Comparison of moments between cases with Mohr-Coulomb and hardening-soil models (HDPE pipe, A-2 soil, 2.8 ft cover).

and the hardening-soil model. Given that a difference between the linear-elastic model and the Mohr-Coulomb model is whether or not soil failure is modeled by plasticity, plasticity is one of the key characteristics of soil models for this project.

The analyses presented here indicate some of the difficulties in predicting structural response of buried culverts subjected to live loads. The soil parameters currently used in design appear to yield soil behavior that is softer than achieved in the field tests. Given the variability of real-world soils and in-field compaction effort, this conservatism is justified in design. Soil parameters could be developed just for the current study that match the soil test data, which in turn produce better estimates of live load response of buried culverts. However, the same question will arise—how should the parameters be modified for design of actual structures that will experience all of the variability noted? Given the success of the Duncan-Selig model and the Selig (1988) properties, it is appropriate to continue with conservative design parameters.

In addition to the soil parameters of a specific soil type, other uncertainties in the field tests made matching field data in the analysis difficult. Backfill densities were reported as the density

Table 2-4. Summary of vertical displacements under wheel (HDPE pipe, A-2 soil, 2.8 ft cover).

Truck	Position	Field Test (in.)			Plaxis 3D (in.)		Ratio: Plaxis 3D / Field Test					
					Mohr-Coulomb	Hardening Soil	Mohr-Coulomb Model			Hardening Soil Model		
		Oct 00	May 01	Aug 02			Oct 00	May 01	Aug 02	Oct 00	May 01	Aug 02
Heavy	3	0.061	0.036	0.039	0.069	0.089	1.13	1.91	1.76	1.47	2.48	2.29
	4	0.065	0.040	0.039	0.076	0.103	1.18	1.91	1.96	1.59	2.58	2.65
Light	3	0.049	0.018	0.022	0.053	0.068	1.07	2.92	2.39	1.38	3.75	3.07
	4	0.049	0.026	0.026	0.058	0.077	1.18	2.23	2.23	1.58	2.98	2.98

Table 2-5. Summary of horizontal chord extensions under wheel (HDPE pipe, A-2 soil, 2.8 ft cover).

Truck	Position	Field Test (in.)			Plaxis 3D (in.)		Ratio: Plaxis 3D / Field Test					
					Mohr-Coulomb	Hardening Soil	Mohr-Coulomb Model			Hardening Soil Model		
		Oct 00	May 01	Aug 02			Oct 00	May 01	Aug 02	Oct 00	May 01	Aug 02
Heavy	3	0.009	0.004	0.005	0.016	0.024	1.74	3.91	3.13	2.69	6.06	4.85
	4	0.016	0.008	0.006	0.019	0.031	1.21	2.43	3.24	1.95	3.90	5.20
Light	3	0.005	0.003	0.003	0.012	0.018	2.40	4.00	4.00	3.67	6.11	6.11
	4	0.007	0.006	0.004	0.015	0.023	2.11	2.46	3.69	3.35	3.91	5.87

Table 2-6. Summary of force results (HDPE pipe, A-2 soil, 2.8 ft cover).

Truck	Position	Thrust (lb/in.)				Moment (lb-in./in.)			
		Crown		Peak		Peak Positive		Peak Negative	
		MC	HS	MC	HS	MC	HS	MC	HS
Heavy	3	19.5	24.6	28.7	32.1	15.7	20.5	-11.1	-15.4
	4	24.5	32.8	33.2	39.8	11.7	14.7	-11.5	-16.5
Light	3	14.9	18.8	22.0	24.3	12.0	15.1	-8.6	-11.7
	4	18.5	24.9	25.2	30.2	8.8	10.5	-8.7	-12.4

measured at the time of backfilling; however, there is considerable activity over the pipes after the backfilling is completed, and this activity likely densifies the soil. For example

- In the long-span study, the soil surface was compacted with a large vibratory roller prior to the live load tests to ensure that the surface soil could carry the heavily loaded truck without significant rutting. This probably densified the clean gravel backfill.
- In the MNDOT study, the backfill was overlaid with 8 in. of gravel and 4 in. of pavement. Again, the backfill over the top crown of the test pipes probably was densified prior to live load testing.
- In the MNDOT study, after the construction was complete, there was still considerable variability in the data because of seasonal differences, temperature variations and, perhaps, other parameters.

Because of these circumstances, the overprediction of displacements and forces was expected in the soil models. The differences between the model predictions and the field data could be addressed by increasing soil properties until the predictions match field data; however, this would be artificial because the soil properties used for the study have been validated repeatedly over the last 20 years. The question then is whether or not to match specified field properties or anticipate densification through subsequent construction in order to match field test results. The use of specified soil properties was selected as being appropriately conservative. Any densification that occurs because of subsequent construction activities should provide additional safety. This approach was further justified given the variability of highway construction sites, potential variations in backfill type and density, and variations in depth of cover.

2.1.4 Recommended Soil Constitutive Model

The preceding sections document the investigation of soil models for analysis of live load effects on buried structures. Based on these studies, a linearly elastic, perfectly plastic soil model, with a Mohr-Coulomb failure criterion, was selected. This selection offered the best mix of capturing the important aspects of soil behavior in transmitting live loads to structures and simplicity in modeling to allow the research team to complete the greatest number of analyses in the least amount of time. In implementing this soil model, the research team recommended that the elastic soil properties be selected based on depth of fill. This technique does not offer all of the benefits of the Duncan-Selig/hardening-soil models in capturing stress-dependent stiffness behavior of soil, but, for the purposes of a live load study, this technique appears to provide sufficient accuracy.

Parameters for the soil model were those reported above based on the Selig (1988 and 1990) properties. The bulk modulus values in Selig (1990) should be considered suitable for analysis when justified by data, but may not be a lower bound. The proposed properties proved somewhat conservative relative to field data.

Soil angles of friction vary depending on the stress state. In the modeling, one may choose whether the angle of friction depends on initial stresses (prior to live load) or on the stresses present because of the live load. This choice did not significantly affect the structural response of culverts to surface live loads. The research team also found that a smaller angle of friction resulted in greater structural responses. Given that soil under live loads is under higher stresses than the state before the live loads are applied, angle of friction of soil under live loads should be lower than for the soil before the live loads are applied. Although this change in the angle of friction because of live loads does not affect the soil strength significantly, the research team believes that it is more accurate to use angles of friction under higher stresses than those based on only geostatic stress state.

The research team used soil angles of friction at a reference confinement of 14.7 psi from Selig's parameters (1988) at any depth in the 3D analysis, instead of variable angles of friction calculated from the stress state before the live load application.

2.2 Selection and Development of Refined Analytical Models

This section describes the general characteristics of the software, soils, model dimensions, structures, live load, and modeling sequence. Examples of typical models are provided in Section 2.2.7.

2.2.1 Software

All core analyses were done with FLAC3D, with supporting or quality control calculations done using SAP 2000, PLAXIS, ANSYS, and FLAC2D. FLAC3D is a continuum code used in analysis, testing, and design by geotechnical, civil, and mining engineers. The software uses an explicit finite difference formulation that can accommodate large displacements and strains and non-linear material behavior, even if yield or failure occurs over a large area or if total collapse occurs. FLAC3D can model some complex behaviors not readily available in other codes, such as problems that consist of several stages, large displacements and strains, non-linear material behavior and unstable systems (even cases of yield/failure over large areas, or total collapse). (Chapter 2.1 of Appendix B has additional information.)

Built-in soil models include elastic, Mohr-Coulomb, and Cam-Clay, but all analyses reported here used the Mohr-Coulomb soil model (except for a thin, elastic layer used to prevent the live load from causing failure of the soil surface, and in some analyses, an elastic layer representing the pavement).

All culvert structures modeled here used shell structural elements—isotropic shell elements were used for concrete, PVC, FRP and smooth metal culverts, and orthotropic shell elements were used for corrugated metal and profile wall culverts. FLAC3D's built-in programming language, FISH, facilitated preparing data sets and extracting/processing results.

2.2.2 Soil Properties

Development of soil constitutive models and properties has been addressed in preceding sections (and in Appendix A). Major decisions include use of the Mohr-Coulomb soil, soil property variations with depth, and the use of soil friction angles representative of high-stress conditions.

All models used one of four soil materials: well-graded or gravelly sand at 85% standard compaction (SW85), well-graded or gravelly sand at 95% standard compaction (SW95), inorganic silts and fine sands at 85% standard compaction (ML85), and inorganic clays at 85% standard compaction (CL85). Mohr-Coulomb soil parameters for SW95, SW85, ML85, and CL85 are provided in Tables 2-7 through 2-10.

2.2.3 Model Dimensions

In general, model dimensions were larger for increasing cover depth and increasing culvert depth. In some instances, the research team initially used smaller model widths, observed

Table 2-7. Parameters for linear-elastic and Mohr-Coulomb models for SW85.

Depth (ft)	Modulus of Elasticity E (psi)	Poisson's Ratio ν	Angle of Friction ϕ (deg)	Dilatation Angle ψ (deg)	Cohesion c (psi)
0 to 1	1,300	0.26	38.0	8.0	0.001
1 to 6	2,100	0.21	38.0	8.0	0.001
6 to 11	2,600	0.19	38.0	8.0	0.001
11 to 18	3,300	0.19	38.0	8.0	0.001

Table 2-8. Parameters for linear-elastic and Mohr-Coulomb models for SW95.

Depth (ft)	Modulus of Elasticity E (psi)	Poisson's Ratio ν	Angle of Friction ϕ (deg)	Dilatation Angle ψ (deg)	Cohesion c (psi)
0 to 1	1,600	0.40	48.0	18.0	0.001
1 to 5	4,100	0.29	48.0	18.0	0.001
5 to 10	6,000	0.24	48.0	18.0	0.001
10 to 18	8,600	0.23	48.0	18.0	0.001

Table 2-9. Parameters for linear-elastic and Mohr-Coulomb models for ML85.

Depth (ft)	Modulus of Elasticity E (psi)	Poisson's Ratio ν	Angle of Friction ϕ (deg)	Dilatation Angle ψ (deg)	Cohesion c (psi)
0 to 1	600	0.25	30.0	0.0	3.0
1 to 6	700	0.24	30.0	0.0	3.0
6 to 13	800	0.23	30.0	0.0	3.0
13 to 18	850	0.3	30.0	0.0	3.0

Table 2-10. Parameters for linear-elastic and Mohr-Coulomb models for CL85.

Depth (ft)	Modulus of Elasticity E (psi)	Poisson's Ratio ν	Angle of Friction ϕ (deg)	Dilatation Angle ψ (deg)	Cohesion c (psi)
0 to 1	100	0.33	18.0	0.0	6.0
1 to 7	250	0.29	18.0	0.0	6.0
7 to 14	400	0.28	18.0	0.0	6.0
14 to 18	600	0.25	18.0	0.0	6.0

results indicating that the models were too narrow, and reran the models using greater width. Table 2-11 summarizes the model dimensions.

2.2.4 Culvert Structures

Nine culvert structures were modeled:

- Concrete arch,
- Concrete pipe
- Concrete box,
- Corrugated metal pipe,
- Corrugated metal arch,
- Fiberglass-reinforced plastic pipe,
- HDPE profile wall pipe,
- PVC pipe, and
- Smooth metal pipe.

The solid cross-section culverts were all modeled as isotropic structures; the corrugated metal pipe, corrugated metal arch, and HDPE profile wall pipe were modeled as orthotropic structures. The properties used for the various culvert structures are listed in Tables 2-12 through 2-16. Concrete box and concrete arch properties were calculated from the section thickness and concrete modulus of 4,030,000 psi (box) and 3,605,000 psi (arch).

Uncracked concrete properties were used in the analyses. The rationale was twofold: (1) cracking was not expected and (2) if cracking did occur, the resulting softer structure would have lower, unconservative structural loads.

All structures were modeled using three-node, planar-shell elements, either isotropic or orthotropic.

The pipe stiffness[2] of the various round pipe models varied by more than three orders of magnitude, from 10 lb/in/in for 96-in.-diameter smooth metal pipe, to 47,000 lb/in/in for 12-in.-diameter concrete pipe (See Figures 2-7 and 2-8).

[2]Pipe stiffness, PS:

$PS = \frac{EI}{0.149r^3}$ where E = modulus of elasticity, I = moment of inertia, r = mean pipe radius

Table 2-11. Summary of model dimensions.

Culvert Type	Culvert Dimensions	Cover Depth (inches)	Model Width (inches)	Model Height (inches)
Round Pipe	12”	12	36	42
		24	54	54
		48	108	78
		96	216	126
Round Pipe	24”	12	72	73
		24	72	84
		48	108	108
		96	216	156
		144	72	204
Round Pipe	48”	12	144	138
		24	144	150
		48	144	174
		96	144	198
		144	144	222
Round Pipe	96”	12	288	252
		24	288	264
		48	288	288
		96	288	336
		144	288	384
Concrete Box	48” x 48”	12	144	138
		24	144	150
		48	144	174
		96	144	222
Concrete Box	96” x 96”	12	288	252
		24	288	264
		48	288	288
		96	288	336
Corrugated Metal Arch	20.1 ft x 9.1 ft	12	240	229
		48	240	265
		96	240	313
Corrugated Metal Arch	30.1 ft x 18.1 ft	12	360	444
		48	360	456
		96	360	528
Concrete Arch	25.4 ft x 10 ft	12	300	252
		48	300	288
		96	300	336
Concrete Arch	43.11 ft x 13.8 ft	12	528	352
		48	528	364
		96	528	436

Table 2-12. Summary of isotropic structural properties for concrete pipe.

Pipe Dia. (in)	OD (in)	Wall Thickness (in)	A (in^2/in)	I (in^4/in)	EA (lb/in)	EI ($lb\text{-}in^2/in$)
12	16	2	2	0.667	7,210,000	2,403,000
24	30	3	3	2.25	10,815,000	8,111,000
48	58	5	5	10.42	18,025,000	37,552,000
96	114	9	9	60.75	32,445,000	219,004,000

Table 2-13. Summary of isotropic structural properties for smooth metal pipe.

Pipe Dia. (in)	OD (in)	Wall Thickness (in)	A (in2/in)	I (in4/in)	EA (lb/in)	EI (lb-in2/in)
24	24.75	0.375	0.375	0.00439	10,875,000	127,000
48	49.25	0.625	0.625	2.25	18,125,000	65,250,000
96	97.874	0.937	0.937	10.42	27,173,000	302,180,000

Table 2-14. Summary of isotropic structural properties for PVC pipe.

Pipe Dia.(in)	OD (in)	Wall Thickness (in)	A (in^2/in)	I (in^4/in)	EA (lb/in)	EI (lb-in^2/in)
12	14.7	1.4	1.4	0.229	140,000	22,900
24	30	2.4	2.4	2.25	240,000	225,000
48	58	3.5	3.5	10.42	350,000	1,042,000

Table 2-15. Summary of orthotropic structural properties for HDPE profile wall pipe.

Pipe Dia.(in)	Profile	Wall Thickness (in)	Direction	A (in^2/in)	I (in^4/in)	EA (lb/in)	EI (lb-in^2/in)
12	2"X1.07"	0.1984	Circumferential	0.1984	0.0305	19840	3050
			Longitudinal	0.06984	0.0000726	6984	7.26
24	4"X2.16"	0.344	Circumferential	0.344	0.1997	34400	19970
			Longitudinal	0.14108	0.00057	14108	57
48	5.98"X3.12"	0.48	Circumferential	0.48	0.634	48000	63400
			Longitudinal	0.22481	0.00219	22481	219
60	8"X3.51"	0.541	Circumferential	0.5407	0.9	54070	90000
			Longitudinal	0.25389	0.00299	25389	299

Table 2-16. Summary of orthotropic structural properties for corrugated metal pipe.

Pipe Dia.(in)	Corrugation	Wall Thickness (in)	Direction	A (in^2/in)	I (in^4/in)	EA (lb/in)	EI (lb-in^2/in)
12	2-2/3"X1/2"	0.0598	Circumferential	0.0646	0.00189	1873400	54810
			Longitudinal	0.000587	1.92E-05	17013	558
24	2-2/3"X1/2"	0.0747	Circumferential	0.0807	0.00239	2340300	69310
			Longitudinal	0.001137	3.75E-05	32982	1088
48	2-2/3"X1/2"	0.1046	Circumferential	0.113	0.00343	3277000	99470
			Longitudinal	0.003083	0.000103	89412	2987
96	3"X1"	0.1046	Circumferential	0.1308	0.01546	3793200	448340
			Longitudinal	0.000706	0.000117	20464	3402

2.2.5 Live Load

Analyses were conducted for dead load (soil loading only) and combined dead plus live load. The dead load response was subtracted from the combined response to determine the live only response. Dead loads (i.e., soil loads) were not factored. Live loads were applied and factored as follows:

$$LL = m_{mpf}\left[1+\frac{IM}{100}\right]P \quad (1)$$

where

m_{mpf} is the multiple presence factor (1.2)

P is the wheel load magnitude (16,000 lb)

IM is the dynamic load allowance $33\left[1-\frac{0.125\cdot H}{12}\right], H \le 8$

H is the depth of cover from road surface to top of culvert, in.

2.2.6 Modeling Sequence

Three states of the model were analyzed and saved for each analysis conducted:

- State 1 is the soil mass in equilibrium, with no culvert or live load. State 1 was achieved by creating the model grid, applying material properties to the soil materials, and placing stresses in the grid.
- State 2 (dead load) is the soil mass plus the culvert, in equilibrium. State 2 was achieved by excavating the soil (with no cycling of the model), installing the culvert in the soil, and then cycling to equilibrium.
- State 3 (dead load plus live load) is State 2 plus application of the live load defined above.

Unless noted otherwise, all numerical results presented in tables and figures in this report are for State 3 minus State 2 (i.e., dead plus live load minus dead load). All graphical out-

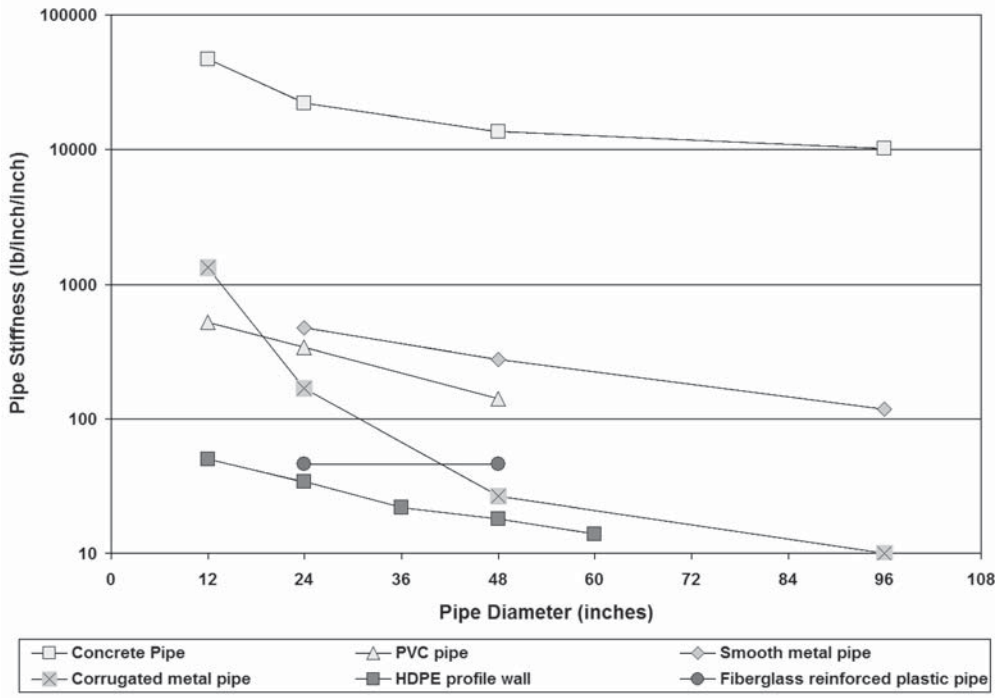

Figure 2-7. Pipe stiffness for the round culverts modelled.

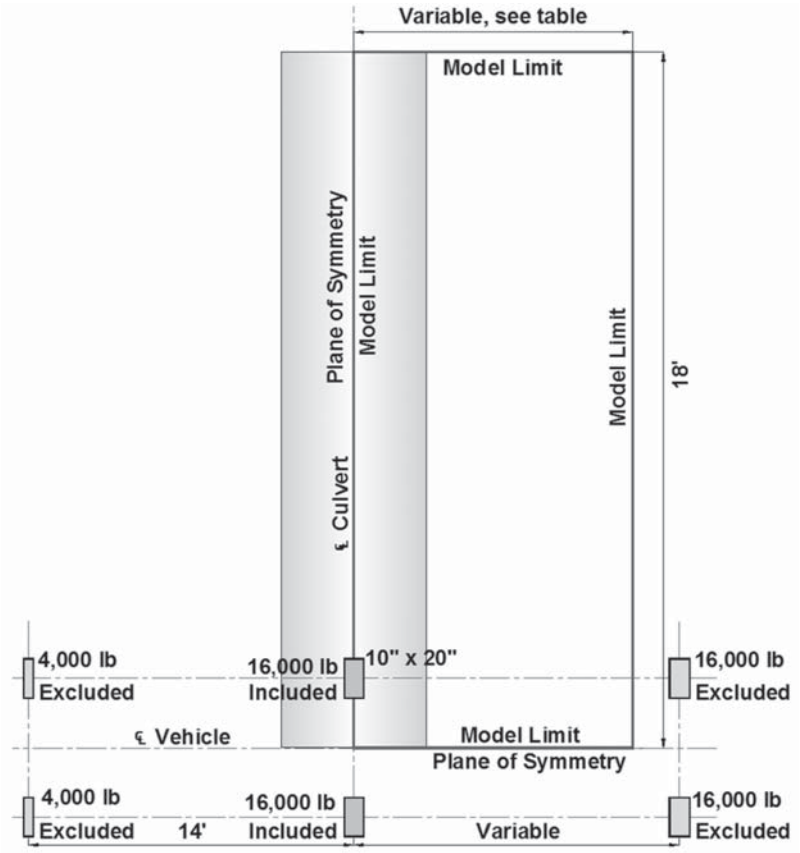

Figure 2-8. Location and intensity of live load, before factoring.

put from FLAC3D is for States 1, 2, or 3 (but not for example State 3 minus State 2).

2.2.7 Typical Soil and Structure Models

It may not be possible to adequately illustrate "typical models" for 830 analyses ranging from 12-in.-diameter pipe to 43-ft arches, and for 12-in. to 12-ft cover. However, figures in this section illustrate the soil zone meshes, culvert structural meshes, and live load application.

Figures 2-9 through 2-12 show typical soil meshes, where the different soil layers are indicated by shading. Figures 2-13 and 2-14 show typical structural meshes. Figure 2-15 shows a typical deformed mesh, where the deformation represents grid dis-

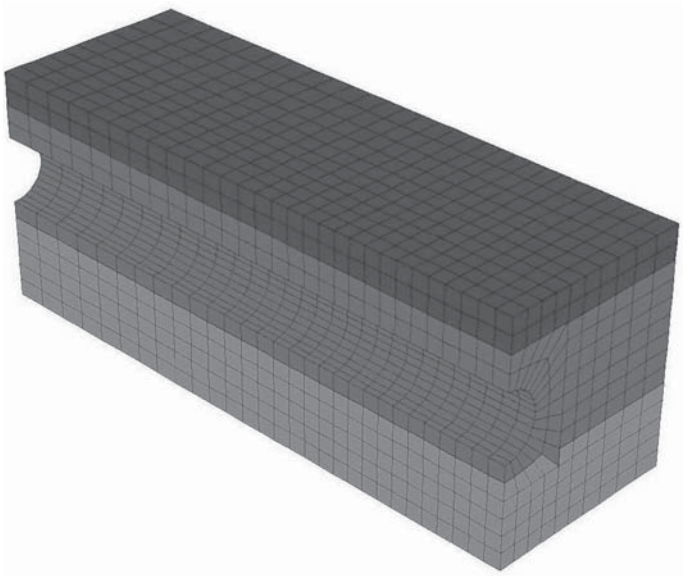

Figure 2-9. Round pipe model for 24″ deep, 24″ diameter (shading indicates soil modulus).

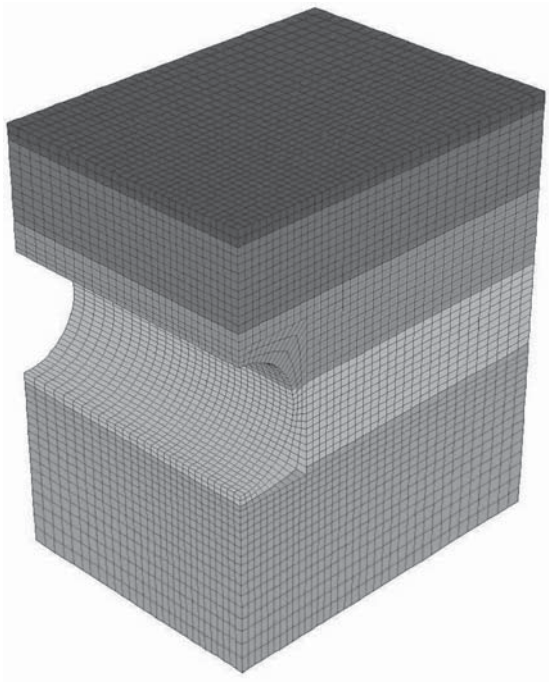

Figure 2-10. Round pipe model for 96″ deep, 96″ diameter (shading indicates soil modulus).

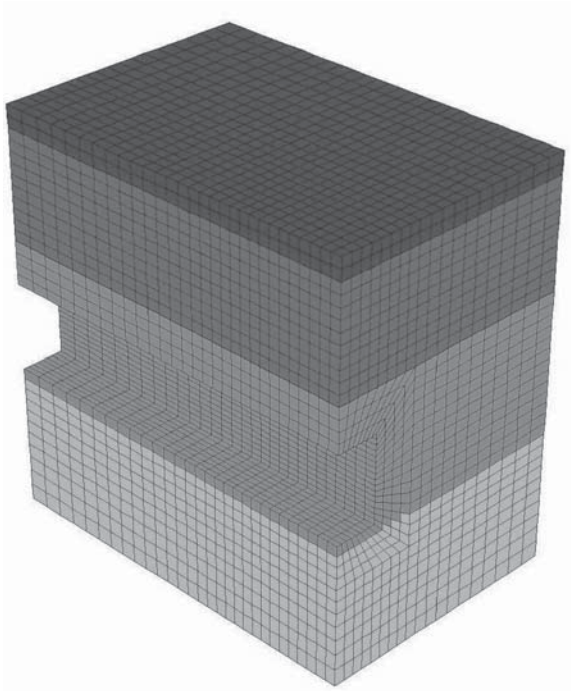

Figure 2-11. Concrete box model for 96″ deep, 48″ × 48″ cross section (shading indicates soil modulus).

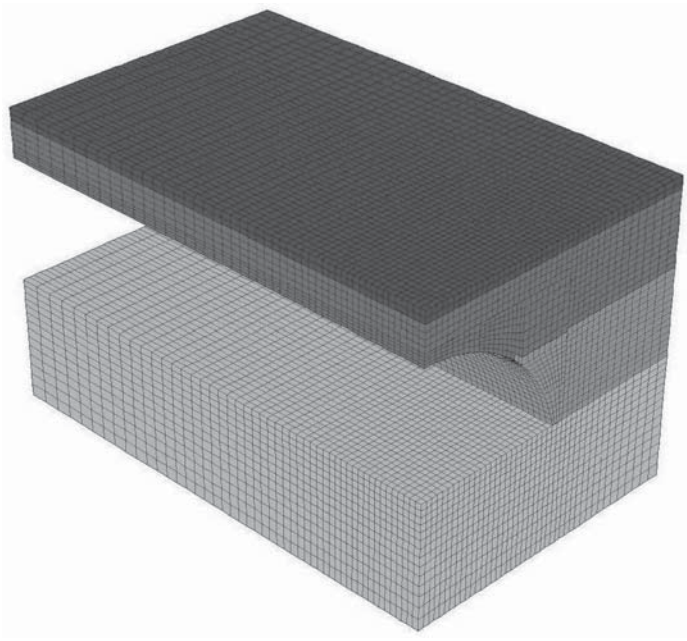

Figure 2-12. Concrete arch model for 48″ deep, 25.4 ft × 10 ft cross section (shading indicates soil modulus).

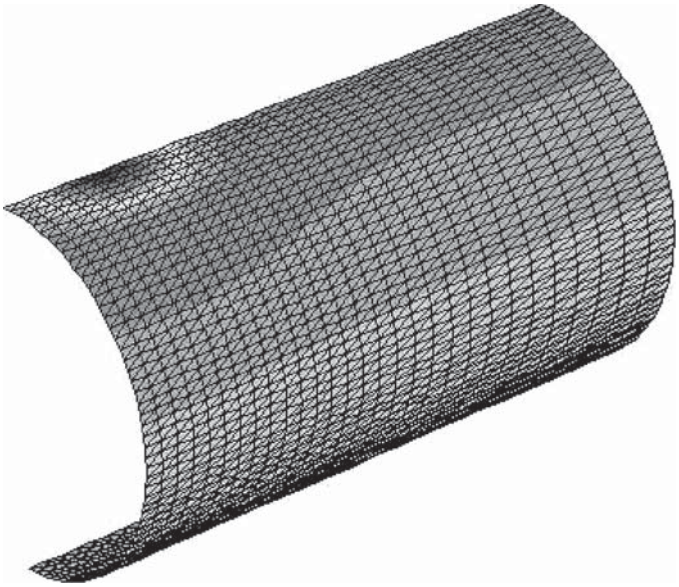

Figure 2-13. Typical structural model for a large round pipe (different shadings indicate the normal pressure on the culvert).

placement and the shading indicates vertical stress. Table 2-17 illustrates the range of mesh sizes.

2.3 Development of SDEs

Current AASHTO procedures for simplified design of culverts vary with the type of pipe and the performance limits that must be evaluated. For example, simplified design of concrete culverts is based on the indirect method where a three-edge bearing load that produces an equivalent bending moment to the in-ground loads is determined, while corrugated metal pipe is evaluated solely on the basis of compressive thrust due to earth load. The proposed SDEs presented in this section were

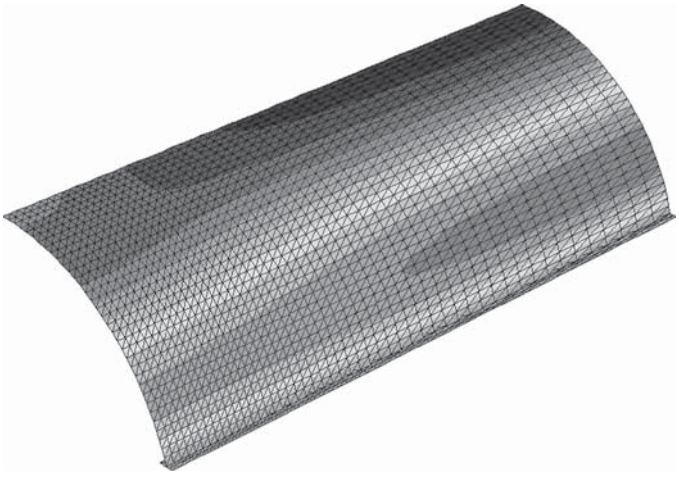

Figure 2-14. Typical structural model for an arch (shading indicates the normal pressure on the culvert).

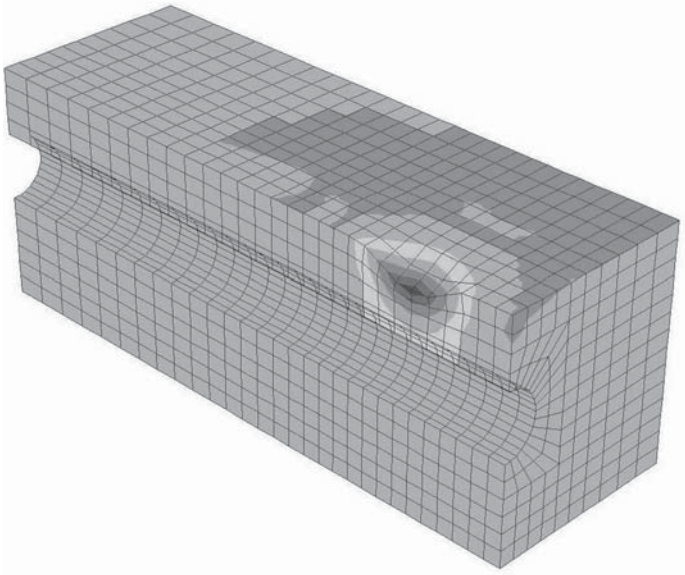

Figure 2-15. Typical live load application, showing deformed grid (that represents vertical stress).

developed to provide the data necessary to consider live load effects in the context of those existing design methods. Thus, the research team first reviews the existing simplified design criteria and then presents analysis of the computer model data in the context of those criteria.

In analyzing the data to develop new simplified procedures, the research team focused on procedures that emphasize simplicity and an actual physical process by which live loads attenuate with increasing depth of fill. The research team avoided simple curve fitting and, where some effects were considered minor, opted for simple equation forms broadly applicable to many types of culverts, rather than greater accuracy that would require the introduction of more coefficients. The research team took this approach because the goal of the project was simplified design procedures and because computer models are increasingly generally available for situations where greater precision is required.

2.3.1 Current Simplified Culvert Design

This section reviews the limit states for culvert types included in the AASHTO specifications and the simplified procedures used to develop designs. Guidelines were developed for analyzing all types of culverts in 2D finite-element

Table 2-17. Range of mesh sizes.

Item	Typical Small Model	Typical Large Model
Number of grid points	2040	186894
Number of zones	1740	170607
Number of structural elements	696	5194
Numbers of structural nodes	390	2862

Table 2-18. Relative stiffness parameters for typical culvert pipe.

Stiffness Parameter	Concrete	Corrugated Metal	Thermoplastic
EI	Stiff	Flexible	Flexible
EA	Stiff	Stiff	Flexible

programs. Design of culverts with finite-element analyses requires a pressure distribution at the ground surface that reduces the total applied load to account for the live load attenuation in the third dimension that is not modeled. This historically has been completed using AASHTO distributions to reduce the live load to the magnitude at the depth of the pipe crown.

The pipe properties that affect pipe-soil interaction are the flexural stiffness, EI, and the axial stiffness, EA (see Table 2-18). Concrete, corrugated metal, and thermoplastic pipe all have different relative combinations of these parameters and thus, the behavior is different for each type of pipe:

- **Concrete pipe.** Concrete pipe carries live (and earth) loads primarily with bending moments because of the high flexural stiffness. The high hoop stiffness also causes the pipe to have high contact pressure.
- **Corrugated metal pipe.** Corrugated metal pipe has relatively low flexural stiffness that allows these pipes to deflect away from load. However, loads are resisted through the high axial stiffness, resulting in high contact pressures and high thrust forces.
- **Thermoplastic pipe.** Thermoplastic pipes (and corrugated polyethylene in particular) have low flexural and low hoop stiffness. The parametric study showed that the pipe moves away from live loads both through flexure and circumferential shortening. This extra motion of the pipe relative to both concrete and corrugated metal results in higher soil strains and, as a result, a significant portion of the load arches around the pipe.

As a result of these three different behaviors, the development of the SDEs resulted in different expressions for each type of pipe. SDEs were first developed for reinforced concrete pipe and box sections, based on McGrath, Liepins, and Beaver (2005), which established distribution widths for box sections with 0 to 2 feet of soil cover. The 2005 study demonstrated that live loads on rigid structures distribute further longitudinally in culverts with longer spans. This result is logical given that a longer span can undergo larger deformations, allowing the redistribution. A value of 0.06 times the span was added to the distribution width to account for this effect. Given that the same effect was noted in more deeply buried box culverts, the use of the term is also applied at greater depths. A further benefit of this term is that the proposed distribution equations produce the same result at 2-ft depth, whether computed using the strip equations for depths of 2 feet or less or the proposed equations for depths of 2 feet or greater.

2.3.1.1 Standard Versus LRFD Specifications

In developing the proposed design equations, the research team compared the proposed calculation procedures and the methods in the current AASHTO LRFD and Standard Specifications. The comparisons revealed two significant differences between the specifications that must be addressed:

- **Multiple presence.** For a single loaded lane, the LRFD Specification includes a 20% increase in service load to account for the likelihood of overloaded trucks. However, because of a reduced load factor in the LRFD code, the factored loads in the two codes are approximately the same. The code comparisons below are on the basis of service loads. To provide a common basis for comparison, loads computed using the Standard Specification are increased by 20%.
- **Impact.** The LRFD Specification uses a linearly variable impact factor reducing from 1.33 at a 0 ft depth to 1.00 at a depth of 8 feet, while the Standard Specifications use a stepwise impact factor that decreases from 1.3 at 0 depth of fill to 1.0 at a depth of 3 feet. The two methods are compared in Figure 2-16, which shows that the LRFD Specifications are more conservative by about 15 to 20% at depths between 2 and 4 feet. This is addressed in the compar-

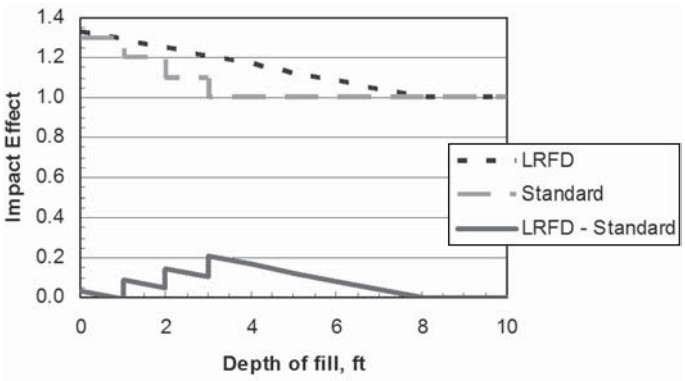

Figure 2-16. Comparison of LRFD and standard specification impact factors.

isons below by increasing the calculated value from the Standard Code.

2.3.1.2 Concrete Culverts

Concrete culverts fall into three categories: pipe, box sections, and arches. Concrete box sections and arches are all designed with either finite-element analyses or computer analyses of a frame model subjected to an applied pressure distribution. Thus, a simplified design procedure for box and arch sections requires development of an appropriate pressure distribution. AASHTO allows design of concrete pipe by two methods: the direct design procedures of the SIDD method and the traditional indirect design procedures. The direct design procedures require a pressure distribution that can be used in conjunction with the Heger distribution developed for earth loads. The indirect procedures require a bedding factor that relates the reinforcing requirements to resist live loads in ground to the reinforcing requirements to pass the three-edge bearing test.

2.3.1.3 Metal Culverts

Metal culverts fall into the categories of pipe (including ellipses and closed bottom arches) and long-spans. Metal pipe is designed solely for compressive thrust as are long-span culverts. *NCHRP Report 473* (McGrath et al., 2002) recommended that long-span metal culverts be designed for moment as well as thrust. The research team analyzed the moment data and did not develop an improved recommendation relative to *NCHRP Report 473,* thus no equation is proposed for moment.

2.3.1.4 Thermoplastic Culverts

Although only one category of culvert is made of thermoplastic materials, these culverts have the most detailed design procedures of the types included in current AASHTO Specifications. Thermoplastic culverts are evaluated for thrust, flexure, and deflection. Current AASHTO Specifications for thermoplastic pipe include polyethylene (PE) and PVC.

2.3.2 Evaluation of Computer Study Data

Proposed simplified design methods were developed from the numerical modeling reported in the preceding section. The approach taken was to consider concrete box culverts first, because box sections have flat top slabs which afford an opportunity to evaluate not only the design forces but the vertical soil stresses on the top slab. Normal pressures on round or elliptical culverts are more difficult to interpret. The findings from box sections were then used as a basis to investigate the other culverts.

2.3.2.1 Concrete Box Sections

Vertical Soil Pressure on the Top Slab. Figure 2-17 presents the vertical soil pressure resulting from live load alone on the cross section of 48-in.-span by 48-in.-rise and 96-in.-span by 96-in.-rise box sections at 24 in. depth of fill directly under the load center. The x-axis is in degrees from the center of the box sections so that the edges of the top slab and bottom slabs are at +45 and –45 degrees, respectively. The various curves represent variations in soil type.

Figure 2-17 shows that the peak vertical pressures are approximately the same and that soil type does not have any significant affect on the distribution. In the figure, the live load distribution on the 48-in.-span box sections has spread to the edge of the boxes, while it is still clearly contained on the surface of the 96-in.-span sections. Distributions for other depths of fill are similar, except at shallower depths of fill the load is within the edges of the top slab for both box dimensions and for deeper fills the load has spread past the edges of the top slab for both box sizes.

The mean load was calculated for all spans and depths of fill as the total force applied to the culvert for a 1-inch length directly under the load. The computed values were compared to the applied soil pressure using the current AASHTO distribution, calculated using Equation 5 (and shown in Table 2-19):

$$LL_{pres} = \frac{LL}{\left(w_t + LLDF \cdot H\right) \cdot \left(l_t + LLDF \cdot H\right)} \quad (2)$$

where

LL_{pres} is the live load pressure at depth H, psi
LL is the total live load applied at surface, lb

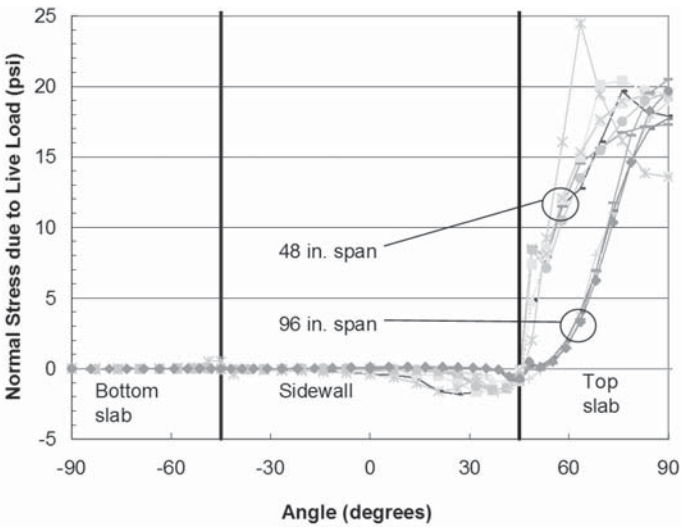

Note: Soil types not differentiated in the figure as there were no substantial differences between the various gradations and compaction levels.

Figure 2-17. Vertical live load soil pressure on box sections, 24 in. cover.

Table 2-19. Comparison of model and calculated load on culvert.

Depth	Model live load	Coeff. of variation	Calc. live load	Live load delta (1)	Total load delta (2)
48 in. Span Box Sections					
in.	lbs/in.	%	lbs/in.	%	%
12	576	4.4%	520	-9.8%	-9.0%
24	382	4.6%	318	-16.7%	-13.0%
48	153	3.9%	135	-11.7%	-4.8%
72	87	3.6%	74	-14.3%	-3.0%
96	57	3.4%	46	-20.1%	-2.3%
144	34	3.0%	25	-28.6%	-1.4%
96 in. Span Box Sections					
in.	lbs/in.	%	lbs/in.	%	%
12	582	4.3%	520	-10.7%	-9.0%
24	381	3.7%	318	-16.4%	-10.4%
48	190	1.2%	175	-7.7%	-2.3%
96	84	3.7%	90	7.1%	0.6%

Notes:
1. Live load delta is the variation between the calculated live load and the model live load.
2. Total load delta is the variation between the calculated and model total load, where the total load is the live load plus the weight of soil directly over the box section, assuming the soil prism load and a soil density of 120 pcf.

w_t is the width of tire (or axle length plus tire width at depths where wheels interact), in.
l_t is the length of tire parallel to span of culvert, in.
LLDF is the rate of increase of load spread with increasing depth of fill, taken as 1.15
H is the depth of fill, in.

Table 2-19 indicates the following:

- Within any size and depth of culvert, the coefficient of variation is small confirming that soil type has very little effect on the load distribution.
- The variation between the model load and the calculated live load is about 10% at a depth of 24 inches and increases with depth for the 48-in. culverts and decreases with depth for the 96-in. culverts.
- When the total load is considered by adding the weight of soil, the variation between the model live load and the calculated live load is a maximum at a depth of 24 inches and decreases to less than 5 percent for all depths 4 feet and greater.

The same analysis completed for an *LLDF* of 1.0 shows a better fit to the data, with the live load delta less than 5 percent except for the deeper fills and the total load delta less than 3 percent at all depths. However, this analysis only evaluates the contact pressure. The final distribution width must also consider the further distribution of load within box sections due to the structural stiffness of the slabs. This is addressed in the following section.

Bending Moment in Box Sections. To analyze the bending moments from the computer study, values were taken at midspan, top slab for the maximum positive moments, and at the tip of the top haunch in the sidewall which is the typical location of the design negative moment. Table 2-20 presents the bending moments averaged for all soil types, and, as for the live load normal pressures, indicates that soil type is not a fac-

Table 2-20. Computer model bending moments.

Depth (ft)	Top slab, midspan		Sidewall, tip of top haunch	
	Bending moment (in.-lb/in.)	Coeff. of variation (percent)	Bending moment (in.-lb/in.)	Coeff. of variation (percent)
48 in. Span Box Sections				
12	2414	3.5%	-1208	2.8%
24	1383	5.1%	-849	5.8%
48	584	4.7%	-424	7.6%
72	341	3.5%	-250	3.9%
96	227	2.5%	-166	4.4%
144	135	2.5%	-99	2.8%
96 in. Span Box Sections				
12	3251	3.0%	-1003	1.9%
24	2060	3.6%	-884	3.7%
48	997	1.6%	-600	1.6%
96	422	4.2%	-301	4.1%

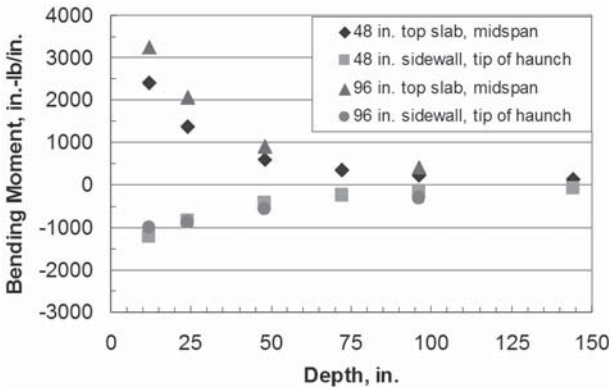

Figure 2-18. Box culvert bending moments vs. depth of fill.

tor in live load distribution onto box sections. The bending moments versus depth of fill are shown in Figure 2-18.

To evaluate the model bending moments relative to current practice, the research team compared the values with the bending moments from the 2D frame analysis program BOXCAR, which was used to generate reinforcing designs for current ASTM and AASHTO box section standards. The BOXCAR analyses were completed for the same load as the computer models (i.e., LRFD design truck [32,000-lb axle load], LRFD impact, and 1.2 multiple presence factor). The LLDF in the BOXCAR analyses was taken as 1.15. Table 2-21 presents the ratios of the BOXCAR bending moments to the computer model bending moments and suggests that current practice is very conservative, especially for the 96 in. span culverts. The comparison is only made for depths of fill 24 inches and greater because AASHTO uses a strip width approach to live load distribution for box sections under depths of fill less than 24 inches which was outside the scope of this project.

Table 2-21 indicates that the conservatism increases with the span, which is reasonable as longer span structures are somewhat more flexible and should distribute loads longitudinally to a greater extent. There are several issues to be considered in increasing load distribution widths as much as the ratios suggested in Table 2-21.

Table 2-21. Comparison of 2D and computer model bending moments.

Depth	BOXCAR/Table 20 bending moments	
	Top slab, midspan	Sidewall, tip of top haunch
48 in. Span Culverts		
24	185%	196%
48	171%	151%
96	149%	130%
96 in. Span Culverts		
24	328%	424%
48	361%	362%
96	313%	268%

- The analysis assumes equal stiffness in both the span and longitudinal directions of the culvert slabs. Although this is typical, cracking parallel to the culvert span can decrease the distribution length slightly.
- Box culverts typically are designed for single lane loadings. Under current distribution widths, the use of a multiple presence factor of 1.2 ensures conservative designs for multilane loadings. Increasing the distribution width would result in overlapping lane loads such that multiple lane loadings would control design, thus, the reduction in design load would not be realized to the extent suggested in Table 2-21.
- The computer models show the entire vertical live load being carried through vertical shear stresses at the sides of the box sections. There is no vertical reaction on the bottom slabs. We remain uncertain if this would be the case for multiple live load cycles. A distributed load on the bottom slab would cause some increase in the top slab moments.
- Precast box sections are rarely longer than 8 feet. Thus, if the load spreading results from internal forces within the culvert, then the spread will be limited.

For the time being, the research team is reluctant to increase the distribution for live loads to box sections significantly greater than allowed by the current LRFD specifications. Thus, the research team proposes the following live load distribution equation for box sections:

$$LL_{pres} = \frac{LL}{(w_t + LLDF \cdot H + 0.06 \cdot D_i) \cdot (l_t + LLDF \cdot H)} \quad (3)$$

where

LL_{pres} is the live load pressure at depth H, psi
LL is the total live load applied at surface, lb
w_t is the width of tire (or axle length plus tire width at depths where wheels interact), in.
l_t is the length of tire parallel to span of culvert, in.
$LLDF$ is the rate of load spread with increasing depth of fill, taken as 1.15 for box culverts in all soil types
H is the depth of fill, in.
D_i is the inside span of the culvert, in.

The term $0.06 \cdot D_i$ allows for a modest increase in the distribution width. The longitudinal distribution width at 2 ft of fill essentially matches the longitudinal distribution for slabs of box sections given in the current LRFD Specifications. Equation 6 increases the longitudinal distribution length and sets the distribution perpendicular to the span slightly longer than in current practice.

Table 2-22. Comparison of proposed and current live loads on 8-ft-span box culvert.

Depth* (ft)	Proposed (lb/ft)	Current		Ratios	
		LRFD (lb/ft)	Modified Stnd** (lb/ft)	Proposed /LRFD	Proposed / Modified Stnd
1	5523	5523	5523	1.00	1.00
1.001	5523	5523	5523	1.00	1.00
1.999	5347	5347	5347	1.00	1.00
2	5387	6038	6844	0.89	0.79
2.001	5385	6036	6840	0.89	0.79
2.999	4139	4528	4012	0.91	1.03
3	4138	4526	4412	0.91	0.94
4	3510	3647	3442	0.96	1.02
5	3105	3216	2675	0.97	1.16
6	2763	2854	1920	0.97	1.44
7	2223	2291	1431	0.97	1.55
8	1765	1815	1097	0.97	1.61
9	1485	1525	949	0.97	1.56
10	1268	1300	830	0.98	1.53
11	1096	1121	732	0.98	1.50
12	978	1000	650	0.98	1.50

*Incremental depths included to show steps in load due to stepwise function for Standard Specification impact

**Modified to negate differences in multiple presence and impact (= actual Standard * 1.2* (LRFD impact/Standard impact)

Comparison with Past Practice. The proposed design method for box culverts can be evaluated by calculating the applied vertical load on the sections and comparing it with the applied load using the current AASHTO Standard and LRFD specifications. The comparison is made for service loads; however, to make the design service loads equivalent, the loads computed according to the Standard Specifications were increased 20 percent to account for the multiple presence factor included in the LRFD Specifications and was modified for the difference in impact factor between the two specifications. Table 2-22 presents the results of the calculations for an 8-ft-span culvert; results are similar for all sizes. Table 2-22 shows the following:

- For depths less than 2 feet of fill, there is no change in the load calculation. The strip width for box section with less than 2 feet of fill was recently addressed by AASHTO.
- There is no significant jump in the proposed load at 2 feet where the calculation method changes from the strip load to the distributed load.
- At a depth of 2 feet, the proposed load calculation is about 10 percent less than current LRFD because of the inclusion of the term "0.06 Span." The drop from the current Standard Specification is more significant because the Standard Specification conservatively applies the surface load as a point load.
- At depths greater than 2 feet, the proposed calculation method is reduced slightly from the current LRFD.
- At depths greater than about 2 feet, the proposed calculation is approximately equal to the Standard Specification for depths from 3 to 4 feet and then increases to about 1.5 times the Standard Specification load at greater depths.

A comparison calculation shows that the load on a single lane with multiple presence factor of 1.2 is larger than in a multiple lane loading for all depths at which live loads are significant. Given that the more liberal distribution of the Standard Specification would result in the two-lane condition controlling, the research team recommends the narrower distribution in part to keep the single-lane condition controlling the design.

2.3.2.2 Concrete Arch Structures

An analysis of concrete arches indicates that the same distribution width proposed for box sections can be used for analyzing reinforced concrete arch sections. A similar finding was made in *NCHRP Report 473* (McGrath et al., 2002) on long-span culverts.

2.3.2.3 Concrete Pipe

Thrust. In evaluating live load distribution onto concrete pipe, the research team first looked at the peak and springline thrusts. Figures 2-19 through 2-21 compare the model values of springline and peak thrusts with the thrusts based on Equation 6. The curve "Calc'd-Crown" was calculated from Equation 6 using a depth of fill to the pipe crown and the curve "Calc'd-Springline" was computed using the depth of fill to the springline.

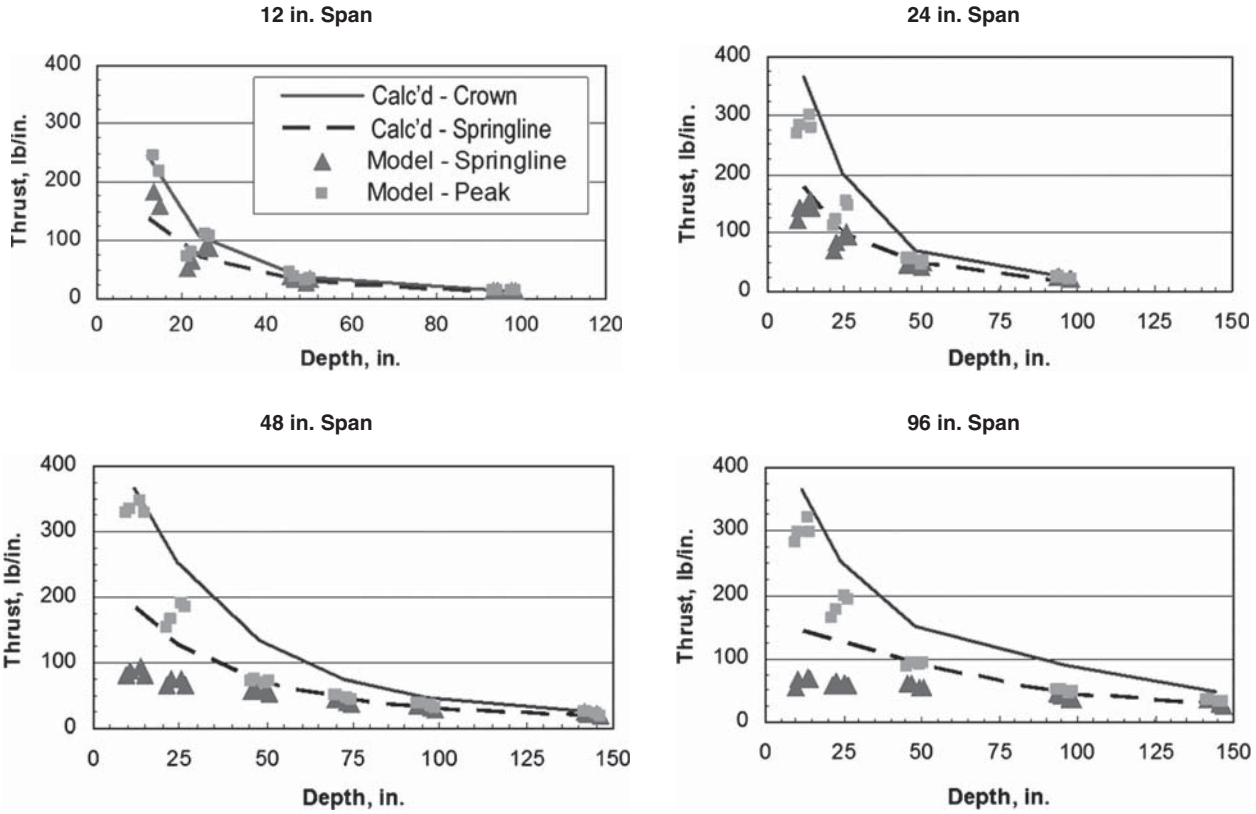

Figure 2-19. Comparison of concrete pipe model thrust with eqn (6)-based values.

Figures 2-19 through 2-21 show that peak thrust is reasonably predicted for all spans and depths of fill by using Equation 6 with the depth of fill taken to the top of the pipe. The springline thrust is reasonably predicted for the 12-in. and 24-in.-span pipe using Equation 6, but is somewhat conservative for the 48-in. and 96-in.-span pipe under shallow fill. These figures also show that the soil type has very little influence on the load distribution for concrete pipe, as was the case with box sections.

The research team investigated the effect of improving the quality of prediction for peak thrust by modifying the LLDF based on diameter and developed the following equations:

$$\text{For } D_i \le 24in \qquad LLDF_{cp} = 1.15 \tag{4}$$

$$\text{For } 24in < D_i \le 96in \qquad LLDF_{cp} = 0.00833 \cdot D_i + 0.95 \tag{5}$$

$$\text{For } D_i > 96in \qquad LLDF_{cp} = 1.75 \tag{6}$$

where

$LLDF_{cp}$ is the live load distribution factor for concrete pipe
D_i is the inside span of the culvert, in.

These equations increase the LLDF for pipe diameters larger than 24 inches, giving a value of 1.35 for 48-in.-diameter pipe

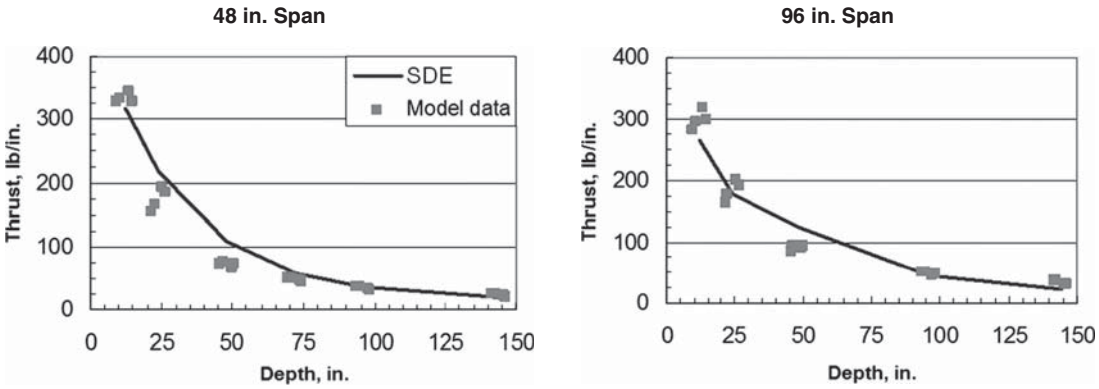

Figure 2-20. Comparison of proposed SDE with model peak thrust in concrete pipe.

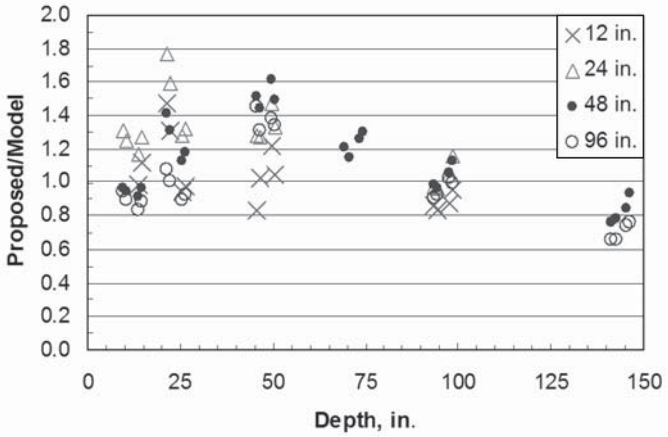

Figure 2-21. Ratios of calculated to computer model thrusts.

and 1.75 for pipe with diameters of 96 inches and larger. The upper limitation on LLDF is imposed because there is prior successful experience with using a distribution factor of 1.75 for design.

Figure 2-20 compares the model data with the modified form of Equation 6 for 48-in.-diameter concrete pipe and Figure 2-21 does the same for 96-in.-diameter concrete pipe. The figure shows a better match—ratios of calculated thrust from the modified equation to model thrust average 1.00 with a standard deviation of 0.22. This compares with an average of 1.14 and a standard deviation of 0.29 for thrusts calculated with equations above. The ratios between the proposed model-predicted peak thrusts and the computer model values are presented in Figure 2-21.

Bedding Factor. Once the live load was determined using the equation above, a bedding factor was required to calculate the required pipe capacity in the indirect design method. The philosophy of indirect design is to size reinforcement to pass the three-edge bearing test under a load that produces the same peak positive bending moment as imposed by the field conditions. The bedding factor is the ratio of the field load to the three-edge bearing load that produces the same bending moment. The bedding factor can thus be calculated as the ratio of the three-edge bearing moment due to the field load to the actual field moment. For earth loads, the bedding factors developed for the current AASHTO Specifications computed a reduced effective field moment to account for the presence of lateral thrust. The approach is presented in ACPA's *Concrete Pipe Design Manual* (1998). In this study, the research team did not consider modifications due to thrust because the location of peak thrust was not necessarily at the crown or invert where the peak moment would occur, and the live load also generated very little thrust as a result of lateral soil pressure. Thus, the research team computed the bedding factor using the simple equations:

$$B_f = \frac{M_{TEB}}{M_{FLD}} \tag{7}$$

$$M_{TEB} = 0.318 \cdot N_{FLD}\left(D_i + t\right) \tag{8}$$

where

B_f is the bedding factor
M_{TEB} is the bending moment in the three-edge bearing test, in.-lb/in.
M_{FLD} is the field bending moment after reduction for compressive thrust, in.-lb/in.
N_{FLD} is the peak thrust in the field, lb/in.
D_i is the inside pipe diameter, in.
t is the pipe wall thickness, in.

Using this approach, the research team computed the bedding factors shown in Figure 2-22 using the peak thrusts and peak positive bending moments from the computer study. In completing these calculations, the research team did not consider installation type as a factor because the peak moments occur in the crown area which is not significantly affected by installation condition. This is consistent with current AASHTO practice. Figure 2-22 shows a trend of bedding factors increasing as the depth of fill goes from 12 to 24 inches and then decreasing with further increases in depth of fill.

The general trend of decreasing bedding factor with increasing depth of fill is the reverse of the trend in the current LRFD live load bedding factors for concrete pipe, which were developed based on 2D analyses. However, both the computer model and the current AASHTO LRFD trend toward a bedding factor of 2.2 for deeply buried pipe. The reason for this change in trend is simply in the method of calculation. In this study, the peak compressive thrust was used as the basis for computing the bedding factor, because there was less variability in predicting the peak thrust than the springline thrust.

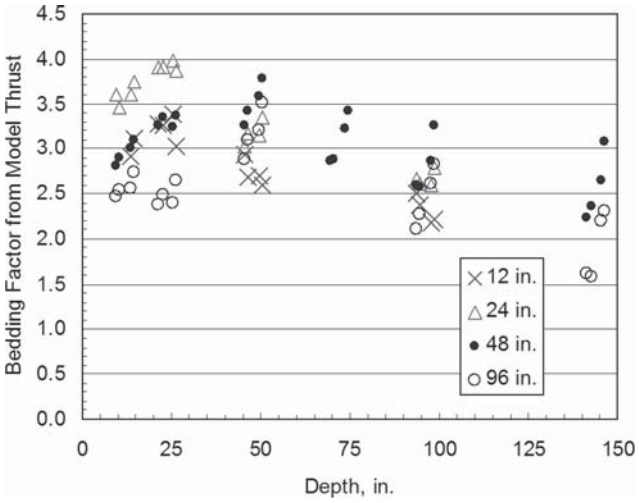

Figure 2-22. Bedding factors computed from computer study.

Table 2-23. Input variables for calculating live load on pipe.

Parameter	Calculation Method			
	Proposed	LRFD	Standard	ACPA
Footprint (in x in)	10 x 20	10 x 20	0 x 0	10 x 20
LLDF	1.15 to 1.75	1.15 (granular soils)	1.75	1.75
Elevation of calculation	top of pipe	top of pipe	top of pipe	0.75 D_i below top of pipe
Bedding factor	2.2	1.1 to 2.2	1.1 to 2.2	1.7 (user option)

The current AASHTO live load bedding factors were computed using the springline thrusts. Given that the AASHTO analyses were based on 2D modeling, the springline thrusts would be higher than the 3D values, thus very different bedding factors from current practice would be expected, regardless of the method of calculation.

The research team proposes a constant bedding factor of 2.2 for all installation conditions, diameters, and depths of fill. This is a lower bound for all conditions and, as seen in the next section, still results in a significantly reduced load on concrete pipe due to the change in load calculation.

Comparison with Past and Current Practice. The variation in required D-load to carry live load is quite variable between the proposed method and current practice. For concrete pipe the research team includes a method from the ACPA Handbook to complete the comparison. Variations in the inputs for the procedure are summarized in Table 2-23. The results of the calculations are presented in Table 2-24 and Table 2-25 for 4-ft-diameter and 12-ft-diameter pipe, respectively.

Table 2-24 and Table 2-25 show a wide discrepancy in current practice. The Standard Specification is generally the most conservative at shallow depths due to the concentrated surface load but is less conservative with depth due to the larger LLDF of 1.75. The ACPA method is the least conservative, but represents a procedure that has been used for many years.

2.3.2.4 Corrugated Metal Pipe

Thrust. Initial calculations for evaluating peak thrust in corrugated metal pipe were completed using the live load pressure computed from Equation 6, multiplied by one-half the smaller of the load spread parallel to the span direction or the pipe diameter. Peak thrust is calculated as

$$N_{peak} = LL_{pres} \cdot \left\{0.5 \cdot \min\left(D_i; l_t + LLDF \cdot H\right)\right\} \quad (9)$$

where

N_{peak} is the estimated peak thrust, lb/in.
LL_{pres} is the nominal live load pressure, psi
l_t is the length of tire parallel to span of culvert, in.
LLDF is the rate of load spread with increasing depth of fill, 1.15

Table 2-24. Comparison of proposed live load D-load on 4-ft-diameter concrete pipe with past practice.

Depth (ft)	Proposed (B_f = 2.2) (lb/ft/ft)	Current Practice			Ratios		
		LRFD (lb/ft/ft)	Modified Stnd* (lb/ft/ft)	Modified ACPA Hndbk* (B_f = 1.7) (lb/ft/ft)	Proposed/ LRFD	Proposed/ Modified Standard	Proposed/ Modified ACPA Hndbk
1	863	1464	2357	537	0.59	0.37	1.61
2	591	755	856	492	0.78	0.69	1.20
3	437	514	462	400	0.85	0.95	1.09
4	296	369	270	266	0.80	1.10	1.11
5	213	268	183	186	0.79	1.16	1.14
6	160	203	131	136	0.79	1.22	1.17
7	123	157	99	102	0.78	1.25	1.20
8	97	125	76	80	0.78	1.28	1.21
9	81	105	65	71	0.77	1.25	1.14
10	70	89	56	64	0.79	1.24	1.10
11	62	77	50	58	0.81	1.23	1.08
12	56	69	44	42	0.81	1.26	1.09

*Standard and ACPA modified to match impact and multiple presence of LRFD

Table 2-25. Comparison of proposed live load D-load on 12-ft diameter concrete pipe with past practice.

Depth (ft)	Proposed (B_f = 2.2) (lb/ft/ft)	Current Practice			Ratios		
		LRFD (lb/ft/ft)	Modified Stnd* (lb/ft/ft)	Modified ACPA Hndbk* (B_f = 1.7) (lb/ft/ft)	Proposed/ LRFD	Proposed/ Modified Standard	Proposed/ Modified ACPA Hndbk
1	227	666	1080	100	0.34	0.21	2.27
2	154	387	422	95	0.40	0.36	1.62
3	129	269	217	101	0.48	0.59	1.27
4	110	203	164	89	0.54	0.67	1.23
5	95	149	120	80	0.64	0.79	1.19
6	83	119	97	70	0.70	0.85	1.18
7	73	96	79	62	0.76	0.92	1.17
8	64	86	73	54	0.74	0.87	1.19
9	56	81	64	49	0.69	0.88	1.14
10	49	76	55	44	0.64	0.89	1.10
11	44	72	49	41	0.61	0.89	1.08
12	39	67	43	37	0.58	0.90	1.05

*Standard and ACPA modified to match impact and multiple presence of LRFD

H is the depth of fill, in.
D_i is the inside span of the culvert, in.

Figures 2-23 and 2-24 show reasonable agreement between the computer model thrusts and the Equation 6 predicted thrusts, except for the large-diameter pipe under shallow conditions. These pipes, with low bending stiffness, probably develop higher thrusts to carry the load as a membrane force rather than in flexure.

Also, analysis of the live load spread versus depth [$l_t + LLDF \cdot H$] indicates that for these pipes the live load has not spread to the width of the crown, thus, there is probably a concentration effect. The following factor was introduced to account for this effect and a slight modification for the 12-in.-diameter pipes.

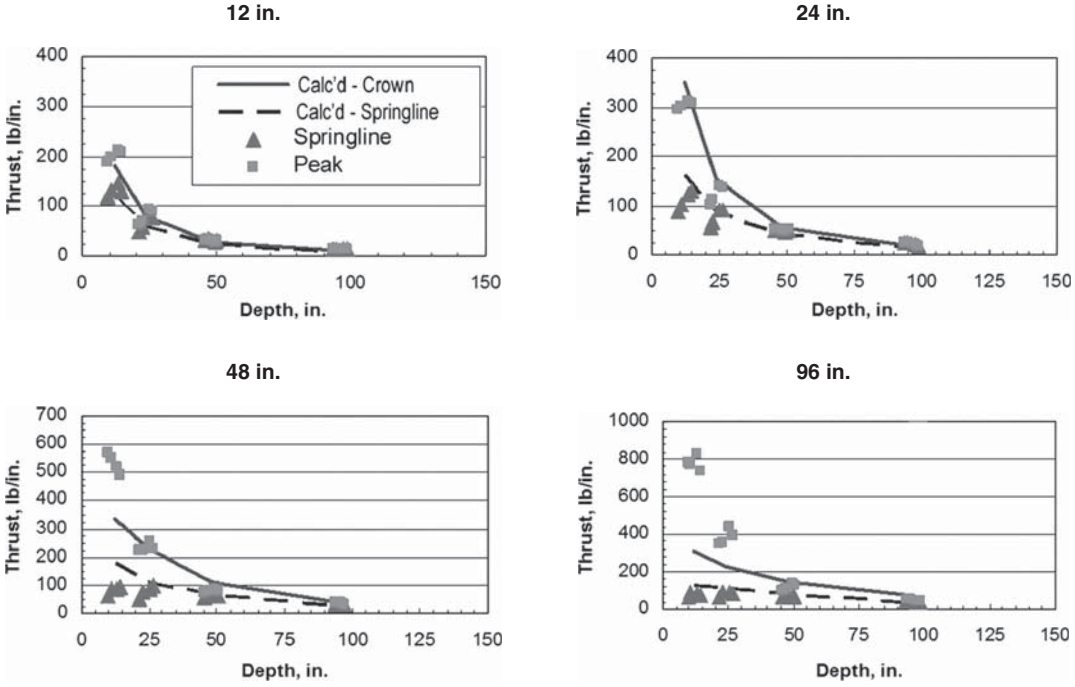

Figure 2-23. Comparison of thrusts between LRFD and computer model for metal pipe.

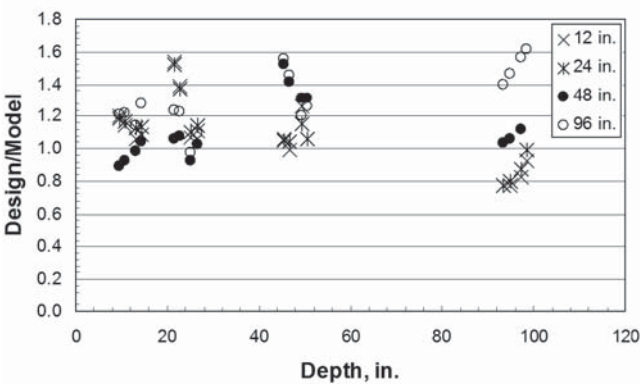

Figure 2-24. Peak thrust ratios for metal pipe—proposed design equation.

$$N_{peak} = F_1 \cdot LL_{pres} \cdot \{0.5 \cdot \min(D_i; l_t + LLDF \cdot H)\} \quad (10)$$

$$F_1 = 0.75 \cdot \frac{D_i}{l_t + LLDF \cdot H} \geq F_{1-Lim} \quad (11)$$

$$F_{1-Lim} = \frac{15}{D_t} \quad \text{subject to:} \quad F_{1-Lim} > 1.0 \quad (12)$$

where

$LL_{pres} \cdot \{0.5 \cdot \min(D_i; l_t + LLDF \cdot H)\}$ is the peak thrust prior to correction, from Eq. 12
l_t is the length of tire parallel to span of culvert, in.
$LLDF$ is the rate of load spread with increasing depth of fill, taken as 1.15
H is the depth of fill, in.
D_i is the inside span of the culvert, in.
F_1 is the correction factor
F_{1-Lim} is the limit value for F_1

With this modification, the ratios of the calculated thrust to the computer model thrust are shown in Figure 2-24. The ratios have a mean value of 1.15 and a standard deviation of 0.21. The only values notably less than 1.0 are the small-diameter pipe under deep fills, where the live load is a trivial component of the total load.

Comparison with Current Practice. Thrust forces computed with the proposed equation are compared with thrust forces computed using the procedures of the LRFD and Standard Specifications in Table 2-26 and Table 2-27.

Table 2-26 and Table 2-27 indicate that metal culverts develop a larger thrust force under shallow fills than predicted by current practice. This becomes more pronounced as the pipe diameter increases. For 4-ft-diameter pipe, this thrust increase exists only at the shallowest depth of fill, 1 ft. For 12-ft-diameter pipe, however, the increase runs to a depth of 6 ft. This finding is consistent with *NCHRP Report 473* (McGrath et al., 2002) results for long-span metal culverts.

2.3.2.5 Corrugated Metal Arches

Predicted thrusts computed using the live load pressure of Equation 6 are compared with the model thrusts in Figure 2-25. Similar to metal pipe, the thrusts show a high maximum thrust at shallow depths relative to that predicted by Equation 6.

Thrusts in corrugated metal arches were studied in *NCHRP Report 473*—a modifying coefficient using the same form was developed:

$$F_{m.arch} = \frac{0.54 \cdot Span}{w_t + LLDF \cdot H + 0.03 \cdot Span} \quad (13)$$

where

$F_{m.arch}$ is the thrust modifier for long-span metal arches
$Span$ is the culvert span, in.
$LLDF$ is the live load distribution factor, 1.15
H is the depth of fill, in.
w_t is the width of tire (or axle length plus tire width at depths where wheels interact), in.

Table 2-26. Comparison of proposed and existing equations for live load thrust in 4-ft-diameter metal pipe.

Depth (ft)	Thrust from Proposed SDE (lb/ft)	Current		Ratios	
		LRFD (lb/ft)	Modified Standard (lb/ft)	Proposed/ LRFD	Proposed/ Modified Standard
1	6122	4392	7070	1.39	0.87
2	2847	3019	3422	0.94	0.83
3	2019	2113	1681	0.96	1.20
4	1317	1342	983	0.98	1.34
5	960	977	669	0.98	1.44
6	726	738	479	0.98	1.51
7	564	573	357	0.98	1.58
8	447	454	275	0.98	1.63
9	376	381	238	0.99	1.58
10	321	325	208	0.99	1.55
11	277	280	182	0.99	1.52
12	247	250	162	0.99	1.52

Table 2-27. Comparison of proposed and existing equations for live load thrust in 12-ft-diameter metal pipe.

Depth (ft)	Thrust from Proposed SDE (lb/ft)	Current		Ratios	
		LRFD (lb/ft)	Modified Standard (lb/ft)	Proposed/ LRFD	Proposed/ Modified Standard
1	15874	4392	7070	3.61	2.25
2	7340	3019	3422	2.43	2.15
3	4169	2263	2206	1.84	1.89
4	2853	1823	1721	1.57	1.66
5	2087	1608	1463	1.30	1.43
6	1582	1427	1260	1.11	1.26
7	1232	1272	1073	0.97	1.15
8	1092	1138	823	0.96	1.33
9	1025	1066	712	0.96	1.44
10	939	975	623	0.96	1.51
11	812	841	548	0.97	1.48
12	725	750	487	0.97	1.49

The proposed design equation is

$$N_{peak.m.arch} = F_{m.arch} \cdot LL_{pres} \cdot \{0.5 \cdot \min(D_i; l_t + LLDF \cdot H)\} \quad (14)$$

The peak thrusts computed with Equation 17 were compared to model thrusts. The ratios of the computed values to the model values are shown in Figure 2-26. The mean value of the ratios is 1.10 with a standard deviation of 0.15. The two values that plot below 0.9 were culverts embedded in clay backfill which is not allowed by AASHTO for long-span culverts.

2.3.2.6 Thermoplastic Pipe (Profile Wall)

Thrust. Analysis of thrust for thermoplastic pipe (profile wall), using Equation 13, is presented in Figures 2-27 through 2-30. The comparison of the calculated values with the computer model thrusts is similar to the other types of pipe except that there is a distinct effect of soil type as shown by the vertical scatter within each data set for depth and diameter.

The effect of soil type was expected because thermoplastic pipe has low hoop stiffness which increases the arching of load around a pipe in stiff soils. Backfill stiffness is a significant factor in earth load arching. Further analysis showed that the thrust in thermoplastic pipe could be predicted from Equation 13 with the following correction for the soil effect:

$$N_{peak} = F_{th} \cdot F_1 \cdot LL_{pres} \cdot \{0.5 \cdot \min(D_i; l_t + LLDF \cdot H)\} \quad (15)$$

$$F_{th} = \frac{0.95}{1 + 0.6 S_H} \quad (16)$$

where

F_{th} is the correction factor for effect of soil type on thrust

S_H is the hoop stiffness factor computed in accordance with AASHTO LRFD Equation 12.12.3.4-4, assuming that the vertical confining stress is 0.15 ksf. and using the short-term modulus of elasticity of the pipe material. (Note: the assumption of the vertical confining stress is somewhat arbitrary, but as the soil stresses due to live

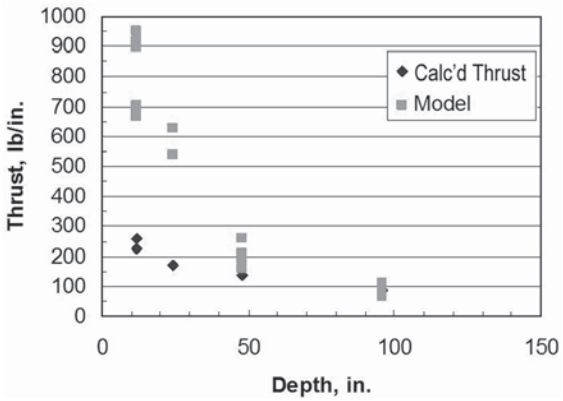

Figure 2-25. Comparison of SDE and computer model thrusts for corrugated metal arches.

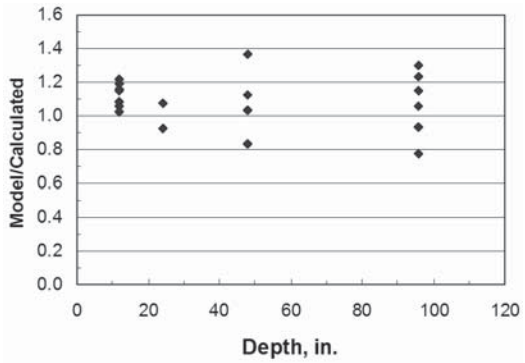

Figure 2-26. Comparison of proposed and model thrusts for long-span metal culverts.

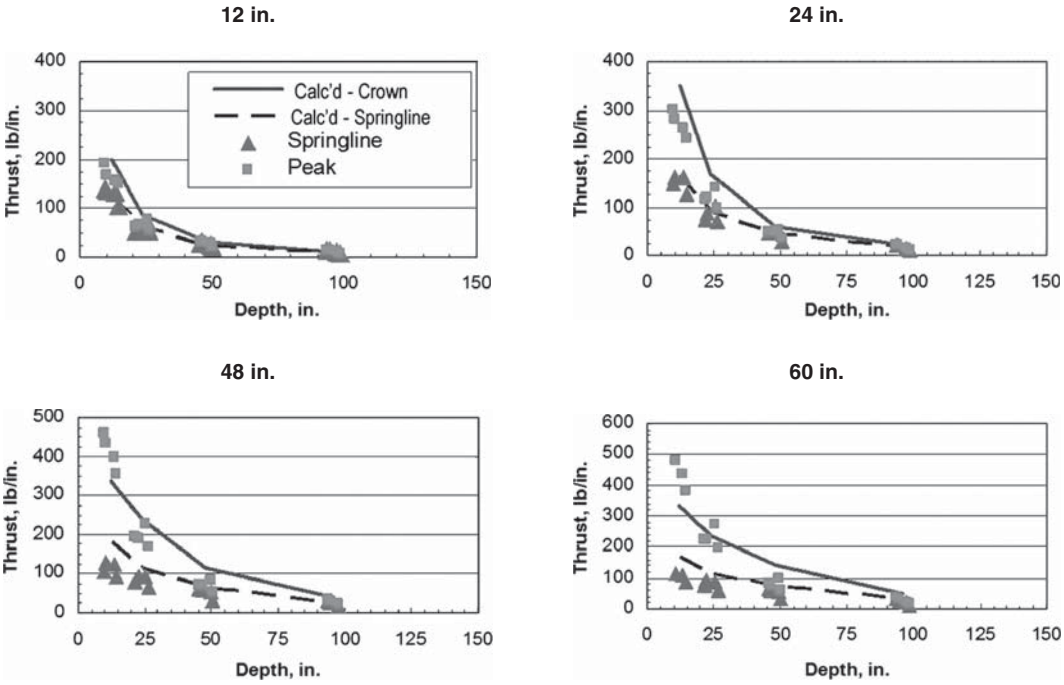

Figure 2-27. Comparison of SDE and computer model thrusts for thermoplastic pipe.

load are variable around the pipe, this provides an adequate approximation.)

Applying this correction, the ratio of the predicted thrusts to the computer model thrusts is presented in Figure 2-28. The mean value of the ratio is 1.21 with a standard deviation of 0.25. Comparison of thrust due to combined earth plus live load is shown in Figure 2-29. In this comparison, long-term earth load was calculated using the current AASHTO procedures for thermoplastic pipe. The long-term earth load is substantially less than the short-term earth load for pipe embedded in SW95 soils, thus the comparison is conservative. Figure 2-29 shows an average ratio of calculated to computer model total thrust of 1.14 with a standard deviation of 0.14. The figure also shows that the variation reduces significantly for depths of fill greater than 24 inches. Current AASHTO specifications require at least 2 feet of cover for thermoplastic pipe.

Bending Moment. The live load bending moment is required to calculate strains required for thermoplastic pipe design. The research team computed non-dimensional bending moment coefficients as

$$c_m = \frac{M}{(T \cdot R)} \tag{17}$$

where

c_m is a dimensionless moment coefficient
M is the bending moment, in.-lb/in.

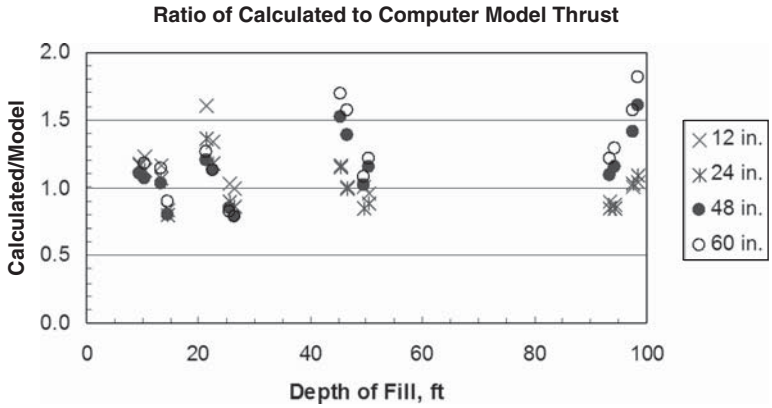

Figure 2-28. Ratio of calculated (Eqn (18)) to computer model peak thrust for thermoplastic pipe.

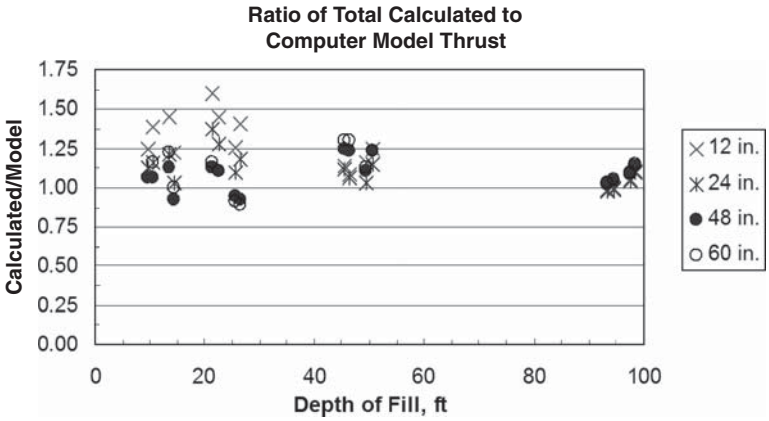

Figure 2-29. Thermoplastic pipe—ratio of calculated to model thrust for earth load plus peak live load thrust.

T is the peak thrust, lb/in.
R is the mean pipe radius. in.

The moment coefficients are plotted by diameter in Figure 2-30 which shows some variation as a result of diameter (symbol type) and soil type (variations within symbols of the same type). The variation due to diameter is chiefly in the smaller diameters under shallow fill. The correction factors in Eq. 21 and Table 2-28 were developed for the two effects.

$$F_{3.th} = \frac{D_i}{48\text{in.}} \qquad \text{constrained by:} \quad 0.65 < F_{3.th} < 1 \tag{18}$$

Computing a revised moment coefficient as

$$c_{m.\text{mod}} = c_m / F_{3.th} / F_{4.th} \tag{19}$$

gives the data plot in Figure 2-31. The data is fairly consolidated and a simple upper bound curve was plotted with the equation

$$UP_{cm} = 0.045 - 0.00032 \cdot H(\text{in.}) \tag{20}$$

The upper bound equation is exceeded for 48-in.- and 60-in.-diameter pipe under 12 inches of fill; however, this is far below the minimum allowable depth of fill for these products.

Combining the upper bound curve with the coefficients gives the equation for computing bending moment:

$$M_{th} = \frac{(N_{peak} \cdot R) \cdot [0.045 - 0.00032 \cdot H]}{F_{3.th} \cdot F_{4.th}} \tag{21}$$

where

M_{th} is the design bending moment, in.-lb/in.
N_{peak} is peak thrust computed from Eq. 18, lb/in.
R is the radius to centroid of pipe wall, in.
H is the depth of fill to top of pipe, in.
$F_{3.th}$ is the coefficient for diameter from Eq. 21
$F_{4.th}$ is the coefficient for diameter from Table 2-28

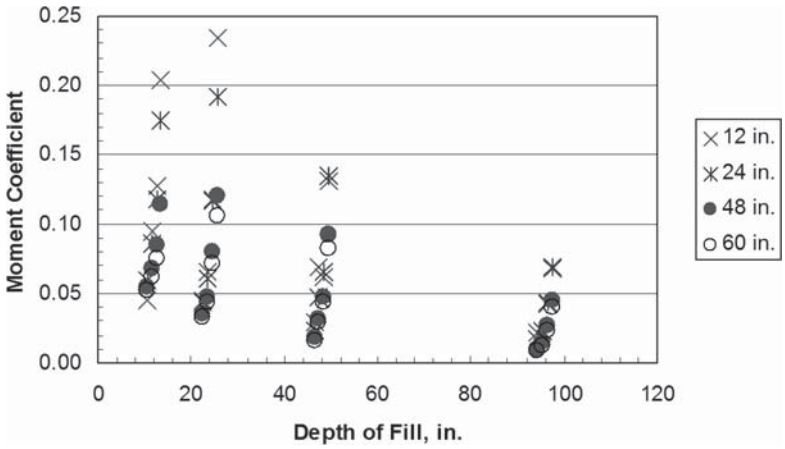

Figure 2-30. Dimensionless moment coefficients from computer model.

Table 2-28. Soil correction factor, $F_{4.th}$, for bending moment in thermoplastic pipe.

Soil Type	$F_{4.th}$
SW95	1.00
SW90, ML95	0.75
SW85, ML90, CL95	0.50
ML85, CL90	0.38
CL85	0.25

Using Eq. 24 bending moments were calculated using the peak thrusts from Eq. 18. The ratios of these calculated moments to the computer model moments are presented in Figure 2-32. The data shows more scatter than the thrust predictions but indicates that the proposed equation is generally conservative. The average ratio is 1.35 with a standard deviation of 0.29.

Comparison with Current Practice. Thrusts computed with the proposed equations are compared with current AASHTO practice in Table 2-29 for 24-in.-diameter pipe in SW95 soil (called Sn95 in the LRFD Specifications) and in Table 2-30 for 24-in.-diameter pipe in ML85 soil (called Si85 in the LRFD Specifications).

The tables show a substantial live load reduction in high-quality backfill where the thermoplastic PE pipe with low hoop and flexural stiffness deforms and allows the soil to carry load around the pipe. In weaker soils, such as ML85, the load reduction is modest relative to the LRFD Specifications and increases relative to the Standard Specifications.

2.3.2.7 PVC Pipe

The PVC pipe modeled in the study was solid wall pipe that is not representative of PVC pipe that would be installed in typical highway culvert installations (which are typically profile wall pipe). Pipe stiffnesses are in the range of 500 psi versus about 50 psi for culvert pipe. Analysis of the data shows that the

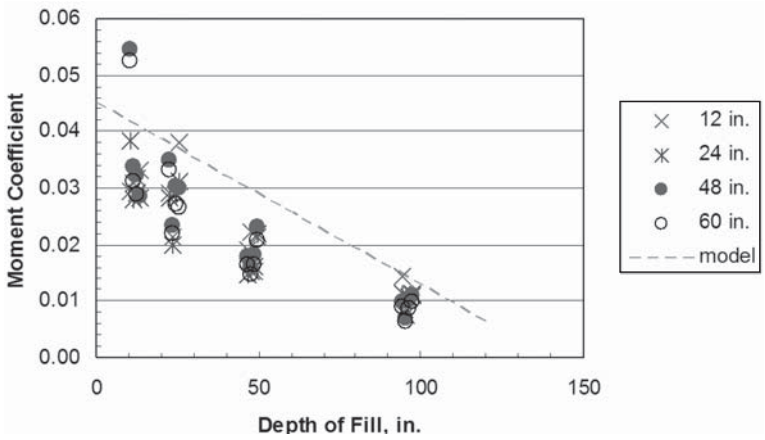

Figure 2-31. Corrected moment coefficient with upper bound curve, thermoplastic pipe.

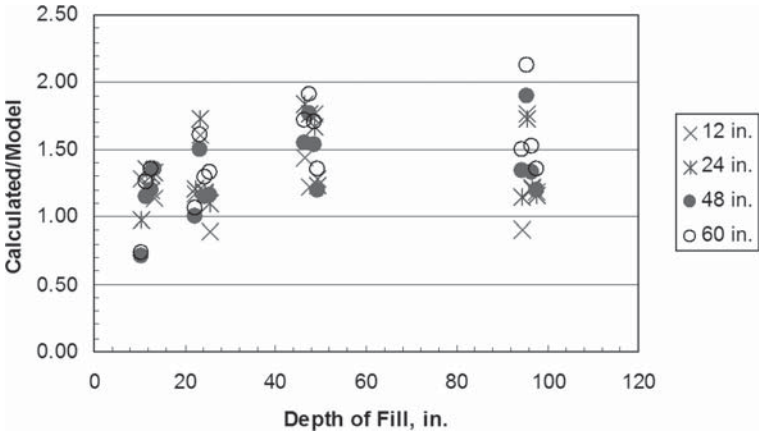

Figure 2-32. Calculated to model moment ratios vs. fill depth for thermoplastic pipe.

Table 2-29. Comparison of proposed thermoplastic thrust with current AASHTO specifications for SW95 soil.

Depth (ft)	Thrust from Proposed SDE (lb/ft)	Current		Ratios	
		LRFD (lb/ft)	Modified Standard (lb/ft)	Proposed/ LRFD	Proposed/ 1.2 x Standard
1	2457	4392	7132	0.56	0.34
2	1091	1927	1880	0.57	0.58
3	602	1057	696	0.57	0.86
4	388	671	422	0.58	0.92
5	282	489	298	0.58	0.95
6	213	369	222	0.58	0.96
7	166	286	172	0.58	0.97
8	131	227	137	0.58	0.96
9	110	191	119	0.58	0.93
10	94	162	103	0.58	0.91
11	81	140	91	0.58	0.89
12	72	125	82	0.58	0.88

pipe can be analyzed for load using Eq. 6. However, this may not be appropriate for culvert pipe, which can be analyzed with the same procedures as proposed for profile wall pipe in the previous section. Figure 2-33 shows the comparison of the calculated to model thrusts for the PVC pipe.

The model ratios average 1.09 with a standard deviation of 0.23, which is high but tolerable for a solid wall pipe with very low hoop stresses.

2.4 Effect of SDEs on Culvert Forces

The research team calculated and compared the critical structural responses for the following culvert types and depth-span combinations:

- Concrete box—6 combinations
- Concrete pipe—100 combinations
- Corrugated metal pipe—42 combinations
- Thermoplastic (profile wall)—80 combinations
- Metal arch—6 combinations
- Concrete arch—8 combinations

The research team provides direct comparison of the structural responses generated under the AASHTO Standard Specification, AASHTO LRFD Specification, and the proposed SDEs. (Appendix D.1 contains MathCAD templates illustrating Standard, LRFD, and Proposed calculations for all structure types; Appendix D.2 lists parametric study results.)

2.4.1 Live Load Equations from AASHTO Standard and LRFD Codes

This section summarizes the live load equations from the AASHTO Standard and LRFD codes. These equations were used to compute the live loads for all culvert types in the comparisons described below. The proposed live load

Table 2-30. Comparison of proposed thermoplastic thrust with current AASHTO specification for ML85 soil.

Depth (ft)	Thrust from Proposed SDE (lb/ft)	Current		Ratios	
		LRFD (lb/ft)	Modified Standard (lb/ft)	Proposed/ LRFD	Proposed/ 1.2 x Standard
1	3645	4392	7132	0.83	0.51
2	1618	1927	1880	0.84	0.86
3	893	1057	696	0.84	1.28
4	575	671	422	0.86	1.36
5	419	489	298	0.86	1.41
6	317	369	222	0.86	1.43
7	246	286	172	0.86	1.43
8	195	227	137	0.86	1.43
9	164	191	119	0.86	1.38
10	140	162	103	0.86	1.36
11	121	140	91	0.86	1.33
12	107	125	82	0.86	1.31

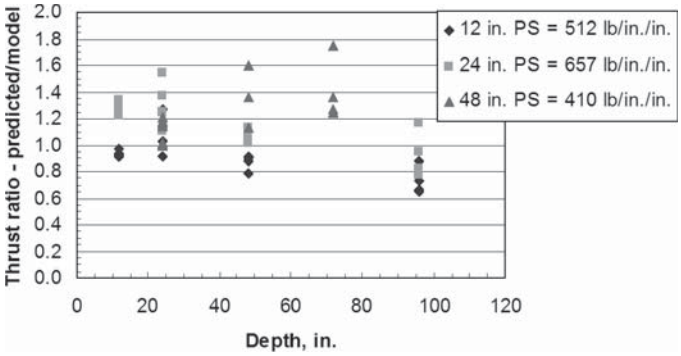

Figure 2-33. Ratios of model thrust to predicted thrust in PVC pipe using Equation 6.

equations for each culvert type are presented in the appropriate section.

2.4.1.1 AASHTO Standard

The live load equations for the AASHTO Standard Specification are

L_{HS20} is the wheel load from the HS20 load case, 16,000 lb:

$$LL = L_{HS20} \tag{22}$$

where LL is the live load force, lb

Determine the wheel interaction depth:

$$H_{\text{int}} = \frac{s_w}{LLDF_s} \tag{23}$$

where
H_{int} is the wheel interaction depth, ft
s_w is the wheel spacing, 6 ft
$LLDF_s$ is the live load distribution factor, 1.75

Determine the live load area and pressure

$$\text{For } H < H_{\text{int}} \qquad A_{LL} = \left(LLDF_s \cdot H\right) \cdot \left(LLDF_s \cdot H\right) \tag{24}$$

$$W_{LL} = LL / A_{LL} \tag{25}$$

$$\text{For } H \geq H_{\text{int}} \qquad A_{LL} = \left(s_w + LLDF_s \cdot H\right) \cdot \left(LLDF_s \cdot H\right) \tag{26}$$

$$W_{LL} = 2 \cdot LL / A_{LL} \tag{27}$$

where
H is the culvert depth, ft
A_{LL} is the live load area, sf
W_{LL} is the live load pressure, psf

Determine the impact fraction

$$\begin{aligned} \text{For} \quad & 0 \leq H \leq 1 \qquad I = 0.3 \\ & 1 \leq H \leq 2 \qquad I = 0.2 \\ & 2 \leq H \leq 3 \qquad I = 0.1 \\ & 3 \leq H \qquad I = 0 \end{aligned} \tag{28}$$

where I is the impact fraction (maximum 30 percent)

The service live load is computed from

$$W_L = \left(1 + I\right) \cdot W_{LL} \cdot \min\left(D_i / 12, LLDF_s \cdot H\right) \tag{29}$$

where D_i is the inside diameter or span of the culvert, inches

2.4.1.2 AASHTO LRFD

The live load equations for the AASHTO LRFD Specification are

$$LL = L_{HS20} \tag{30}$$

where
L_{HS20} is the wheel load from the HS20 load case, 16,000 lb
LL is the live load force, lb

Determine the wheel interaction depth

$$H_{\text{int}} = \frac{s_w - w_t / 12}{LLDF_l} \tag{31}$$

where
H_{int} is the wheel interaction depth, ft
s_w is the wheel spacing, 6 ft
w_t is the tire patch width, 20 in.
$LLDF_l$ is the live load distribution factor, 1.15

Determine the live load area and pressure

$$\text{For } H < H_{\text{int}} \quad A_{LL} = \left(\frac{w_t}{12} + LLDF_l \cdot H\right) \cdot \left(\frac{l_t}{12} + LLDF_l \cdot H\right) \tag{32}$$

$$W_{LL} = LL / A_{LL} \tag{33}$$

$$\text{For } H \geq H_{\text{int}} \quad A_{LL} = \left(\frac{w_t}{12} + s_w + LLDF_l \cdot H\right) \cdot \left(\frac{l_t}{12} + LLDF_l \cdot H\right) \tag{34}$$

$$W_{LL} = 2 \cdot LL / A_{LL} \tag{35}$$

where
H is the culvert depth, ft
l_t is the tire patch length, 10 in.
A_{LL} is the live load area, sf
W_{LL} is the live load pressure, psf

Determine the governing load length

$$\text{For } H < 0.833 \qquad L_{t.gov} = l_t / 12 \tag{36}$$

$$\text{For } H \geq 0.833 \qquad L_{t.gov} = \frac{l_t}{12} + LLDF_l \cdot H \tag{37}$$

where $L_{t.gov}$ is the governing load length, ft

Determine the dynamic load allowance

$$\text{For } H < 8\,ft \qquad IM = 33 \cdot \left(\frac{1 - H/8}{100} \right) \tag{38}$$

$$\text{For } H \geq 8\,ft \qquad IM = 0 \tag{39}$$

where IM is the dynamic load allowance

Determine the service live load

$$W_L = MPF \cdot (1 + IM) \cdot W_{LL} \cdot \min(D_i/12, L_{t.gov}) \tag{40}$$

where

MPF is the multiple presence factor, 1.2

D_i is the inside diameter or span of the culvert, in.

2.4.2 Proposed SDEs

2.4.2.1 Live Loads

The proposed live load equations differ for each culvert type, so they are presented in sections 2.4.3.1 through 2.4.8.1.

2.4.2.2 Dead Loads

Dead loads vary according to the culvert type, so they are presented in sections 2.4.3.2 through 2.4.8.2.

2.4.2.3 Service and Factored Loads

Service and factored loads used in the design comparisons were

$$TL_s = DL + LL \tag{41}$$

$$TL_{F,STD} = \gamma_d \cdot DL + \gamma_l \cdot LL \tag{42}$$

$$TL_{F,LRFD} = \gamma_d \cdot DL + \gamma_l \cdot LL \tag{43}$$

$$TL_{F,SDE} = \gamma_d \cdot DL + \gamma_l \cdot LL \tag{44}$$

where

DL is the total dead load

LL is the total live load

TL_S is the total service load

$TL_{F,STD}$ is the factored load for the AASHTO Standard Specification

$TL_{F,LRFD}$ is the factored load for the AASHTO LRFD Specification

$TL_{F,SDE}$ is the factored load for the proposed specification

γ_d is the dead load factor, from Table 2-31

γ_l is the live load factor, from Table 2-31

Table 2-31 contains the dead load and live load factors referred to above.

2.4.3 Concrete Box Comparison

Concrete box design calculations were done using the direct design method, using the software BOXCAR to calculate structural responses. BOXCAR (BOXCAR, 2000) is a four member frame program with the stiffness matrix modified to account for the haunch stiffness. For live load input to BOXCAR, the same total live load was used for each case, but with live load distribution areas. These distribution areas were determined from AASHTO Standard, AASHTO LRFD, and SDEs.

2.4.3.1 Live Load Equations

The proposed live load equations used for concrete box design calculations are as presented in Section 2.4.1.2, except the interaction depth, live load area, and pressure are as follows.

Determine the wheel interaction depth

$$H_{\text{int}} = \frac{s_w - \frac{w_t}{12} - \frac{0.06 D_i}{12}}{LLDF_l} \tag{45}$$

Table 2-31. Dead load and live load factors, γ_d and γ_l.

Culvert Type	AASHTO LRFD		AASHTO Standard		Simplified Design Equation	
	Dead Load	Live Load	Dead Load	Live Load	Dead Load	Live Load
Concrete Pipe	1.3	1.75	1.3	2.17	1.3	1.75
Concrete Box	1.35	1.75	1.35	2.17	1.35	1.75
Corrugated Metal Pipe	1.95	1.75	1.95	2.17	1.95	1.75
Thermoplastic (Profile Wall)	1.95	1.75	1.95	2.17	1.95	1.75
Metal Arch	1.95	1.75	1.95	2.17	1.95	1.75
Concrete Arch	1.3	1.75	1.3	2.17	1.3	1.75

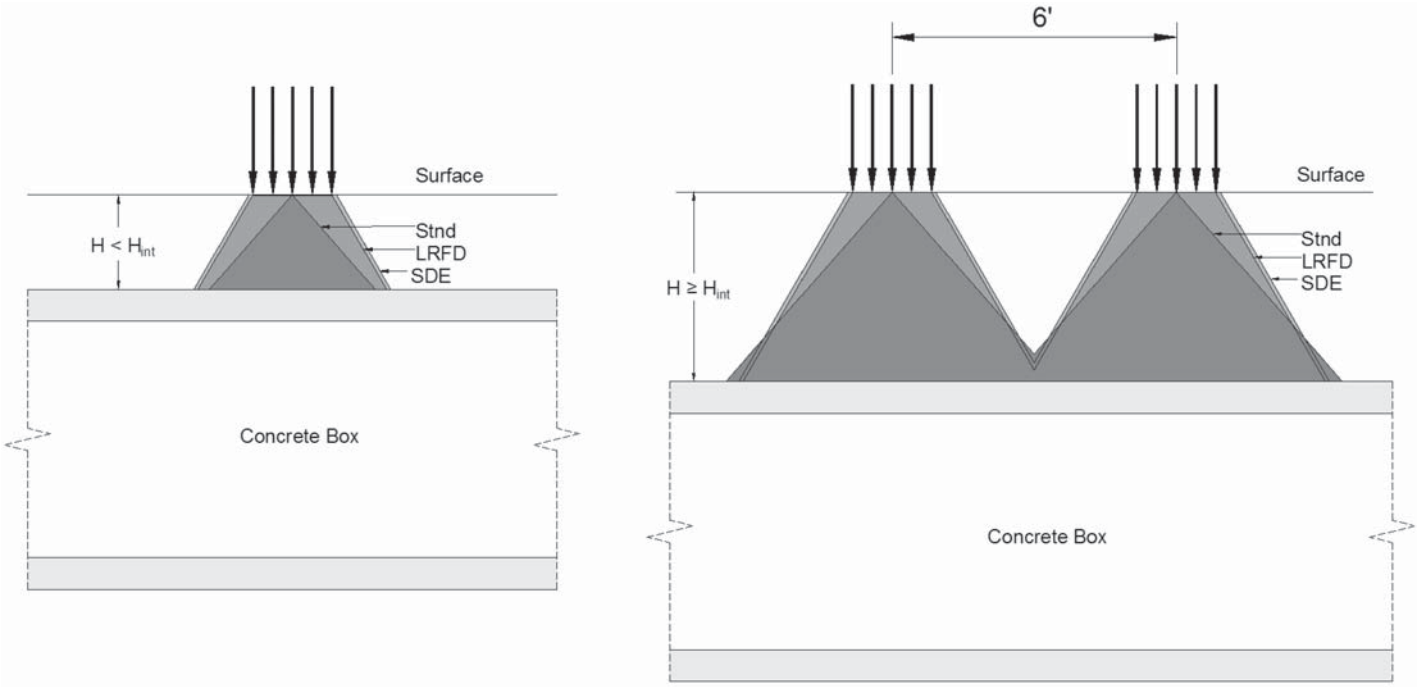

Figure 2-34. Live load variation with depth for concrete box culverts.

where

H_{int} is the wheel interaction depth, ft
s_w is the wheel spacing, 6 ft
w_t is the tire patch width, 20 in.
$LLDF_l$ is the live load distribution factor, 1.15
D_i is the inside span of the culvert, in.

For $H < H_{int}$

$$A_{LL} = \left(\frac{w_t}{12} + LLDF_l \cdot H + 0.06 \cdot D_i/12\right) \cdot \left(\frac{l_t}{12} + LLDF_l \cdot H\right) \quad (46)$$

For $H \geq H_{int}$

$$A_{LL} = \left(\frac{w_t}{12} + s_w + LLDF_l \cdot H + 0.06 \cdot D_i/12\right) \cdot \left(\frac{l_t}{12} + LLDF_l \cdot H\right) \quad (47)$$

where

H is the culvert depth, ft
w_t is the tire patch width, 20 in.
l_t is the tire patch length, 10 in.
$LLDF_l$ is the AASHTO LRFD live load distribution factor, 1.15

Figure 2-34 compares the variation of live load with depth for concrete boxes, for the Standard, LRFD, and proposed SDE. The SDE distribution starts out wider than LRFD, but increases width with depth at the same rate.

In BOXCAR, the details of live load input were

1. Use live load option "Other" in Boxcar-Design (page 4) and specify 1 wheel
2. Set the LLDF to 0.00001 (to avoid dividing by zero)
3. Set the tire footprint to the area defined by the denominator of the appropriate live load equation above

2.4.3.2 Dead Load Equations

The dead loads were computed by BOXCAR from the parameters listed in Table 2-32.

2.4.3.3 Geometry and Material Properties

Table 2-33 lists the concrete box geometry and material properties used in the design comparison.

Table 2-32. BOXCAR dead load parameters for box culvert parametric study.

Parameter	Value
Soil density	120 pcf
Minimum lateral pressure coefficient	0.25
Maximum lateral pressure coefficient	0.5
Installation type	Embankment/ Compacted
Soil-structure interaction factor	1.083
Fluid density	62.5 pcf

Table 2-33. Concrete box culvert properties for parametric study.

Span (ft)	Rise (ft)	Thickness (in)	Haunch (in)	Cover (ft)	Reinforcing Yield Stress (psi)	Concrete Strength (psi)	Concrete Unit Weight (pcf)
4	4	5	5	2	65,000	5,000	150
4	4	5	5	4	65,000	5,000	150
4	4	5	5	8	65,000	5,000	150
8	8	9	9	2	65,000	5,000	150
8	8	9	9	4	65,000	5,000	150
8	8	9	9	8	65,000	5,000	150

2.4.3.4 Comparison of Standard, LRFD, and Proposed

Figures 2-35 through 2-38 compare the structural responses for reinforced concrete box culverts. These four figures, and comparison figures for all culvert types, have a common format. Each figure contains two comparisons: AASHTO Standard versus proposed SDEs, and AASHTO LRFD versus proposed SDEs. The figures are constructed with the AASHTO value as the abscissa and the SDE as the ordinate. Each figure has a thick line for abscissa values equal to ordinate values. The region below this line, where SDE values are less than the AASHTO values, is shaded one gray tone, to distinguish from the region above this line, where SDE values are greater than AASHTO values, shaded in a different gray tone. All culvert depths are plotted in one figure. In some graphs, the data pairs created by plotting one data point for the (Stnd,SDE) combination and one data point for the (LRFD,SDE) combination are easy to discern (for example Figure 2-35). Comparing the location of these data pairs provides insight into the differences between the Standard and LRFD values.

Top-slab middle moments range from about 30 kip-in/ft to about 180 kip-in/ft, while bottom-slab middle moments range from about 30 kip-in/ft to about 140 kip-in/ft. About two-thirds of the comparisons have SDE values slightly greater than the AASHTO values. Top-slab and bottom-slab maximum shear comparisons are similar. For both moment and shear comparisons, the SDEs, on average, produce slightly higher moments and shears.

The research team expects similar results for larger-span concrete box culverts.

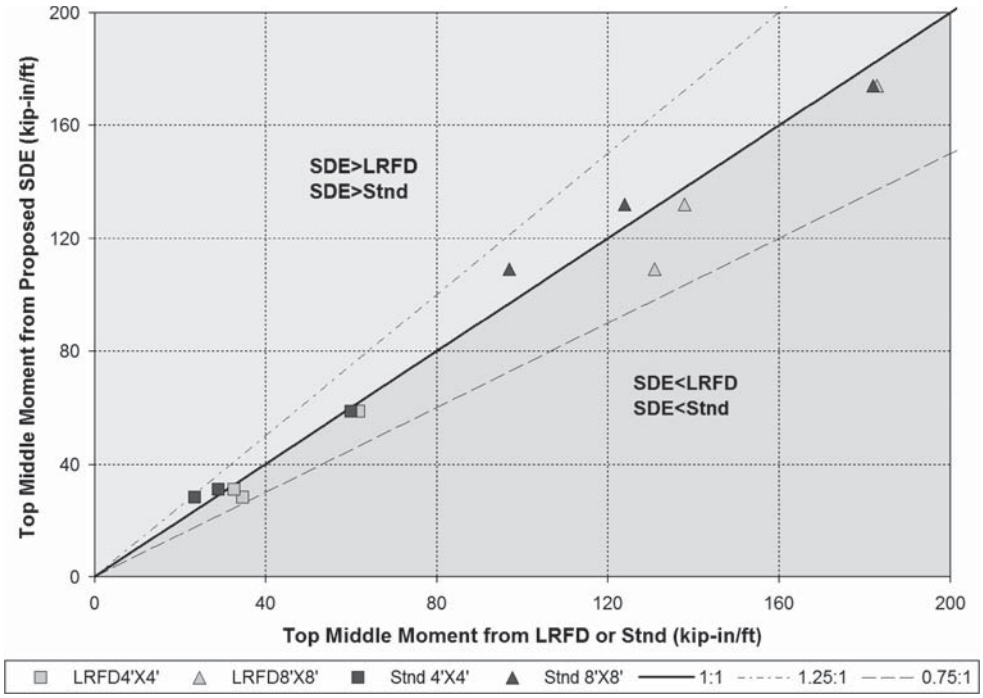

Figure 2-35. Top middle moment comparison for concrete boxes.

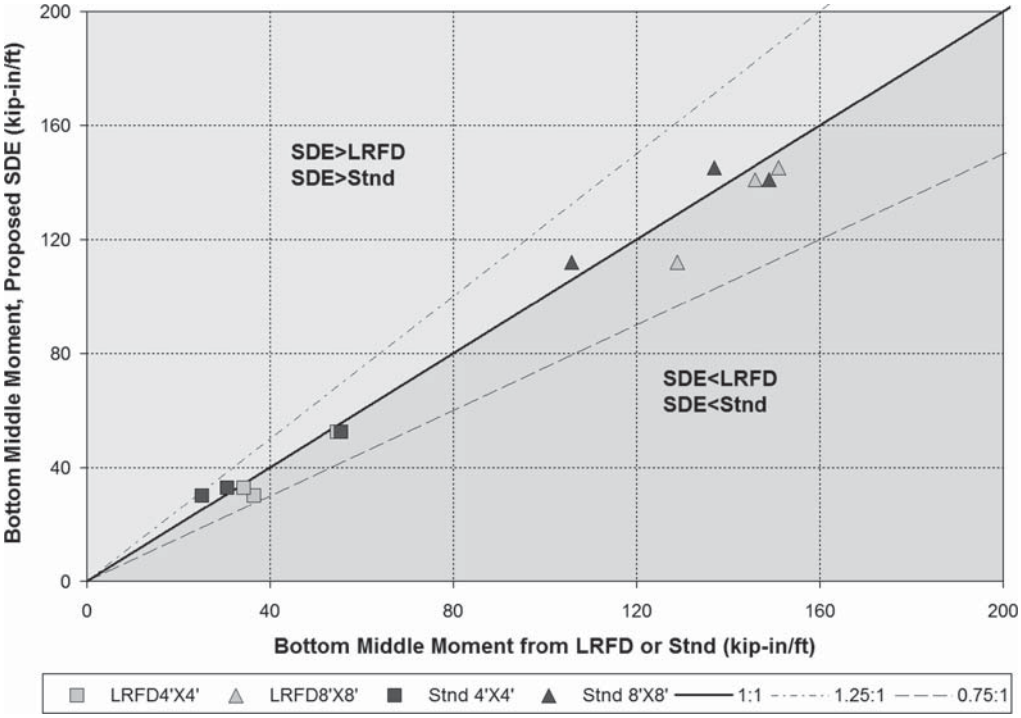

Figure 2-36. Bottom middle moment for concrete boxes.

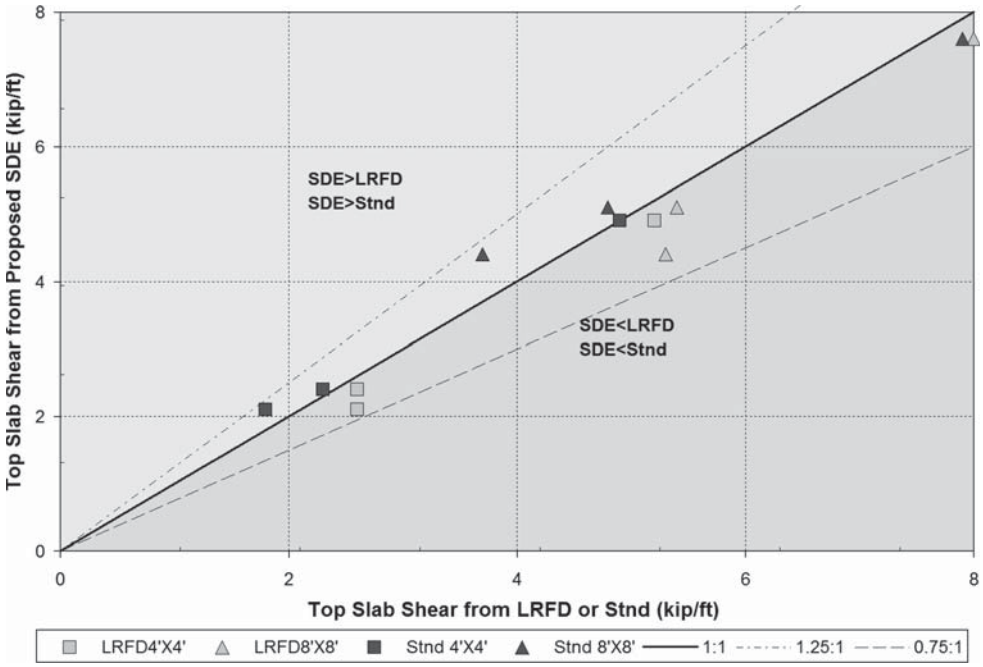

Figure 2-37. Top slab shear comparison for concrete boxes.

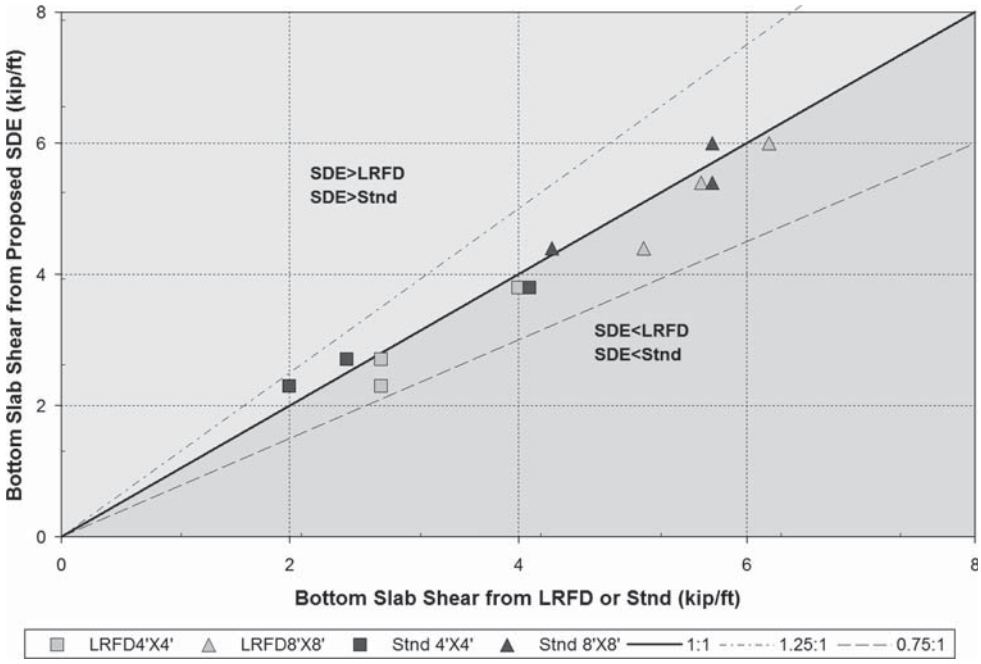

Figure 2-38. Bottom slab shear comparison for concrete boxes.

2.4.4 Concrete Pipe Comparison

Concrete pipe design comparisons were done using the direct design method. The determination of earth loads and live load pressure distributions on the structure were selected by the bedding and installation conditions. The thrust, moment and shear analysis for each installation type was performed using the SIDD methods (ASCE, 2000).

2.4.4.1 Live Load Equations

The proposed live load equations used for concrete pipe design calculations are similar to the AASHTO LRFD equations presented in Section 2.4.1.2, except as follows:

For $D_i \geq 24in$ $\quad LLDF_{cp} = 1.15$ (48)

For $24in < D_i \leq 96in$ $\quad LLDF_{cp} = 0.00833 \cdot D_i + 0.95$ (49)

For $D_i > 96in$ $\quad LLDF_{cp} = 1.75$ (50)

where $LLDF_{cp}$ is the live load distribution factor for concrete pipe

Determine the wheel interaction depth

$$H_{\text{int}} = \frac{s_w - \frac{w_t}{12} - \frac{0.06 D_i}{12}}{LLDF_{cp}} \quad (51)$$

Determine the live load area and pressure

For $H < H_{\text{int}}$ $\quad A_{LL} = \left(\frac{w_t}{12} + LLDF_{cp} \cdot H + 0.06 \cdot D_i/12\right) \cdot \left(\frac{l_t}{12} + LLDF_{cp} \cdot H\right)$ (52)

For $H \geq H_{\text{int}}$ $\quad A_{LL} = \left(\frac{w_t}{12} + s_w + LLDF_{cp} \cdot H + 0.06 \cdot D_i/12\right) \cdot \left(\frac{l_t}{12} + LLDF_{cp} \cdot H\right)$ (53)

Determine the governing load length

For $H < 0.833$ $\quad L_{t.gov} = l_t/12$ (54)

For $H \geq 0.833$ $\quad L_{t.gov} = \frac{l_t}{12} + LLDF_{cp} \cdot H$ (55)

where

H is the culvert depth, ft
w_t is the tire patch width, 20 in
l_t is the tire patch length, 10 in.
D_i is the inside span of the culvert, in.
$L_{t.gov}$ is the governing load length

Figure 2-39 compares the variation of live load with depth for concrete pipe, for the Standard, LRFD and proposed SDE. The SDE distribution starts out wider than LRFD, and increases in width with depth at a faster rate.

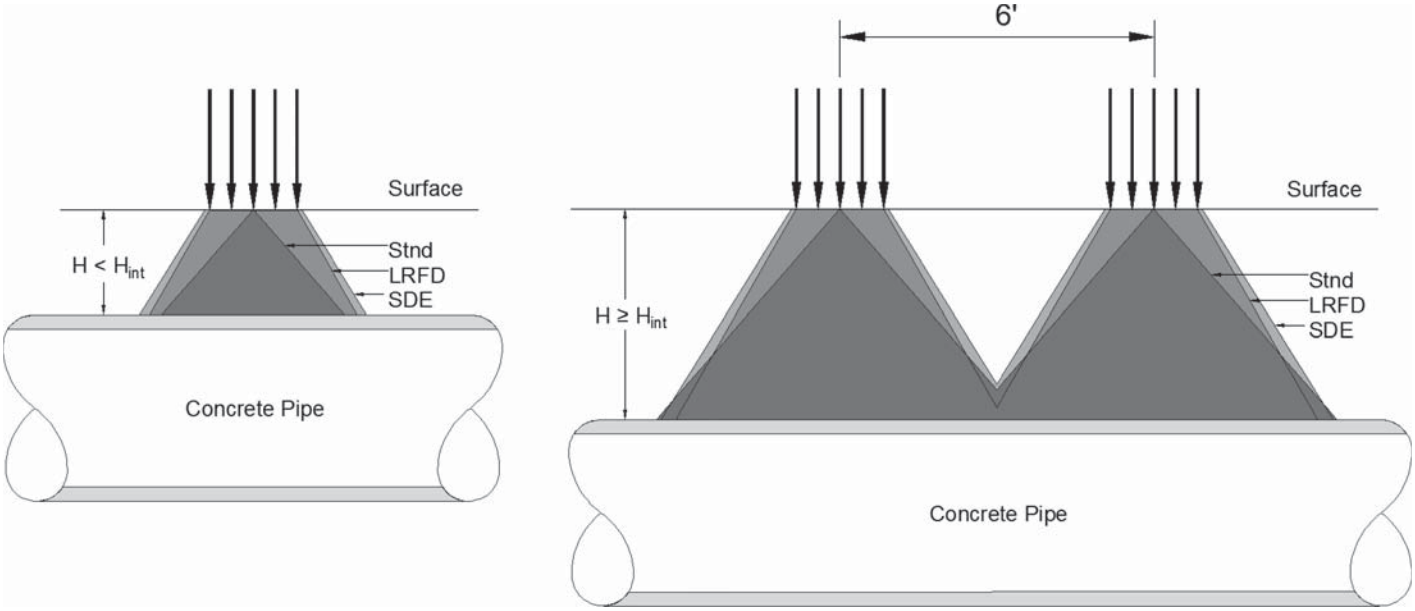

Figure 2-39. Live load variation with depth for concrete pipe culverts.

2.4.4.2 Dead Load Equations

Concrete pipe dead loads were computed from

$$W_p = w_c \cdot \frac{\pi}{4} \cdot \left(D_o^2 - D_i^2\right)/144 \tag{56}$$

$$W_e = F_e \cdot w_e \cdot \left(H + 0.0089 \cdot D_o\right) \cdot D_o/12 \tag{57}$$

$$W_f = w_f \cdot \frac{\pi}{4} \cdot \left(\frac{D_i}{12}\right)^2 \tag{58}$$

where

H is the culvert crown depth, in.
D_i is the culvert inside diameter, in.
D_o is the culvert outside diameter, in.
W_p is the pipe dead load, lb/ft
W_e is the earth dead load, lb/ft
W_f is the fluid dead load, lb/ft
w_c, w_e, and w_f are the concrete unit weight, earth unit weight, and fluid unit weight, respectively.
F_e is the soil-structure interaction factor, 1.35

The total service dead load is

$$DL = W_P + W_E + W_F \tag{59}$$

2.4.4.3 Moment, Thrust and Shear Calculations

To find the design moments, thrusts and shear, the SIDD nondimensional coefficients C_{mi}, C_{ni}, and C_{vi} were used for determining the moment thrust and shear, respectively, at governing locations at the crown, invert, springline and at the critical locations for shear in the invert and crown regions. Calculations were done for the four SIDD installation types.

$$M_i = \frac{D_m}{2} \sum C_{mi} \cdot W_i \tag{60}$$

$$N_i = \sum C_{mi} \cdot W_i \tag{61}$$

$$V_i = \sum C_{vi} \cdot W_i \tag{62}$$

where W_i takes the values W_P, W_E, W_F and W_L.

Additional details may be found in ASCE 2000.

2.4.4.4 Comparison of Standard, LRFD, and Proposed SDEs

Figures 2-40 through 2-43 compare the structural responses for reinforced concrete pipe. These figures, and comparison figures for all culvert types, have a common format, described in Section 2.4.3.4. All four figures for RCP are similar. For low values, corresponding to small-diameter culverts, the SDE values are similar to or slightly greater than LRFD or Standard values. For higher values, corresponding to larger diameter culverts, the SDE values are similar to or less than (sometime significantly less than) AASHTO values.

In all four figures, one group of four data points has SDE values substantially below the AASHTO values. This data is for a 48-in.-diameter RCP at 1-ft depth of burial and compares the AASHTO standard to proposed SDE. The moment or shear values plot so far off the 1:1 because the Standard Specifications treat the live load as a point load for burial depths of 1 foot.

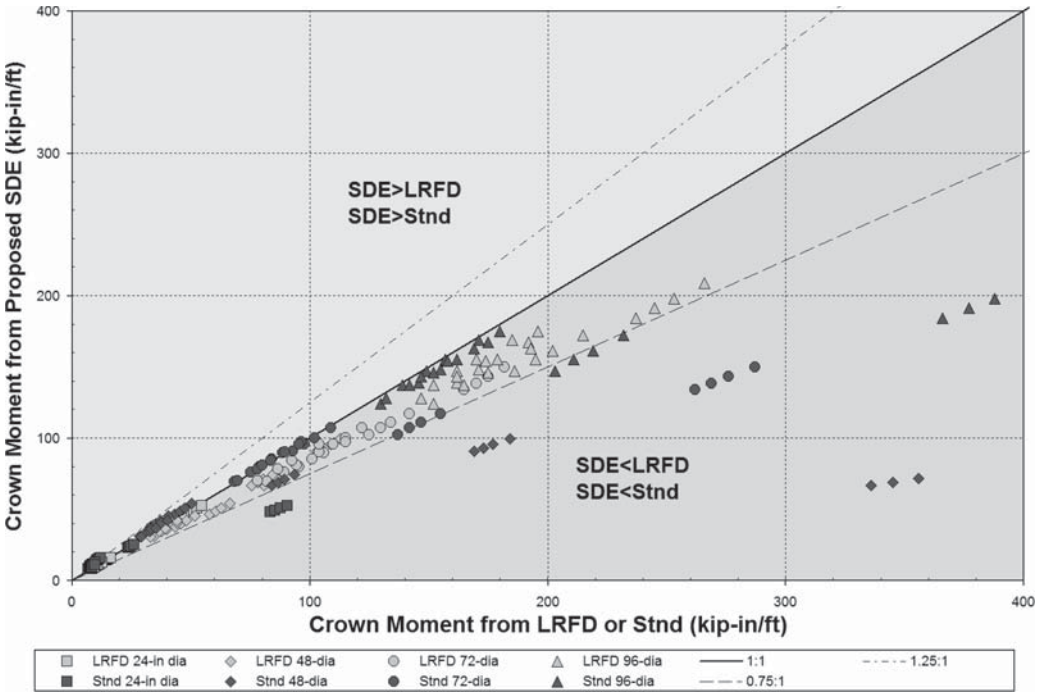

Figure 2-40. Crown moment comparison for RCP.

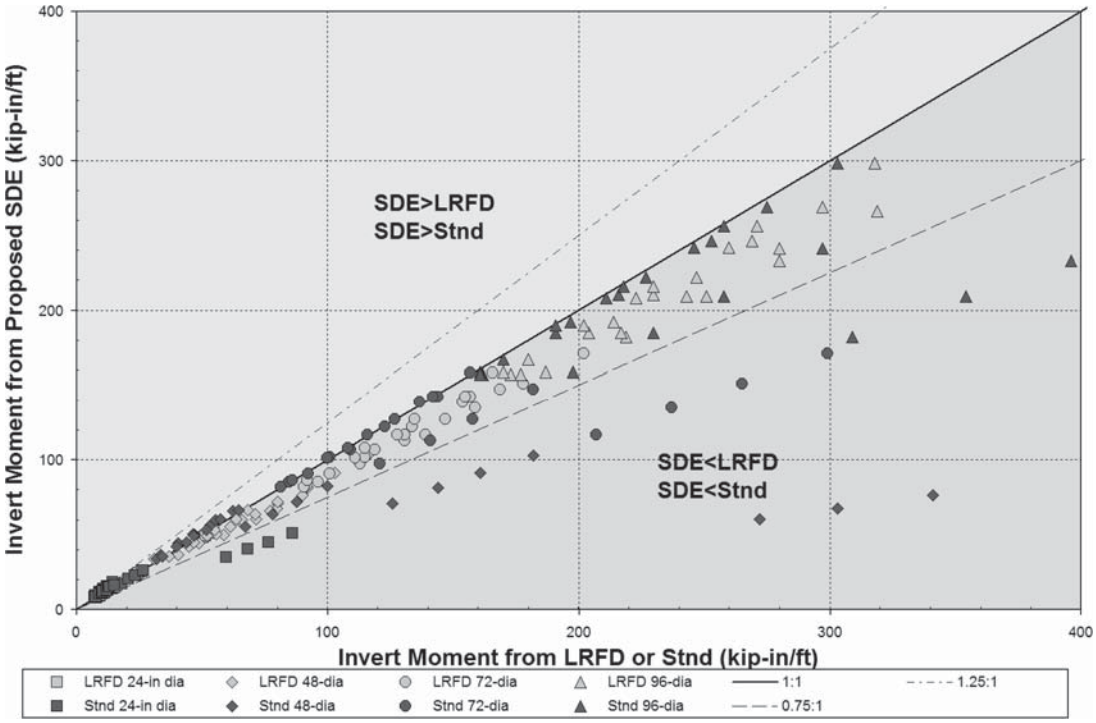

Figure 2-41. Invert moment comparison for RCP.

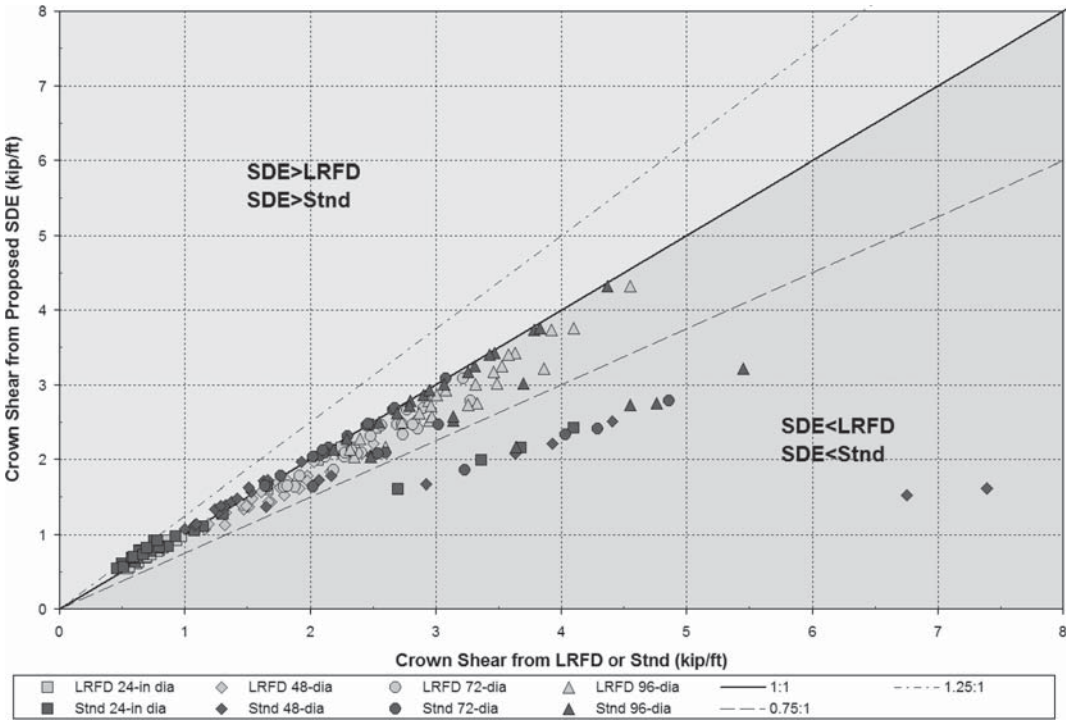

Figure 2-42. Crown shear comparison for RCP.

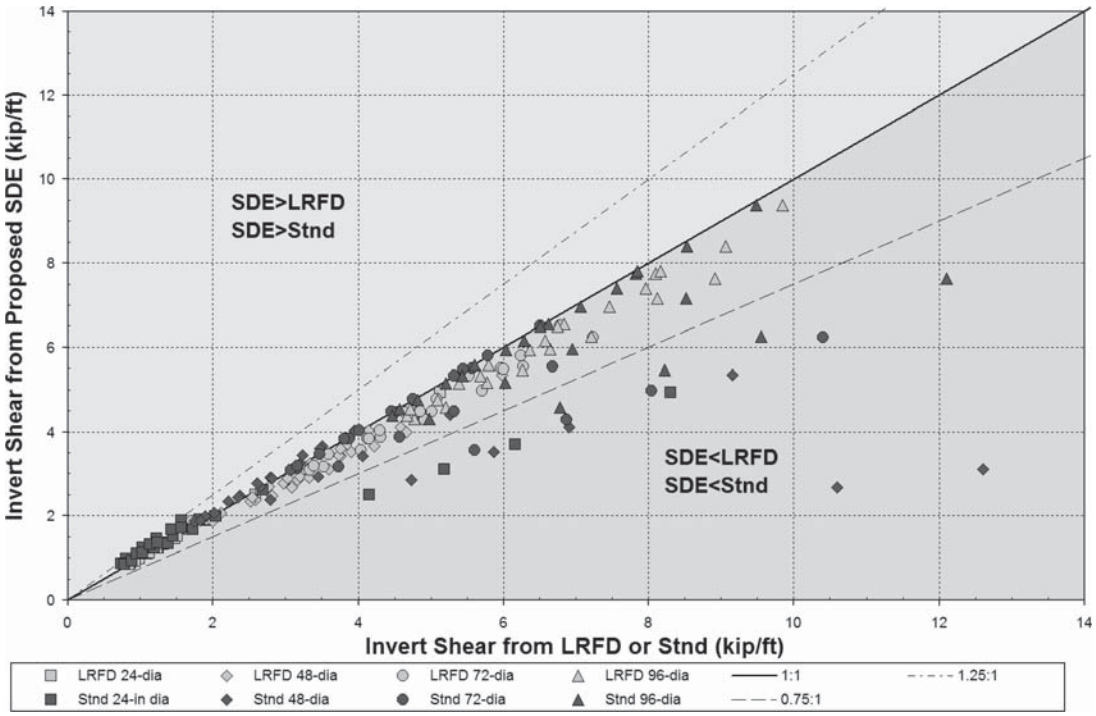

Figure 2-43. Invert shear comparison for RCP.

2.4.5 Corrugated Metal Pipe Comparison

The corrugated metal pipe culvert comparison was made using the peak factored thrust per unit length of wall.

2.4.5.1 Live Load Equations

The proposed live load equations used for corrugated metal pipe are as presented in Section 2.4.1.2, except the live load area is as follows.

Determine the wheel interaction depth

$$H_{\text{int}} = \frac{s_w - \frac{w_t}{12} - \frac{0.06 D_i}{12}}{LLDF_l} \tag{63}$$

For $H < H_{\text{int}}$

$$A_{LL} = \left(\frac{w_t}{12} + LLDF_l \cdot H + 0.06 \cdot \frac{D_i}{12} \right) \cdot \left(\frac{l_t}{12} + LLDF_l \cdot H \right) \tag{64}$$

For $H \geq H_{\text{int}}$

$$A_{LL} = \left(\frac{w_t}{12} + s_w + LLDF_l \cdot H + 0.06 \cdot \frac{D_i}{12} \right) \cdot \left(\frac{l_t}{12} + LLDF_l \cdot H \right) \tag{65}$$

where

H is the culvert depth, ft
w_t is the tire patch width, 20 in.
l_t is the tire patch length, 10 in.
$LLDF_l$ is the AASHTO LRFD live load distribution factor, 1.15
D_i is the inside span of the culvert, in.
s_w is the wheel spacing, 6 ft

Figure 2-44 compares the variation of live load with depth for corrugated metal pipe, for the Standard, LRFD and proposed SDE. The SDE distribution starts out wider than LRFD, but increases in width with depth at the same rate as the LRFD.

2.4.5.2 Dead Load Equations

Corrugated metal pipe dead loads were computed from

$$W_e = F_e \cdot w_e \cdot \left(H + 0.0089 \cdot D_o \right) \cdot D_o / 12 \tag{66}$$

where

W_e is the earth dead load, lb/ft
w_e is the earth unit weight, lb/cubic ft
F_e is the soil-structure interaction factor, 1.0

The total dead load is

$$DL = W_e \tag{67}$$

2.4.5.3 Thrust Calculations

For AASHTO Standard Specifications, the total factored thrust is

$$T_t = \frac{TL_{F,STD}}{2} \tag{68}$$

where T_t is the factored thrust per unit length (lb/ft)

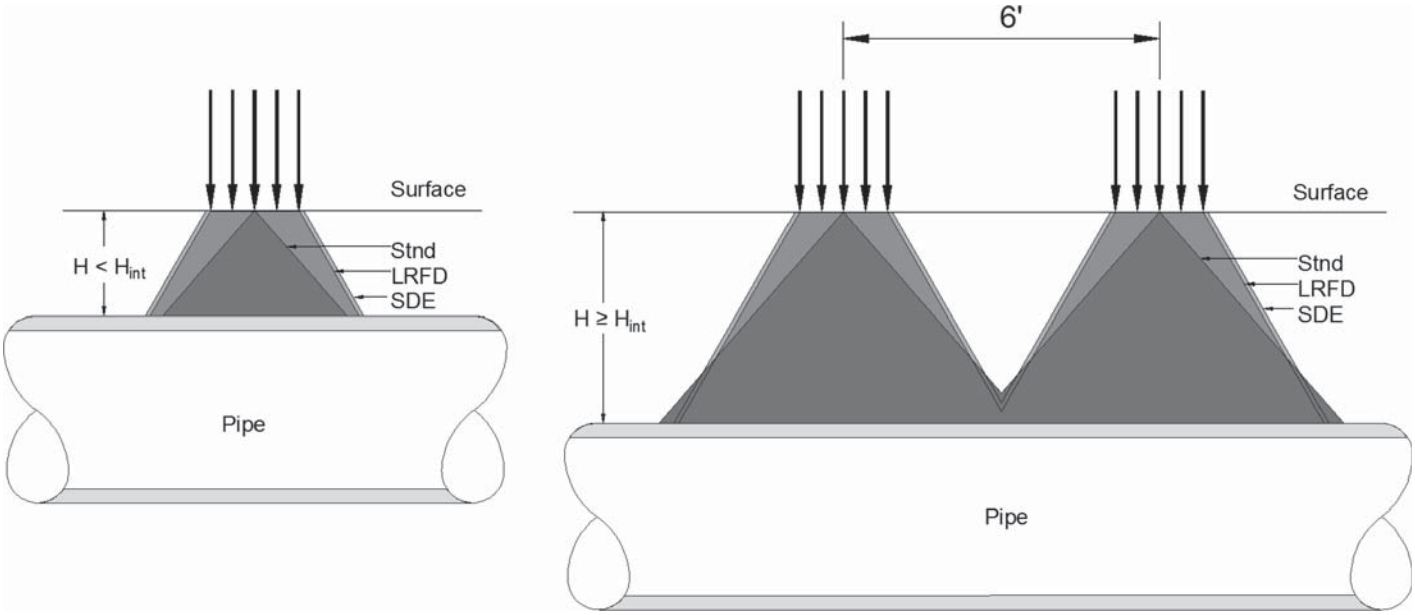

Figure 2-44. Live load variation with depth for corrugated metal pipe.

For AASHTO LRFD Specifications

$$T_t = \frac{TL_{F,LRFD}}{2} \tag{69}$$

For the proposed live load equations, the following live load adjustment is required:

$$F_{1,\lim} = \text{maximum}\left(15/D_t, 1\right) \tag{70}$$

$$F_1 = \text{maximum}\left(F_{1,\lim}, 0.75 \cdot \left(\frac{D_i/12}{L_t/12 + LLDF_l \cdot H}\right)\right) \tag{71}$$

$$T_t = \frac{\gamma_d \cdot DL + \gamma_t \cdot \left(LL \cdot F_1\right)}{2} \tag{72}$$

2.4.5.4 Comparison between Standard, LRFD and Proposed

Figure 2-45 compares the peak thrust for corrugated metal pipe. This figure, and comparison figures for all culvert types, have a common format, described in Section 2.4.3.4.

The figure illustrates that, for most cases, the design peak thrust determined from the Standard Method, LRFD Method, and the SDEs are similar. In most cases, the peak thrust from the SDEs are slightly greater than from the Standard Method and about the same or slightly less than the LRFD Method. Outliers occur for large-diameter pipes under shallow burial, typically diameters above 5 feet and depths of 2 to 3 feet and less. The high peak thrusts required by the SDEs are the result of the computer model results from this study and are also consistent with *NCHRP Report 473* (McGrath et al., 2002) results for long-span metal culverts. Additional details may be found in Section 2.3.2.4.

2.4.6 Thermoplastic Pipe (Profile Wall)

This section compares profile wall thermoplastic pipes design on the basis of the peak factored thrust. The vertical confining stress is 0.15 ksf (the assumption of the vertical confining stress is somewhat arbitrary, but as the soil stresses due to live load are variable around the pipe, this provides an adequate approximation) using the short term modulus of elasticity of the pipe material. The comparison was done for four soil types (i.e., SW95, SW85, ML85, and CL85).

2.4.6.1 Live Load Equations

The proposed live load equations used for profile wall thermoplastic pipe are as presented in Section 2.4.1.2, except the live load area is as follows:

Determine the wheel interaction depth

$$H_{\text{int}} = \frac{s_w - \frac{w_t}{12} - \frac{0.06D_i}{12}}{LLDF_l} \tag{73}$$

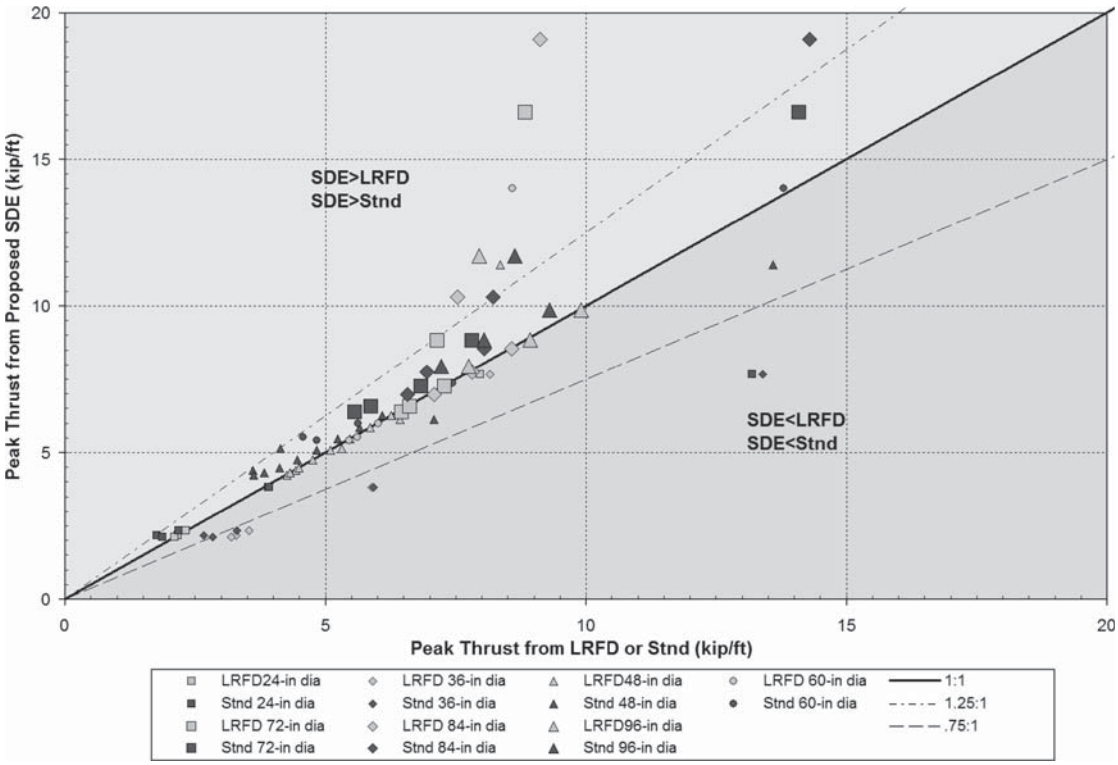

Figure 2-45. Peak thrust comparison for corrugated metal pipe.

For $H < H_{int}$

$$A_{LL} = \left(\frac{w_t}{12} + LLDF_l \cdot H + 0.06 \cdot \frac{D_i}{12}\right) \cdot \left(\frac{l_t}{12} + LLDF_l \cdot H\right) \quad (74)$$

For $H \geq H_{int}$

$$A_{LL} = \left(\frac{w_t}{12} + s_w + LLDF_l \cdot H + 0.06 \cdot \frac{D_i}{12}\right) \cdot \left(\frac{l_t}{12} + LLDF_l \cdot H\right) \quad (75)$$

where

H is the culvert depth, ft
w_t is the tire patch width, 20 in.
l_t is the tire patch length, 10 in.
$LLDF_l$ is the AASHTO LRFD live load distribution factor, 1.15
D_i is the inside span of the culvert, in.
s_w is the wheel spacing, 6 ft

Figure 2-46 compares the variation of live load with depth for thermoplastic pipe, for Standard, LRFD, and the proposed SDE. The SDE distribution starts out wider than LRFD, but increases in width with depth at the same rate as the LRFD.

2.4.6.2 Dead Load Equations

Profile wall pipe dead loads were computed from

$$PL = w_e \cdot \left(H + 0.0089 \cdot D_o\right) \cdot D_o / 12 \quad (76)$$

$$S_h = \frac{\phi_s \cdot M_s \cdot R}{E \cdot A_p} \quad (77)$$

$$VAF = 0.76 - 0.71 \cdot \left(\frac{S_h - 1.17}{S_h + 2.92}\right) \quad (78)$$

$$W_e = VAF \cdot PL \quad (79)$$

where

w_e is the earth unit weight, pcf
W_e is the earth dead load, lb/ft
H is the culvert depth, ft
D_o is the outside span of the culvert, in.
ϕ_s is the resistance factor for soil stiffness, 0.9
M_s is the constrained soil modulus at 150 psf, per the tables in Figure 2-47, excerpted from the AASHTO code
R is the radius to the centroid of the culvert wall, in.
E is the pipe material modulus of elasticity, as specified in Table 12.12.3.3-1 of the AASHTO code, 110,000 psi
A_p is the pipe unit area, in²/in

Values of D_o, R and A_p used in the calculations are provided in Table 2-34.

The total dead load is

$$DL = W_e \quad (80)$$

2.4.6.3 Thrust Calculations

For AASHTO Standard Specifications, the total factored thrust is

$$T_t = \frac{TL_{F,STD}}{2} \quad (81)$$

where T_t is the factored thrust per unit length (lb/ft)

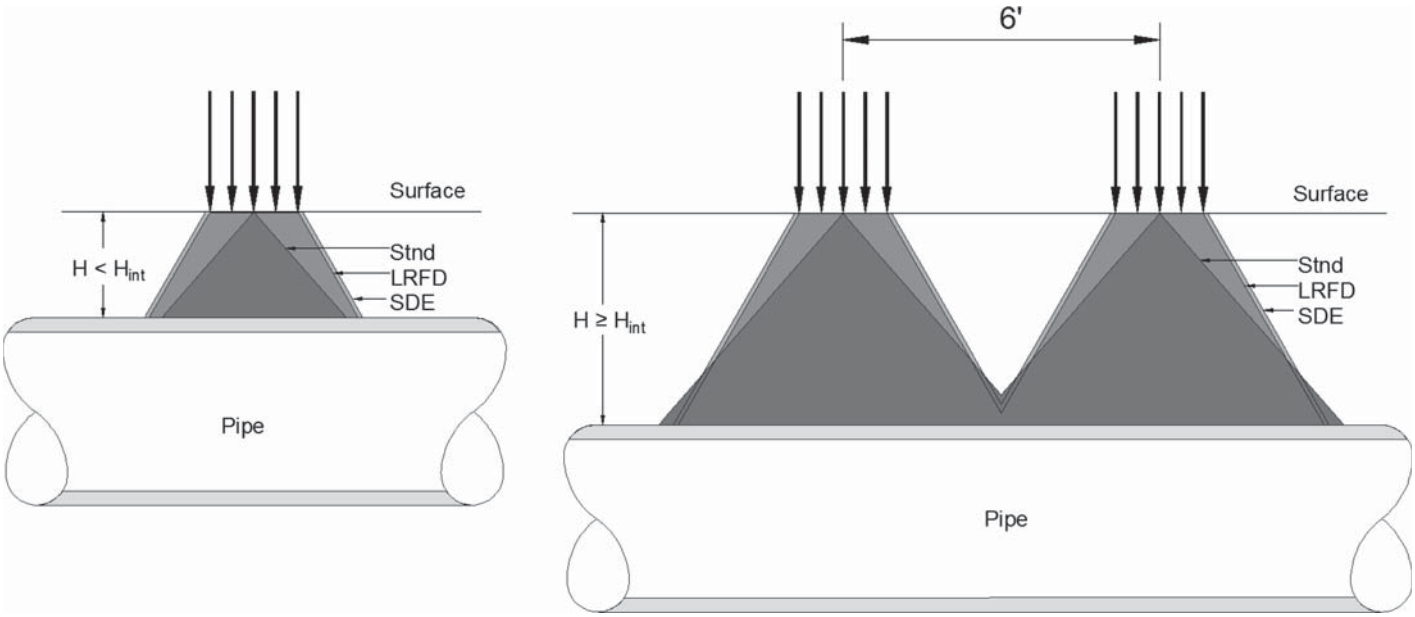

Figure 2-46. Live load variation with depth for thermoplastic pipe culverts.

Table 12.12.3.4-1 M_s Based on Soil Type and Compaction Condition.

P_{sp} Stress level (ksf)	Sn-100 (ksi)	Sn-95 (ksi)	Sn-90 (ksi)	Sn-85 (ksi)
0.15	2.350	2.000	1.275	0.470
0.75	3.450	2.600	1.500	0.520
1.50	4.200	3.000	1.625	0.570
3.00	5.500	3.450	1.800	0.650
6.00	7.500	4.250	2.100	0.825
9.00	9.300	5.000	2.500	1.000
P_{sp} Stress level (ksf)		Si-95 (ksi)	Si-90 (ksi)	Si-85 (ksi)
0.15		1.415	0.670	0.360
0.75		1.670	0.740	0.390
1.50		1.770	0.750	0.400
3.00		1.880	0.790	0.430
6.00		2.090	0.900	0.510
9.00				
P_{sp} Stress level (ksf)		Cl-95 (ksi)	Cl-90 (ksi)	Cl-85 (ksi)
0.15		0.530	0.255	0.130
0.75		0.625	0.320	0.175
1.50		0.690	0.355	0.200
3.00		0.740	0.395	0.230
6.00		0.815	0.460	0.285
9.00		0.895	0.525	0.345

1. The soil types are defined by a two-letter designation that indicates general soil classification, Sn for sands and gravels, Si for silts and Cl for clays. Specific soil groups that fall into these categories, based on ASTM D 2487 and AASHTO M 145, are listed in Table 2.
2. The numerical suffix to the soil type indicates the compaction level of the soil as a percentage of maximum dry density determined in accordance with AASHTO T 99.

Table 12.12.3.4-2 Equivalent ASTM and AASHTO Soil Classifications.

Basic Soil Type (1)	ASTM D 2487	AASHTO M 145
Sn (Gravelly sand, SW)	SW, SP (2) GW, GP sands and gravels with 12% or less fines	A1, A3 (2)
Si (Sandy silt, ML)	GM, SM, ML also GC and SC with less than 20% passing a No. 200 sieve	A-2-4, A-2-5, A4
Cl (Silty clay, CL)	CL, MH, GC, SC also GC and SC with more than 20% passing a No. 200 sieve	A-2-6, A-2-7, A5, A6

1. The soil classification listed in parentheses is the type that was tested to develop the constrained soil modulus values in Table 1. The correlations to other soil types are approximate.
2. Uniformly graded materials with an average particle size smaller than a No. 40 sieve shall not be used as backfill for thermoplastic culverts unless specifically allowed in the contract documents and special precautions are taken to control moisture content and monitor compaction levels.

Figure 2-47. AASHTO tables with modulus coefficients for thermoplastic pipe (profile wall).

Table 2-34. Outside diameter, mean radius and pipe unit area.

Nominal Diameter (in)	Outside Diameter D_o (in)	Mean Radius R (in)	Pipe Unit Area A_p (in^2/in)
24	28.32	13.08	0.344
48	54.24	25.56	0.48
60	67.02	31.75	0.541

For AASHTO LRFD Specifications

$$T_t = \frac{TL_{F,LRFD}}{2} \tag{82}$$

For the proposed live load equations, the following live load adjustments are required:

$$F_{1,\lim} = \max\left(15/D_i, 1\right) \tag{83}$$

$$F_1 = \max\left(F_{1,\lim}, 0.75 \cdot \left(\frac{D_i/12}{L_t/12 + LLDF_l \cdot H}\right)\right) \tag{84}$$

$$F_2 = \frac{0.95}{1 + 0.6 \cdot S_h} \tag{85}$$

$$T_t = \frac{\gamma_d \cdot DL + \gamma_l \cdot LL \cdot F_1 \cdot F_2}{2} \tag{86}$$

2.4.6.4 *Comparison between Standard, LRFD and Proposed*

Figure 2-48 provides comparisons of the peak thrust for thermoplastic pipe. This figure and comparison figures for all culvert types have a common format, described in Section 2.4.3.4.

The figure shows that the peak thrust for most cases are very similar. In general, the peak thrust from the SDEs is slightly greater than the peak thrust from the AASHTO Standard Method. Similarly, the peak thrust from the SDEs is slightly less than the peak thrust from the AASHTO LRFD Method.

Several data clusters are noteworthy. Four Standard Method data points at about 13.5 kips/ft correspond to four LRFD Method data points at about 8.5 kips/ft. These eight values are for 48-in.-diameter pipe buried 1 foot. The difference between the values is the different live load factors between the Standard and LRFD Methods, and special treatment required by the Standard Method for burial depths of less than 2 feet. The data points that plot below the 1:1 line between 6.0 and 7.5 kips/ft are for 2 feet of burial. For these cases, the SDEs are consistently less than either the Standard or LRFD values.

2.4.7 Corrugated Metal Arches

This section compares peak factored thrust for corrugated metal arches. In flexible large-span culverts, the design and performance depend on the interaction of the structure and the surrounding soil. Properties of the backfill envelope as well as in situ material have a major effect on the performance of these structures. AASHTO does not currently specify a factor for long-span metal arch to handle the interaction of the structure and the surrounding soil. A thrust modifier for long-span metal arch will be used in the SDE.

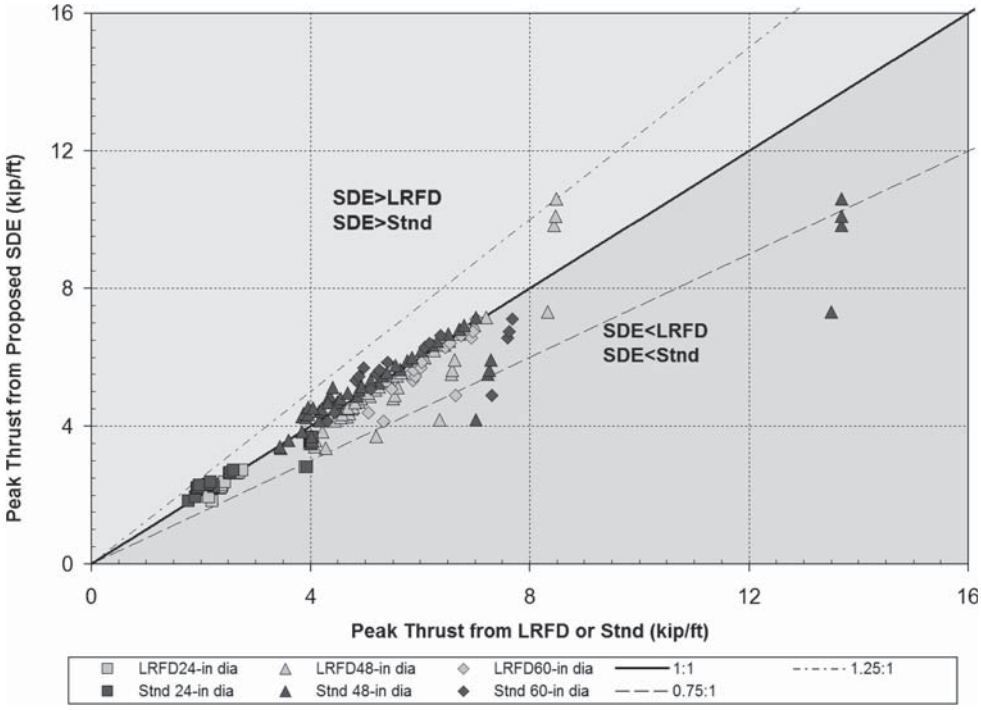

Figure 2-48. Peak thrust comparison for thermoplastic pipe (profile wall).

2.4.7.1 Live Load Equations

The proposed live load equations used for corrugated metal arches are as presented in Section 2.4.1.2, except the live load area is as follows.

Determine the wheel interaction depth

$$H_{\text{int}} = \frac{s_w - \frac{w_t}{12} - 0.06S}{LLDF_l} \tag{87}$$

For $H < H_{\text{int}}$

$$A_{LL} = \left(\frac{w_t}{12} + LLDF_l \cdot H + 0.06 \cdot S\right) \cdot \left(\frac{l_t}{12} + LLDF_l \cdot H\right) \tag{88}$$

For $H \geq H_{\text{int}}$

$$A_{LL} = \left(\frac{w_t}{12} + s_w + LLDF_l \cdot H + 0.06 \cdot S\right) \cdot \left(\frac{l_t}{12} + LLDF_l \cdot H\right) \tag{89}$$

where

H is the culvert depth, ft
w_t is the tire patch width, 20 in.
l_t is the tire patch length, 10 in.
S is the culvert span, feet
$LLDF_l$ is the AASHTO LRFD live load distribution factor, 1.15
s_w is the wheel spacing, 6 ft

The service live load is determined from

For AASHTO LRFD

$$W_L = MPF \cdot (1 + IM) \cdot W_{LL} \cdot \min(S, L_{t,gov}) \tag{90}$$

For AASHTO Standard

$$W_L = (1 + I) \cdot W_{LL} \cdot \min(S, LLDF_s \cdot H) \tag{91}$$

For proposed SDEs

$$W_L = MPF \cdot (1 + IM) \cdot W_{LL} \cdot \min(S, L_{t,gov}) \tag{92}$$

Where S is the culvert span, ft, and the other factors are as defined in previous sections.

Figure 2-49 compares the variation of live load with depth for corrugated metal arches, for the Standard, LRFD and proposed SDE. The SDE distribution starts out wider than LRFD, but increases in width with depth at the same rate as the LRFD.

2.4.7.2 Dead Load Equations

Corrugated metal arch dead loads are calculated from

$$W_e = w_e \cdot H \cdot S \tag{93}$$

where

w_e is the earth unit weight, pcf
W_e is the earth dead load, lb/ft
H is the culvert depth, ft
S is the outside span of the culvert, ft

The total dead load is

$$DL = W_e \tag{94}$$

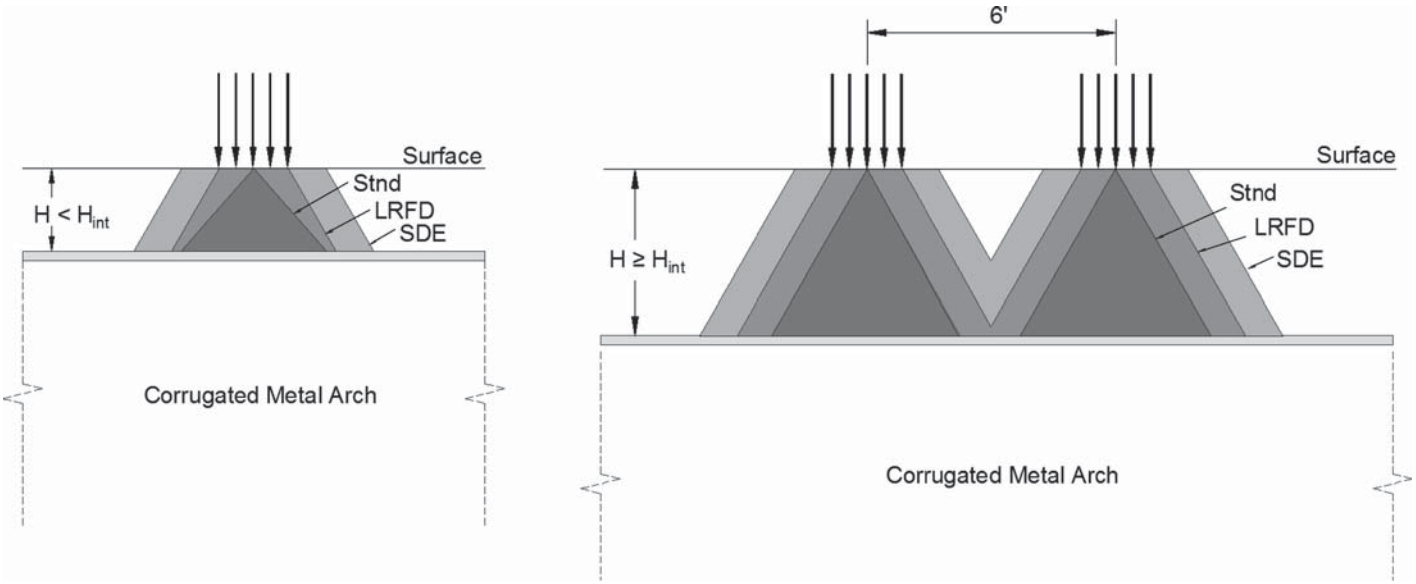

Figure 2-49. Live load variation with depth for corrugated metal arches.

2.4.7.3 Thrust Calculations

For AASHTO Standard Specifications, the total factored thrust is

$$T_t = \frac{TL_{F,STD}}{2} \tag{95}$$

where T_t is the factored thrust per unit length (lb/ft)

For AASHTO LRFD Specifications

$$T_t = \frac{TL_{F,LRFD}}{2} \tag{96}$$

For the proposed live load equations, the following live load adjustments are required:

$$F_{m.arch} = \frac{0.54 \cdot S}{\frac{w_t}{12} + LLDF_l \cdot H + 0.03 \cdot S} \tag{97}$$

$$T_t = \frac{\gamma_d \cdot DL + \gamma_l \cdot LL \cdot F_{m.arch}}{2} \tag{98}$$

2.4.7.4 Comparison between Standard, LRFD and Proposed

Figure 2-50 compares the peak thrust for corrugated metal arches. This figure and comparison figures for all culvert types have a common format, described in Section 2.4.3.4.

Design calculations were done for two arch sizes (20′-1″ × 9′-1″ and 30′-1″ × 18′) and four depths of burial. The 20-ft-span arch was designed for 1, 4, and 8 feet of burial, and the 30-ft-span arch was designed for 1, 2, and 8 feet of burial. Results for depths of 4 and 8 feet, where the dead loads are significant, show that the SDE results are essentially identical to the results from the Standard and LRFD methods (these are the data pairs at 12, 21, and 30 kip/ft). For burial depths of 1 foot and 2 feet, where live loads are greater, the SDEs produce peak thrusts 1.3 to 2.1 times greater than the corresponding values from Standard and LRFD Methods. The principal cause for the difference is the factor $F_{m,arch}$.

2.4.8 Concrete Arches

This section describes design calculations for concrete arches for AASHTO LRFD, AASHTO Standard, and proposed SDEs. Comparisons were made for peak thrust, peak shear, peak positive moment, and peak negative moment. Structural responses to the applied dead and live loads were computed using the 2D structural analysis program (SAP, 2000).

2.4.8.1 Live Load Equations

The proposed live load equations used for concrete arches are as presented in Section 2.4.1.2, except the live load area is as follows.

Determine the wheel interaction depth

$$H_{\text{int}} = \frac{s_w - \frac{w_t}{12} - 0.06S}{LLDF_l} \tag{99}$$

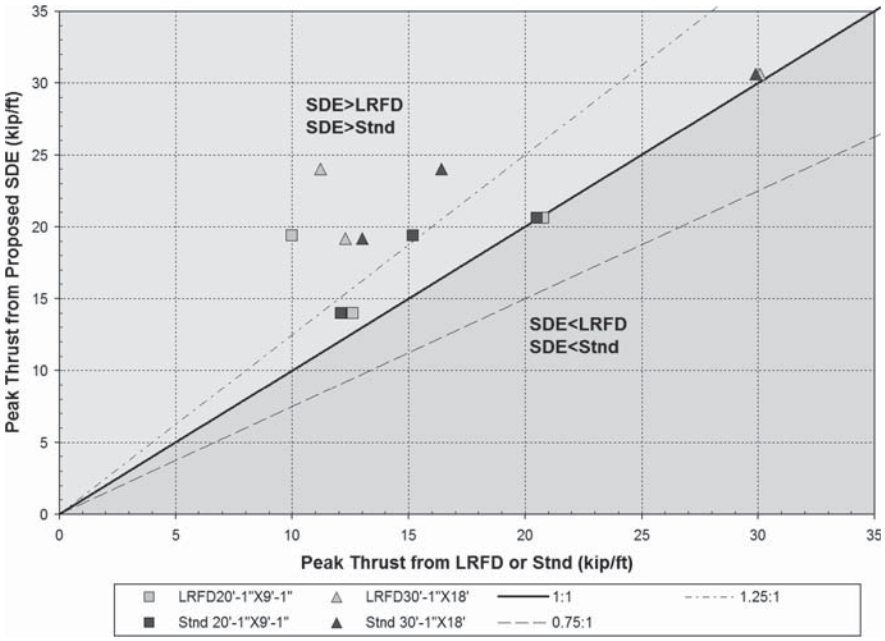

Figure 2-50. Peak thrust comparison for corrugated metal arches.

For $H < H_{int}$

$$A_{LL} = \left(\frac{w_t}{12} + LLDF_l \cdot H + 0.06 \cdot S\right) \cdot \left(\frac{l_t}{12} + LLDF_l \cdot H\right) \quad (100)$$

For $H \geq H_{int}$

$$A_{LL} = \left(\frac{w_t}{12} + s_w + LLDF_l \cdot H + 0.06 \cdot S\right) \cdot \left(\frac{l_t}{12} + LLDF_l \cdot H\right) \quad (101)$$

where

H is the culvert depth, ft
w_t is the tire patch width, 20 in.
l_t is the tire patch length, 10 in.
S is the culvert span, ft
$LLDF_l$ is the AASHTO LRFD live load distribution factor, 1.15
s_w is the wheel spacing, 6 ft

The service live loads were determined from

For AASHTO LRFD

$$W_L = MPF \cdot (1 + IM) \cdot W_{LL} \cdot \min(S, L_{t,gov}) \quad (102)$$

For AASHTO Standard

$$W_L = (1 + I) \cdot W_{LL} \cdot \min(S, LLDF_s \cdot H) \quad (103)$$

For proposed

$$W_L = MPF \cdot (1 + IM) \cdot W_{LL} \cdot \min(S, L_{t,gov}) \quad (104)$$

Where S is the culvert span, ft, and the other factors are as defined in previous sections.

Live loads were applied to the SAP2000 model in the locations illustrated in Figure 2-51, which also compares the variation of live load with depth for the Standard, LRFD, and proposed SDE. The SDE distribution starts out wider than LRFD, but increases in width with depth at the same rate as the LRFD.

2.4.8.2 Dead Load Equations

Typical earth-pressure distributions were used to evaluate thrust, shear, and moment in large-span arch culverts. Soil loads were calculated as follows:

$$\sigma_{ye} = K_e \cdot z \cdot w_e \quad (105)$$

$$\sigma_{yc} = K_c \cdot z \cdot w_e \quad (106)$$

$$\sigma_{xx} = K_h \cdot z \cdot w_e \quad (107)$$

where

σ_{ye} is the vertical pressure at the culvert edge, psf
σ_{yc} is the vertical pressure at the culvert centerline, psf
σ_{xx} is the horizontal pressure along the side of the culvert, psf

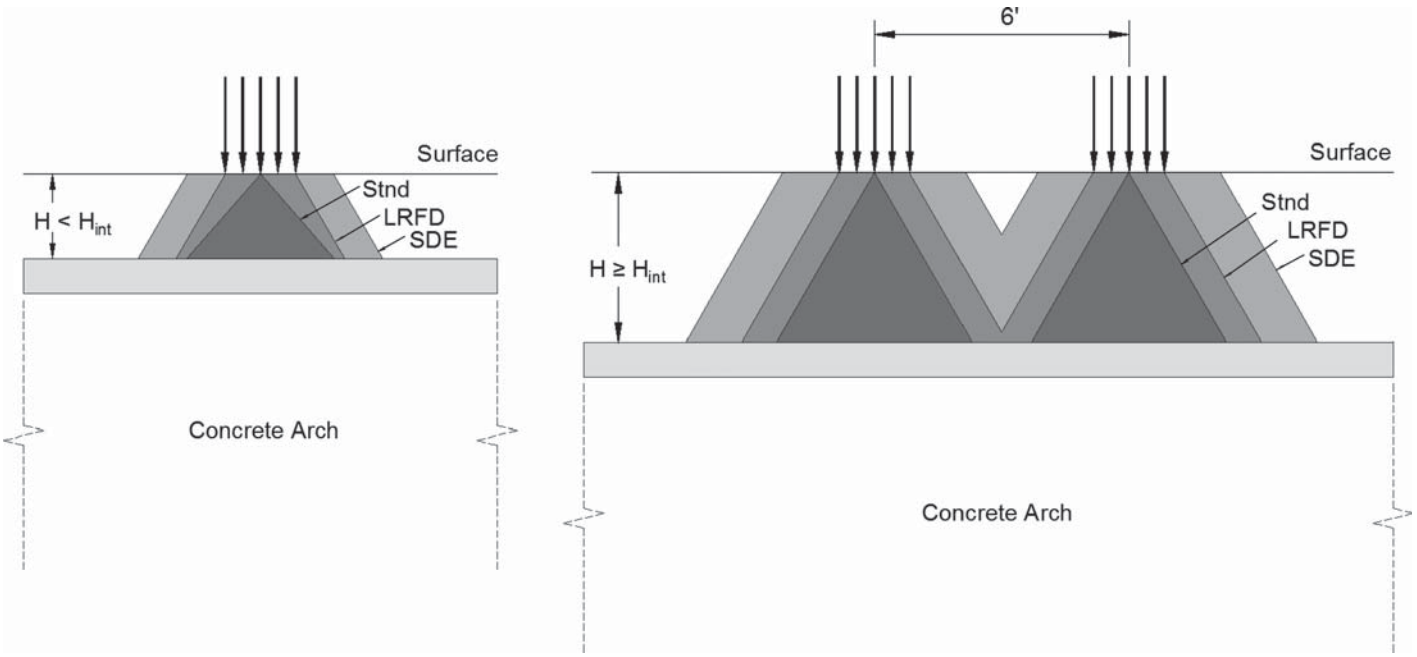

Figure 2-51. Live load variation with depth for concrete arches.

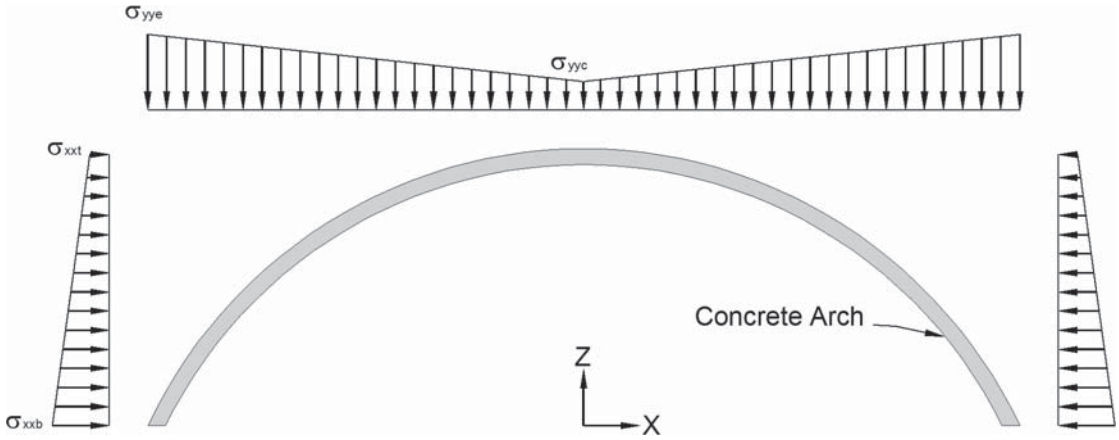

Figure 2-52. Concrete arch dead loads.

w_e is the earth unit weight, 120 pcf
z is the vertical distance from the surface to the point of interest, ft
K_e is the edge pressure coefficient, 1.2
K_c is the center pressure coefficient, 1.0
K_h is the horizontal pressure coefficient, 0.4

Concrete loads were calculated as follows:

$$W_{arch} = A_a \cdot w_c$$

where
W_{arch} is the weight of the concrete arch, lb/ft
A_a is the area of the concrete arch, square ft
w_c is the unit weight of concrete, 150 pcf

The dead loads applied to the SAP2000 model are illustrated in Figure 2-52.

2.4.8.3 Geometry and Material Properties

The geometry of the concrete arches is listed in Table 2-35. The concrete unit weight was 150 pcf.

2.4.8.4 Moment, Shear and Thrust Calculations

The 2D structural analysis program, SAP2000, was used to calculate the structural response to the loads described in the previous sections. Two analyses were performed for each arch-depth combination: one analysis was done with no lateral footing movement, and one analysis was done with lateral footing movement equal to 0.001 times the mean span, based on the recommendations of *NCHRP Report 473* (McGrath et al., 2002).

Table 2-35. Concrete arch geometry.

Nominal Span	Actual Span	Rise	Inside Radius
25'-4"	25' - 3-9/16"	10'-0"	13'-0"
43'-11"	43' - 11-3/8"	13'-8"	24'-6"

2.4.8.5 Comparison between Standard, LRFD, and Proposed SDEs

Figures 2-53 through 2-56 compare the peak thrust, peak shear, peak positive moment, and peak negative moment for concrete arches, respectively. These figures and comparison figures for all culvert types have a common format, described in Section 2.4.3.4.

Figure 2-53 illustrates that the peak thrusts calculated using the proposed SDEs are very similar to those calculated using the Standard and LRFD Methods. The peak thrusts are not significantly influenced by the footing boundary conditions.

Figure 2-54 illustrates the peak shear values calculated using the three methods. This graph shows that the footing movement condition has a much greater influence on peak shear values than peak thrust values. Peak shear values calculated using the proposed SDEs are very similar to those from the LRFD Method. There is no clear pattern to the SDE-Standard comparison—some are significantly more, some significantly less.

Figure 2-55 compares positive moments for the three live loads. The footing movement condition has a profound effect on positive moment—all data points with SDE-calculated values less than 10 kip-in/ft are for no footing movement, while all those greater than 10 kip-in/ft are for footing movement. In general, the positive moments determined using SDE live loads are the same or less than those determined from using Standard or LRFD loads, sometimes significantly less.

Figure 2-56 illustrates the peak negative moments from the three live load cases. SDE-based values on average are about

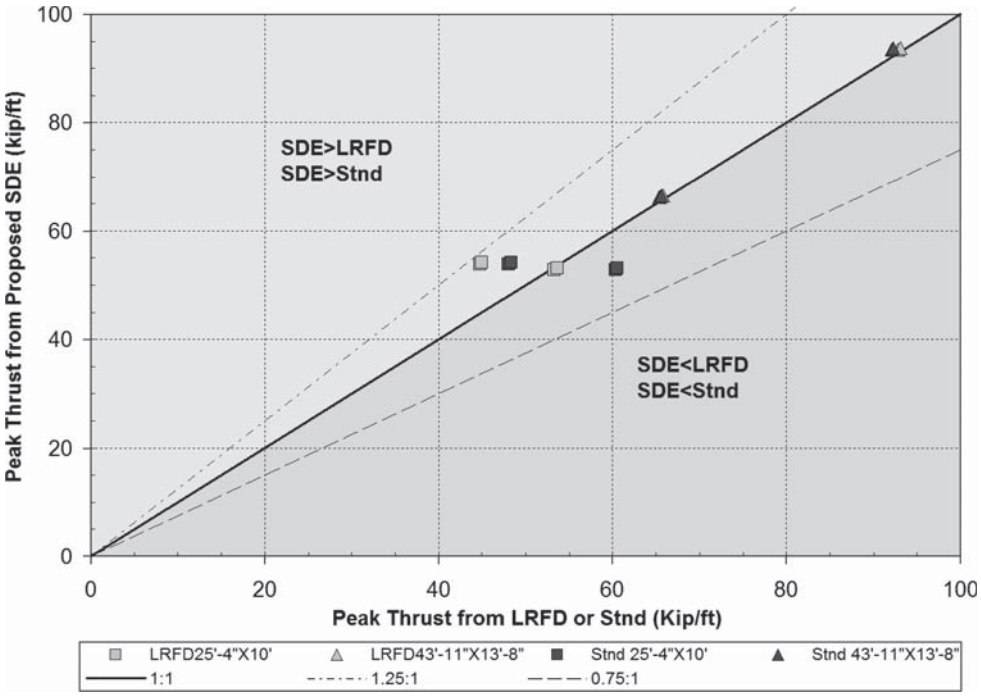

Figure 2-53. Peak thrust values for concrete arches.

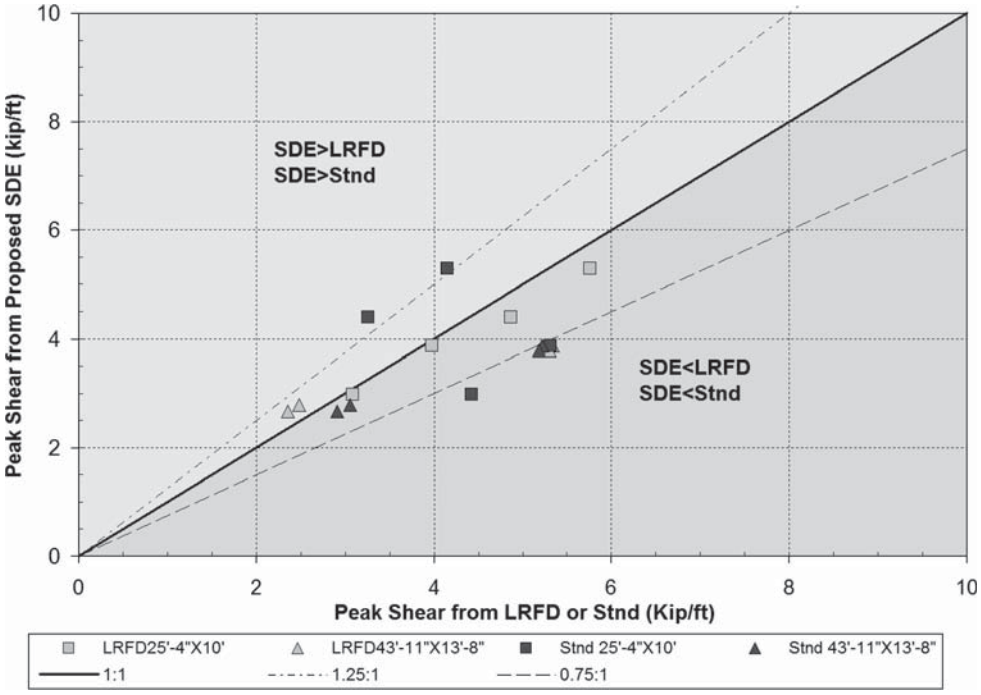

Figure 2-54. Peak shear values for concrete arches.

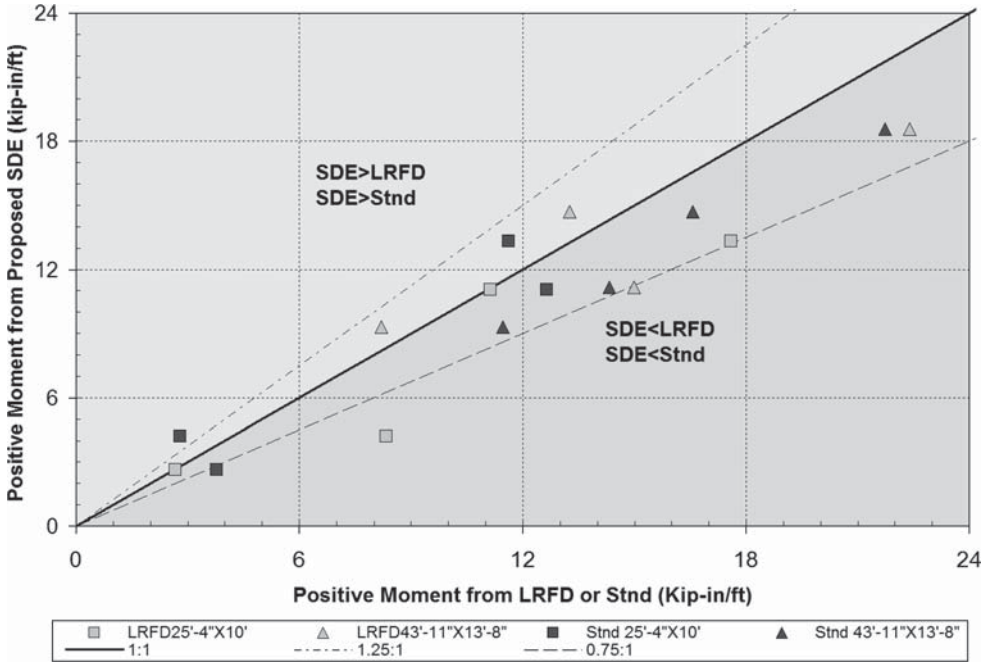

Figure 2-55. Peak positive moment values for concrete arches.

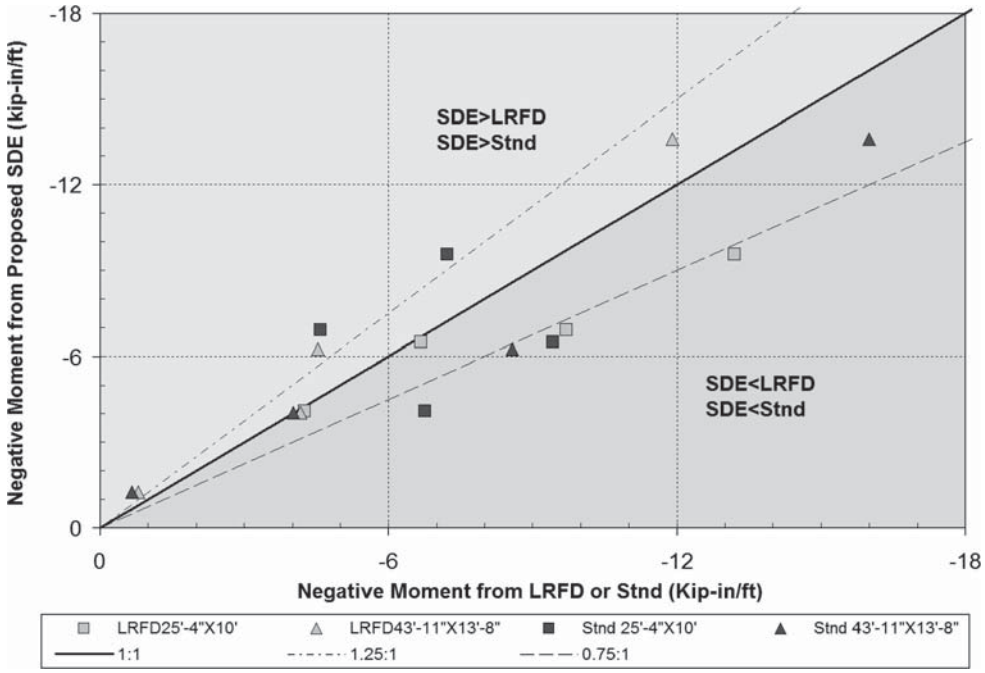

Figure 2-56. Peak negative moment values for concrete arches.

the same as from the Standard and LRFD loads, although there is a lot of scatter.

2.5 Guidelines for Use of Refined Analysis Methods

This project has conducted extensive 3D modeling of the transfer of surface live loads to buried culverts. From the results, the research team has proposed SDEs that permit culvert design without modeling. However, many design situations have conditions not covered by the SDEs. In these situations, 2D and 3D modeling may be used for design. The research team developed guidelines for conducting 2D and 3D modeling, based on the work reported in previous sections and on additional 2D and 3D modeling.

The guidelines are presented in detail in Appendix E. The 2D guidelines provide a means for selecting the surface load intensity to be applied to a 2D model. The 3D guidelines address

software, live load application, representations of the pavement and the soil, model dimensions, element size, symmetry and boundary conditions, representations of culvert structures, and the soil-culvert interface.

2.5.1 Guideline for 2D Analysis

2.5.1.1 Longitudinal and Transverse Subsurface Spreading

2D computer models have an inherent limitation when computing the effect of surface live loads. Because the models are 2D, the load spreading that occurs in the longitudinal direction, parallel to the axis of the culvert, cannot be correctly computed. The model represents a single, vertical slice through the real-world geometry.

Figure 2-8 illustrated the location and intensity of the live load. The vehicle centerline is in the left-right plane of symmetry and the culvert centerline is in the up-down plane of symmetry. This section refers to the left-right direction as the transverse direction and the up-down direction as the longitudinal direction.

The fundamental equation in all live load spread calculations is that the total force at depth H is equal to the total force at the surface:

$$F_S = F_H \tag{108}$$

The surface pressure is

$$P_S = \frac{LL}{w_t \cdot l_t} \tag{109}$$

For 3D spreading, the live load pressure at depth is the force divided by the area:

$$P_H = \frac{LL}{(w_t + LLDF \cdot H)(l_t + LLDF \cdot H)} \tag{110}$$

where

P_H is the vertical pressure at depth H
LL is the live load force at the surface, 16,000 lb unfactored
w_t is the transverse dimension of the tire patch, typically 10 in.
l_t is the longitudinal dimension of the tire patch, typically 20 in.
$LLDF$ is the live load distribution factor, 1.75 for Standard, for LRFD: 1.15 for granular fill, 1.0 for other fills

In the case of 2D modeling, models correctly determine the load spread in the transverse direction (in the plane of the model). In the longitudinal direction, 2D models do not compute load spreading. Hence, the live load must be factored (or "spread") to achieve the spreading that cannot be modeled.

Assuming that the transverse live load spread will be computed by the model, the vertical pressure at depth is

$$P_H^{2D} = \frac{LL}{(l_t + LLDF \cdot H)} \tag{111}$$

and at the surface

$$P_S^{2D} = \frac{LL}{l_t} \tag{112}$$

Hence, the ratio of the live load pressure at depth to the surface live load pressure is

$$\frac{P_H^{2D}}{P_S^{2D}} = \frac{l_t}{(l_t + LLDF \cdot H)} \tag{113}$$

2.5.1.2 2D and 3D Modeling

Preceding sections report the results of extensive 3D modeling of a range of culvert types, soils, and depths. All modeling was done with service live loads. Selected 3D models, with Mohr-Coulomb soil behavior were rerun with 16,000 lb live load, for comparison with analogous 2D modeling. The culvert types, sizes, depths, and soils were as follows:

1. Materials: Concrete Pipe (RCP), Corrugated Metal Pipe (CMP), Profile Wall Pipe (PW)
2. Size:
   a. RCP using 24-, 48-. and 96-in. dia.
   b. CMP using 12-, 24-, 48-, and 96-in. dia.
   c. PW using 12-, 24-, 48-, and 60-in. dia.
3. Soil Type: SW85
4. Cover Depth: 12, 24, 48, and 96 in.

The 2D models used FLAC3D (with a 2D geometry), unfactored loads, and elastic soil behavior. Elastic soil behavior was chosen because elastic models are most common.

Peak thrust and crown moment were compared by computing the following ratios of 3D structural response to 2D structural response:

$$TDRR_i^T = \frac{T_{p,3d}}{T_{p,2d}} \tag{114}$$

$$TDRR_i^{MC} = \frac{M_{c,3d}}{M_{c,2d}} \tag{115}$$

where

$TDRR_i^T$ is the Two-Dimensional Response Ratio for peak thrust, and
$TDRR_i^{MC}$ is the Two-Dimensional Response Ratio for crown moment.

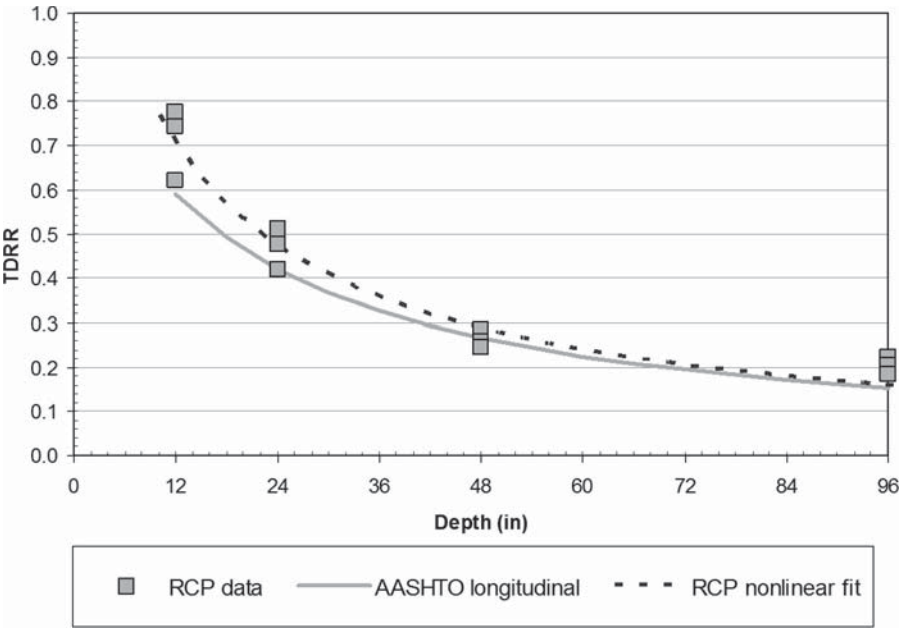

Figure 2-57. Peak thrust TDRR for concrete pipe (AASHTO refers to Eqn (113)).

Figures 2-57 through 2-59 illustrate the peak thrust 2D response ratio. The peak thrust generally does not occur at the crown of the culvert. Each figure includes the curve resulting from Eq. 113, with *f* equal to 1.15.

The peak thrust figures show that the TDRR is strongly influenced by culvert type. Figure 2-57, illustrating RCP results, shows that peak thrust response is very close to the longitudinal spread equation (Eq. 113). In comparison, Figure 2-58 shows that the profile wall response is about 1.5 times greater than Eq. 113. Figure 2-59 shows that the CMP response is similar to Eq. 113 at depths greater than 48 inches, but significantly higher at shallower depths.

Figures 2-60 through 2-62 illustrate the crown moment 2D response ratio. Each figure includes the curve resulting from

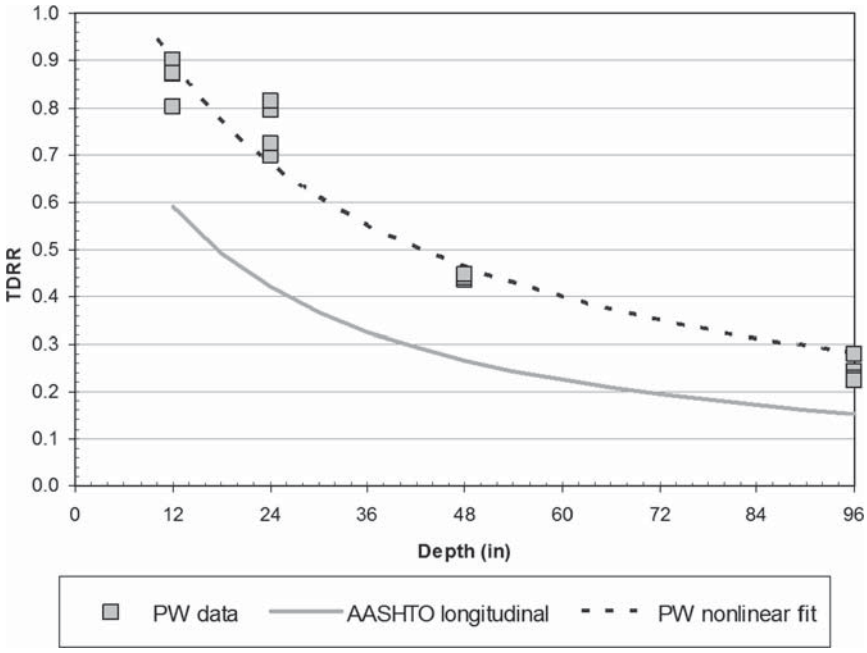

Figure 2-58. Peak thrust TDRR for profile wall (AASHTO refers to Eqn (113)).

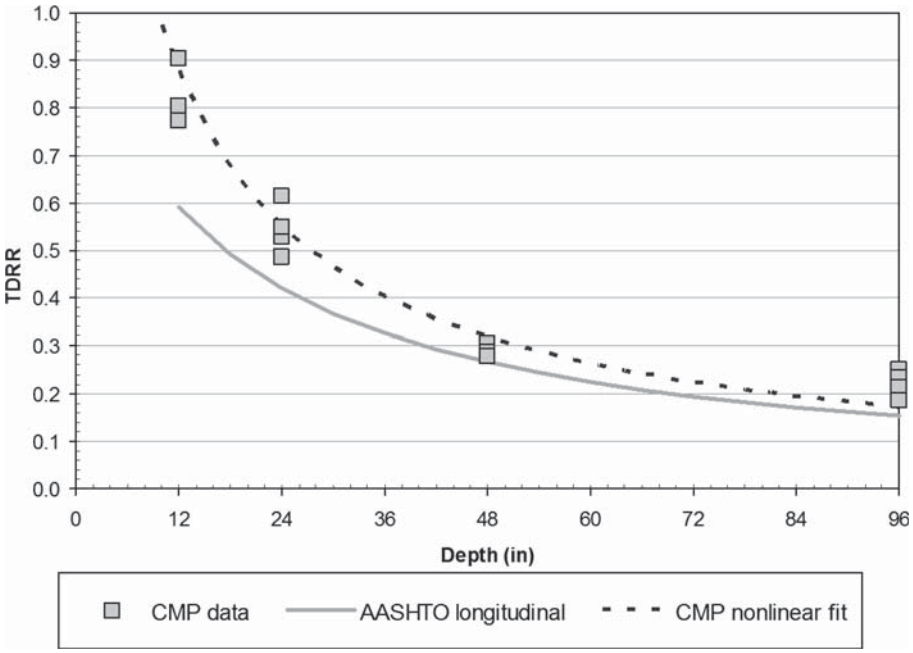

Figure 2-59. Peak thrust TDRR for corrugated metal pipe (AASHTO refers to Eqn (113)).

Equation 113, with *LLDF* equal to 1.15. Like the results for peak thrust, the crown moment results are strongly influenced by culvert type. For RCP (Figure 2-60), the model response is less at shallow depths and greater at 96 inches. The profile wall data (Figure 2-61) shows significant variation due to culvert diameters and is also significantly greater than Equation 113 for all depths. CMP results (Figure 2-62) are about the same as Equation 113 at 12 inches, but increase with increasing depth.

2.5.1.3 2D Guideline

To characterize the variations illustrated in the figures of the previous section, nonlinear curve fitting was used to select parameters for a variant of Equation 116, with one additional parameter:

$$\frac{P_H^{2D}}{P_S^{2D}} = TDRR = \frac{a \cdot l_t}{\left(l_t + b \cdot H\right)} \tag{116}$$

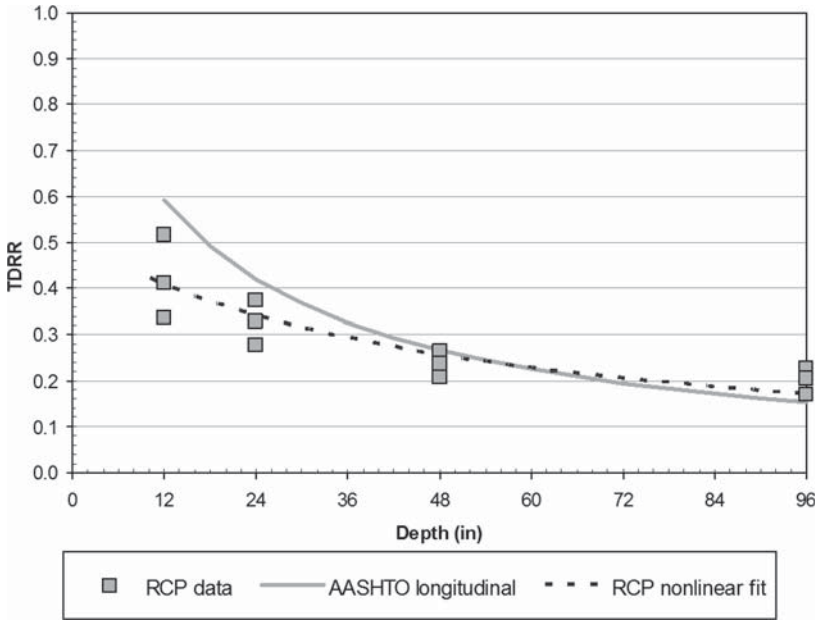

Figure 2-60. Crown moment TDRR for concrete pipe (AASHTO refers to Eqn (113)).

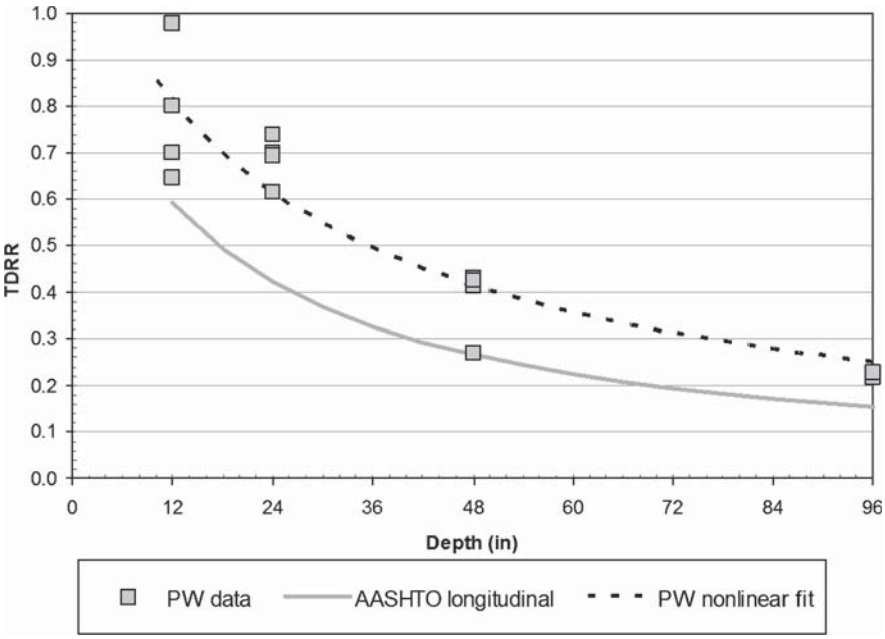

Figure 2-61. Crown moment TDRR for profile wall (AASHTO refers to Eqn (113)).

where *a* is the additional parameter and *LLDF* is replaced by *b*.

These parameters are to be selected from curve fitting. Microsoft Excel's Solver function was used to select values for these parameters, but minimizing the sum of the square differences between the function in Equation 116 and the data points. The nonlinear fit curves plotted on each figure illustrate that the curves fit the data relatively well.

Table 2-36 illustrates the resulting parameter values for Equation 116; and Figures 2-63 and 2-64 illustrate the composite graphs (all data and curves) for peak thrust and crown moment, respectively.

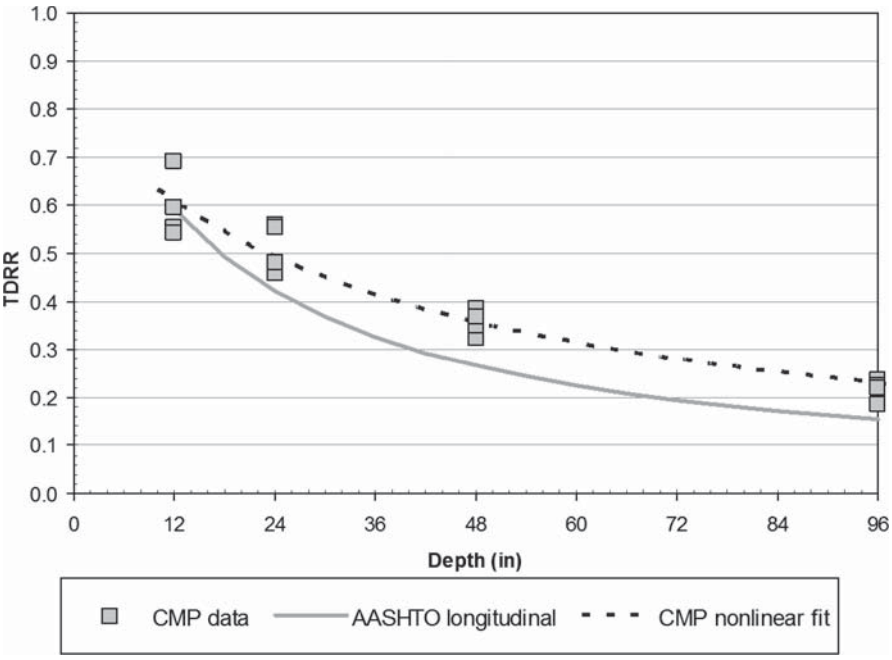

Figure 2-62. Crown moment TDRR for corrugated metal pipe (AASHTO refers to Equation 113).

Table 2-36. Two-dimensional response ratio equation parameters.

Culvert Type	Structural Response	Constant a	Constant b
Concrete Pipe	Peak Thrust	1.387	1.595
	Crown Moment	0.509	0.411
Profile Wall	Peak Thrust	1.303	0.757
	Crown Moment	1.195	0.787
Corrugated Metal Pipe	Peak Thrust	2.132	2.379
	Crown Moment	0.794	0.511

Figure 2-63 illustrates that nearly all data shows a TDRR greater than the longitudinal load spread from Eq. 113, and that there is a significant variation in the data depending on culvert type. Hence, the fitted curves also have significant variations. Figure 2-64 illustrates similar results for crown moment, except that the RCP data is less than Equation 116 for depths of 48 inches or less.

The resulting guideline for the surface pressure to be used for conducting 2D analyses is

$$P_S^{2D} = \frac{P_S^{3D} \cdot a \cdot l_t}{\left(l_t + b \cdot H\right)} \tag{117}$$

where

P_S^{2D} is the 2D surface pressure,
P_S^{3D} is the 3D surface pressure,
a and b are parameters from Table 2-36.

The parameters for peak thrust and crown moment are sufficiently different that separate analyses should be conducted for each.

2.5.2 Guideline for 3D Analysis

2.5.2.1 General Software Guidelines

Following are general software guidelines for conducting 3D analyses of live loads on culverts:

1. 3D elements, geometry, boundary conditions, etc.
2. Shell structural elements:
   a. Isotropic shell elements for isotropic culvert materials
   b. Orthotropic shell elements for orthotropic culvert materials
3. Ability to model live loads placed on the soil surface
4. At least the following constitutive models
   a. Elastic (for pavement)
   b. Mohr-Coulomb (for soil)
5. Soil-culvert interface logic that permits arbitrary interface strength and stiffness

2.5.2.2 Live Load Magnitude, Contact Area, Location

Analyses were conducted for dead load (soil loading only) and combined dead plus live load. The dead load response was subtracted from the combined response to determine the

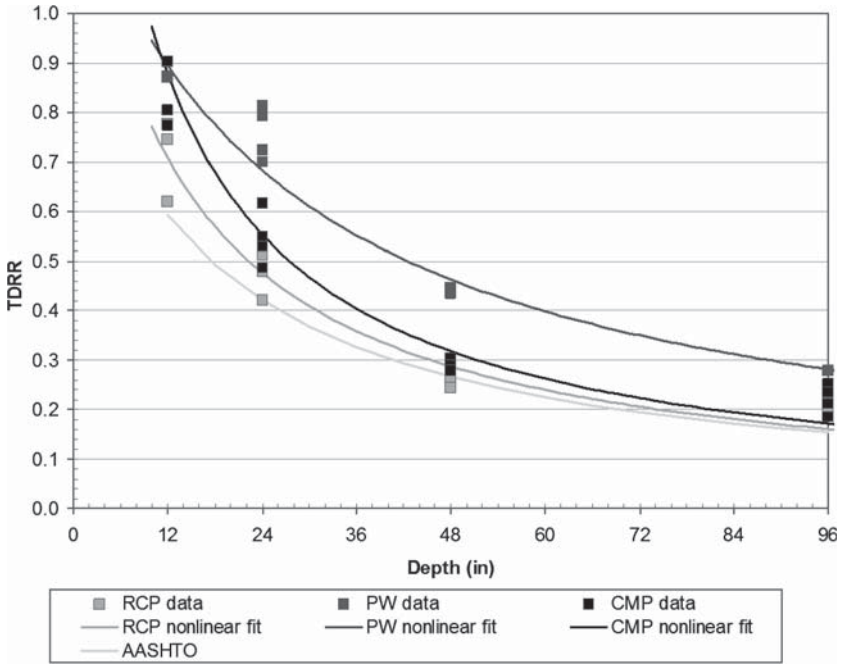

Figure 2-63. Composite graph for peak thrust two-dimensional response ratio (AASHTO refers to Equation 113).

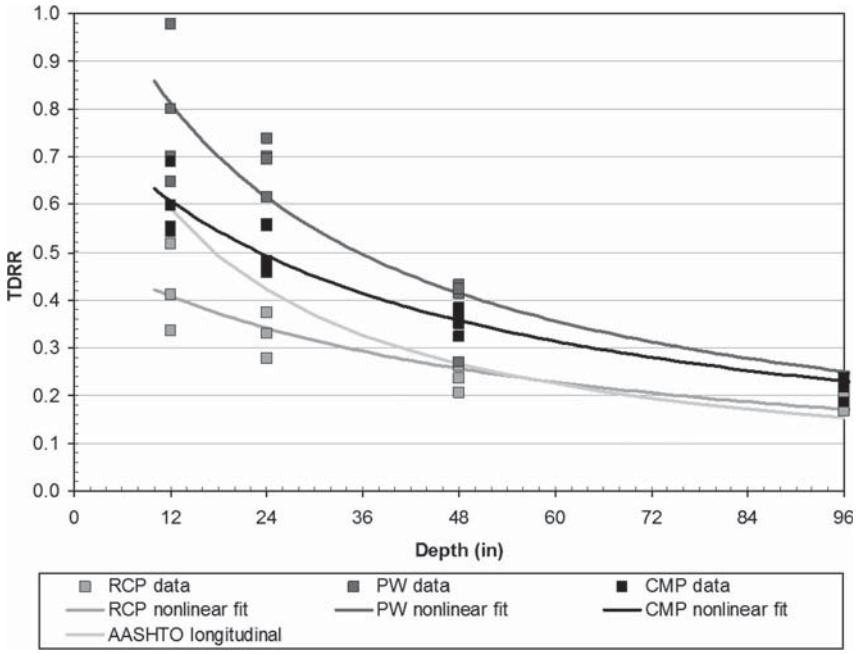

Figure 2-64. Composite graph for crown moment two-dimensional response ratio (AASHTO refers to Equation 113).

live only response. Dead loads, that is soil loads, were not factored. Live loads were applied and factored as follows:

$$LL = m_{mpf}\left[1+\frac{IM}{100}\right]P \qquad (118)$$

where

m_{mpf} is the multiple presence factor (1.2)

P is the wheel load magnitude (16,000 lb)

IM is the dynamic load allowance $33\left[1-\frac{0.125\cdot H}{12}\right], H \le 8$

H is the depth of cover from road surface to top of culvert, in.

In Figure 2-8, two surface load patches are included in the models, either explicitly or via symmetry, while the other load patches at the front and rear of the vehicle are not included. For some conditions, it may be necessary to include the other load patches.

2.5.2.3 Factored versus Unfactored Live Loads

The culvert community is divided on the issue of modeling using factored versus unfactored live loads. As a result, the study included a comparison of structural responses to unfactored and factored live loads.

If the structure and surrounding soil have linear-elastic material properties, structural responses to the factored live loads will differ from those to the unfactored live loads by a load factor. However, backfill surrounding the structure is nonlinear, and the ratio of structural response to the factored load to the response to the unfactored live load will not be exactly equal to the load factor. To examine the effect of soil nonlinearity, soil-structure interaction analyses were performed and compared for culverts subjected to factored and unfactored live loads. The analyses were for various 2D and 3D conditions, structure types, soil behavior, and software.

Based on the cases we examined, structural responses to the factored live load can be estimated by scaling unfactored live load responses by the load factor. The exceptions are thrusts for shallow burial.

2.5.2.4 Representing the Pavement

During the study, the number of models with and without concrete pavement was approximately equal. In models with concrete pavement, the pavement was represented by a single layer of zones with the elastic behavior and properties suitable for concrete. In models without pavement, live loads produced excessive localized bearing failure of the soil. As a result, the surface layer of zones was modeled using the same properties as the underlying zones, but with elastic rather than Mohr-Coulomb behavior.

Results showed that pavement spreads the load and shields the culvert. Because of the significant affect of this load spreading and shielding and given that live loads are possible prior to

paving or during roadway rehabilitation, the research team concluded that unpaved is the controlling case. The influence of pavement is greater for shallow culvert cover depth and flexible culverts and is smaller for stiffer culverts and deeper burial. For example, the ratios of unpaved to paved response were 1.0 to 3.3, for a 48-inch RCP culvert, with 2 feet of cover and SW85 soil. In contrast, the ratios of unpaved to paved response were 0.85 to more than 30, for a 48-inch profile wall culvert with 2 feet of cover and SW85 soil. Ratios were computed for crown and invert moment, crown and springline thrust, and crown and invert displacement.

2.5.2.5 Soil Constitutive Models

In this study, the research team found that a linearly elastic, perfectly plastic model with a Mohr-Coulomb failure criterion was appropriate. This selection offers the best mix of capturing the important aspects of soil behavior in transmitting live loads to structures. The Mohr-Coulomb constitutive model does not offer all of the benefits of the Duncan-Selig/hardening-soil models in capturing stress-dependent stiffness behavior of soil, but for a live load study, the Mohr-Coulomb model appears to provide sufficient accuracy.

2.5.2.6 Soil Properties

All models used one of four soil materials: well-graded or gravelly sand at 85-percent standard compaction (SW85), well-graded or gravelly sand at 95-percent standard compaction (SW95), inorganic silts and fine sands at 85-percent standard compaction (ML85), and inorganic clays at 85-percent standard compaction (CL85). The research team recommends that angles of friction at a reference confinement of 14.7 psi from Selig's parameters (1988) be used at any depth in the 3D analysis instead of variable angles of friction calculated from the stress state before the live load application. (Mohr-Coulomb soil parameters for SW95, SW85, ML85, and CL85 are presented in Chapter 3.4.2 of Appendix E. If site-specific soil properties are known, these values should be used instead of the values presented in the appendix.)

Near-surface soil modulus measurements using the Humboldt GeoGauge, lightweight deflectometer, and dynamic cone penetrometer (DCP) produce near-surface values significantly higher than the values presented in the preceding paragraphs. The modulus values for SW85 and SW95 are lower bounds for DCP data from one site. Many DCP values are 2 to 5 times greater.

Because the focus of NCHRP Project 15-29 was live load effects, inhomogeneous culvert bedding was not modeled, so the research team cannot offer any guidelines for modeling culvert bedding.

2.5.2.7 Model Dimensions and Element Size

In general, model dimensions were larger for increasing cover depth and increasing culvert diameter (span). In some instances, the research team initially used smaller model widths, observed results indicating that the models were too narrow, and reran the models using greater width. (Chapter 3.5 of Appendix E summarizes the model dimensions.)

The size of continuum elements used in the study varied depending on the size of the culvert and the location of the element in the model. In general, smaller elements were used for smaller culvert diameters and larger elements were used for larger culvert diameters. Element size also increased with distance away from the live load—the largest elements were typically at the bottom corner of the model at the end farthest from the live load. Table 2-37 lists the continuum and structural element sizes for nine selected models. Given that the continuum element sizes near the culvert are wedge-shaped, the inner and outer width are listed.

During the study, the research team found the element sizes were sufficiently small to produce good results.

Table 2-37. Continuum and structural element sizes for selected models.

Case	Minimum Continuum Element Size (inches)	Maximum Continuum Element Size(inches)	Minimum Structural Element Size(inches)	Maximum Structural Element Size(inches)
12-inch round	1.6-3.8 x 6 x 6	6 x 6 x 11	1.6 x 6	1.6 x 11
24-inch round	2.4-4.1 x 6 x 6	6 x 10 x 11	2.4 x 6	2.4 x 11
48-inch round	2.4-3.2 x 6 x 6	9 x 11 x 11	2.4 x 6	2.4 x 11
96-inch round	3.8-4.5 x 6 x 6	12 x 12 x 11	3.8 x 6	3.8 x 11
120-inch round	3.4-3.8 x 3.9 x 6	23 x 24 x 11	3.4 x 6	3.4 x 11
25.4 ft x 10 ft conc. arch	12 x 6 x 6	12 x 12 x 18	6 x 6	6 x 18
43.1 ft x 13.8 ft conc. arch	3 x 7 x 6	18 x 18 x 18	7 x 6	7 x 18
20.1 ft x 9.1 ft metal arch	3 x 6 x 6	17 x 12 x 18	6 x 6	6 x 18
30.1 ft x 18 ft metal arch	3 x 8 x 6	17 x 18 x 18	8 x 6	8 x 18

2.5.2.8 Symmetry and Boundary Conditions

Planes of symmetry may be used to reduce the size of and simplify models. All culvert structures modeled were symmetric about a vertical plane of symmetry through the culvert axis. The culvert structures were also of uniform cross section, so planes of symmetry could be used to reduce the length of the models.

The live load magnitudes and geometry illustrated in Figure 2-8 are symmetric about the centerline of the vehicle (which is perpendicular to the centerline of the culvert). The live load is not symmetric about the centerline of the culvert, if all three axles are included. However, for a single, relatively shallow culvert, the front and rear axles do not significantly affect culvert loads. As a result, the research team ignored the live loads from the front and rear axles. The result is a live load distribution that is symmetric about the culvert axis. Nearly all models in this study employed two planes of symmetry to reduce model size. A few analyses did not use the plane of symmetry through the culvert axis to check the analysis results.

Boundary conditions for the continuum (soil) parts of the models were straightforward—live loads were applied as pressures on the model top surface and all other surfaces had free or fixed displacements. The conditions were as follows:

1. Model top—The top was free, with a 10- by 20-inch patch of live load applied as shown in Figure 2-8.
2. Model bottom—The top was fixed in the vertical direction and free otherwise.
3. Model ends—The model ends, where the ends of the culvert were exposed, were fixed in the direction parallel to the culvert axis and free otherwise.
4. Model sides—The model side that contained the culvert centerline was fixed in the horizontal direction perpendicular to the culvert axis and free otherwise. The model side opposite the culvert centerline had the same boundary condition, meaning that it was also a plane of symmetry.

Boundary conditions for the culvert were similar:

1. Culvert ends—The culvert ends, where the end of the culvert was exposed, were fixed in translation in the direction of the culvert axis and were fixed in rotation about the vertical and transverse direction. All other degrees of freedom were free.
2. Culvert crown and invert—The culvert crown and invert, where cut by the plane of symmetry, were fixed in translation perpendicular to the culvert axis and were fixed in rotation about the longitudinal and vertical direction. All other degrees of freedom were free.

During the study, the research team became concerned that translational fixity of the culvert ends was increasing the stiffness of the overall culvert structure. A few analyses were rerun with no translation fixity of the culvert ends. The results were only slightly different, confirming that this boundary condition was not affecting the results.

2.5.2.9 Culvert Structure Representation

Culvert structures may be represented as

1. Continuum elements, where the structure is built up as a series of continuum elements across the thickness of the structure. This method was used in 2D analyses to model box culvert haunch behavior, as a basis for selecting structural element properties.
2. Multiple structural elements, where the culvert is built up of structural elements. This method was used to model the complex interior structure of profile wall pipe for comparison with orthotropic structural elements.
3. Single structural elements, where a single element (of zero thickness) is used to represent a segment of the culvert. This method was used for most analyses.

In all cases, the structures were linear elastic.

The three methods have advantages and disadvantages, but in general, the built-up methods (either continuum elements or structural elements) were only used in special cases where a single, zero-thickness structural element was not adequate. In this study, single structural elements were used to represent the culverts in all production analyses.

In 3D, structural elements for representing culverts must accommodate both bending action and membrane action. As a result, shell elements are necessary and were used for all production analyses. The formulation of shell elements does not permit the calculation of transverse shear forces.

2.5.2.10 Requirements for Iso- and Orthotropic Structural Elements

Culverts composed of solid material and regular geometry may be represented by isotropic structural elements (i.e., bending and membrane properties are the same in all directions). This category of culverts includes concrete boxes and concrete pipe, smooth steel pipe, and smooth thermoplastic pipe.

Both plastic and metal culvert products use cross-sectional shapes that are orthotropic, meaning the structural properties vary by direction. These culvert shapes typically have much higher circumferential bending stiffness than longitudinal bending stiffness. In addition, the circumferential membrane stiffness is much higher than the longitudinal membrane stiffness. In plane shear stiffness is reduced from that of flat plate of the same thickness. In order to accurately model

buried pipes with such properties, accurate and well-behaved 3D orthotropic structural elements that permit specification of different stiffnesses for bending and membrane behavior are needed.

Before a discussion of modeling with 3D shells, the analogous issue in two dimensions will be described. A 2D beam formulation permits specification of the following properties:

1. Material Young's modulus, E
2. Member area, A, used to calculate the axial stiffness EA of the member
3. Member moment of inertia, I, used to calculate the bending stiffness EI of the member

If the beam were of solid cross section, A and I could be calculated from the beam width and thickness. However, commonly used beams are not of solid cross section and hence the area, A, and moment of inertia, I, must be specified separately.

Modeling of a 3D shell presents a similar challenge. The current formulation of shell elements in many structural analysis programs is based on a "solid" representation of the shell. For profile wall pipes, which are not solid, and for corrugated metal culverts, which are not "solid" due to the corrugations, two bending stiffnesses and two membrane stiffnesses must be specified to capture the structural behavior. Typical software permits only three of the four stiffness pairs (i.e., EAtransverse, EAlongitudinal, EItransverse, and EIlongitudinal) to be specified independently. At the start of the study, FLAC3D also had this restriction, but Itasca Consulting Group modified the software to permit the four stiffness pairs to be input independently. Results were confirmed by several culvert and non-culvert test cases.

Two guidelines resulted. When modeling orthotropic culverts

1. Use orthotropic shell elements for all culvert types that are orthotropic, and
2. Confirm via simple demonstration analyses that the 3D analysis software correctly models orthotropic materials. (The research team found that a model of a plywood plate with 2×4 stiffeners in one direction was effective in confirming model behavior.)

2.5.2.11 Culvert Joints

In distributing live loads through fill onto buried structures, practice has been to ignore the presence of joints in a pipe. This results in two potential issues:

1. The discontinuity created by a pipe joint will prevent load spreading though the pipe, resulting in an overstress.
2. A joint loaded on one side, but not the other, will undergo differential deflection, resulting in a joint leak.

Parameters that could affect this condition include

1. Pipe bell and spigot joints are often heavier and stronger than the barrel, providing more strength to resist the live load. Bells are typically thicker than pipe barrels, and the spigots, which may not be thicker than the barrels, are contained within the bell which provides additional confinement.
2. Pipe joints completed by wrap around couplings provide a mechanical connector to two adjacent lengths of pipe that likely provides shear transfer.
3. Unlike box culvert slabs, buried pipes are not assumed to have any inherent load distribution capability (i.e., in a box culvert under less than 2 feet of fill, a live load is distributed over a width about 4 feet wider than the actual loaded width, while in pipe the loaded length is typically assumed to carry the entire load.)
4. Most thermoplastic pipes are required to pass joint shear tests that require imposition of an unbalanced load without causing leakage. Concrete pipes have a joint shear test, but drainage pipes are not typically subjected to it. Metal pipes do not currently have a joint shear test.
5. Most pipes have excess structural capacity at the minimum depths of fill allowed by specifications. Minimum depths of fill are set to control road surface performance and are virtually always, if not always, set at depths where the pipe has extra capacity to carry unanticipated loads.

The research team is not aware of any definitive studies on the above issues and thus cannot state with certainty that the presence of a joint can be ignored when distributing live loads through earth fills; however, the lack of any problems associated with this matter is compelling. It is well known that pipes can be subjected to severe abuse during installation and are often installed in backfill conditions that do not comply with specifications or are subjected to large construction loads that exceed design loads. Despite this, problems are limited and often only result from extreme loading conditions.

Each culvert type has one or more different joint types, each with different behavior. The research team's full-scale models use shell elements to represent the culverts. In order to provide the basis for incorporating joints in full-scale models, large, complex models using continuum elements would need to be developed, tested, and analyzed for each joint type. The macro structural properties of each joint could then be incorporated in a structural element model. Consideration of gasket pressures would also be required.

The research team believes that the technical points outlined above are sufficiently compelling that, when combined with the practical considerations, support a decision to address jointed culverts in the commentary.

2.5.2.12 Soil-Culvert Interface

The soil-culvert interface connects the continuum elements representing the soil to the structural elements representing the culvert. Historically, it was common to model soil-culvert interaction with no interface—the soil and culvert structure were bonded and, in fact, had common nodes.

Now, in typical formulations, the interface has stiffness and strength properties, which vary depending on compression or tension loading. If modeled in this manner, nonlinear behavior may occur in the interface between the culvert and the soil, or in the soil.

The influence of the soil-culvert interface stiffness on culvert response was not investigated, so the research team offers no guidelines.

For preliminary 2D analyses, the interface strength was 50% of the soil shear strength. To examine the effect of interface strength on structural response, the research team analyzed the concrete and thermoplastic pipe with backfill modeled by the Mohr-Coulomb constitutive model with the interface strength equal to 100% of the soil shear strength. Structural responses to live loads did not change significantly when the interface strength was changed from 50% of the soil shear strength to 100%, although the cases with the 100% strength showed slightly larger peak responses than those with the 50% strength, except for moments of the thermoplastic pipe with 2-ft cover. A change in the interface strength affected thrusts more than moments. Structural responses of the thermoplastic pipe were affected more by a change of interface strength than those of the concrete pipe. Structural responses of the 6-ft cover cases were affected more by a change of interface strength than those of the 2-ft cover cases; however, responses of the 6-ft cover cases were much smaller than those for the 2-ft cover cases.

For 3D analyses, the influence of soil-culvert interface strength was investigated, for a few culvert types, sizes, and depths, by varying the interface strength. Four interface strengths were considered:

1. Fully bonded—No relative deformation was permitted between the soil and the culvert.
2. 100% soil strength—Interface strength was 100% of the soil friction angle and 100% of the soil cohesion.
3. 50% soil strength—Interface strength was 50% of the soil friction angle and 50% of the soil cohesion.
4. Unbonded—Interface friction and cohesion were zero.

Interfaces had a Mohr-Coulomb failure criterion.

Most production analyses were conducted for interfaces with strength properties of 100% of the soil strength. As with the 2D results, the 3D results show that the reasonable interface strengths do not have significant influence on the structural response.

2.5.2.13 Modeling Sequence

Three states of the model were analyzed and saved for each analysis conducted:

- State 1 is the soil mass in equilibrium, with no culvert or live load. State 1 was achieved by creating the model grid, applying material properties to the soil materials, and placing stresses in the grid.
- State 2 (dead load) is the soil mass plus the culvert, in equilibrium. This state was achieved by excavating the soil (with no cycling of the model), installing the culvert in the soil, and then cycling to equilibrium.
- State 3 (dead load plus live load) is State 2 plus application of the live load defined above.

While saving and reviewing States 1 and 2 is not necessary in order to find State 3, the research team recommends conducting analyses in this manner.

CHAPTER 3

Interpretation, Appraisal, and Applications

Previous chapters have described the computer model basis for, development of, and assessment of the effect of new SDEs for live loads on buried structures. This chapter summarizes the SDEs, describes the recommended changes to the AASHTO LRFD Design Specifications, and discusses the overall design and reliability margin.

3.1 SDEs

This section summarizes the proposed live load SDEs. The form of the live load equations is similar for all types of pipe.

3.1.1 AASHTO LRFD Live Load Equations

The live load equations for the AASHTO LRFD Specification are

$$LL = L_{HS20} \tag{1}$$

where

L_{HS20} is the wheel load from the HS20 load case, 16,000 lb, and
LL is the live load force, lb

Determine the wheel interaction depth

$$H_{\text{int}} = \frac{s_w - w_t/12}{LLDF_l} \tag{2}$$

where

H_{int} is the wheel interaction depth, ft
s_w is the wheel spacing, 6 ft
w_t is the tire patch width, 20 in.
$LLDF_l$ is the live load distribution factor, 1.15

Determine the live load area and pressure

$$\text{For } H < H_{\text{int}} \quad A_{LL} = \left(\frac{w_t}{12} + LLDF_l \cdot H\right) \cdot \left(\frac{l_t}{12} + LLDF_l \cdot H\right) \tag{3}$$

$$W_{LL} = LL/A_{LL} \tag{4}$$

$$\text{For } H \geq H_{\text{int}} \quad A_{LL} = \left(\frac{w_t}{12} + s_w + LLDF_l \cdot H\right) \cdot \left(\frac{l_l}{12} + LLDF_l \cdot H\right) \tag{5}$$

$$W_{LL} = 2 \cdot LL/A_{LL} \tag{6}$$

where

H is the culvert depth, ft
l_t is the tire patch length, 10 in.
A_{LL} is the live load area, sf
W_{LL} is the live load pressure, psf

Determine the governing load length

$$\text{For } H < 0.833 \qquad L_{t,gov} = l_t/12 \tag{7}$$

$$\text{For } H < 0.833 \qquad L_{t,gov} = \frac{l_t}{12} + LLDF_l \cdot H \tag{8}$$

where $L_{t,gov}$ is the governing load length, ft

Determine the dynamic load allowance

$$\text{For } H < 8\,ft \qquad IM = 33 \cdot \left(\frac{1 - H/8}{100}\right) \tag{9}$$

$$\text{For } H \geq 8\,ft \qquad IM = 0 \tag{10}$$

where IM is the dynamic load allowance

Determine the service live load

$$W_L = MPF \cdot (1 + IM) \cdot W_{LL} \cdot \min\left(D_i/12, L_{t,gov}\right) \tag{11}$$

where

MPF is the multiple presence factor, 1.2
D_i is the inside diameter or span of the culvert, in.

3.1.2 Concrete Box Live Load Equations

The proposed live load equations used for concrete box design calculations are as presented in Section 3.1.1, except the interaction depth, live load area, and pressure are as follows.

Determine the wheel interaction depth

$$H_{\text{int}} = \frac{s_w - \frac{w_t}{12} - \frac{0.06 D_i}{12}}{LLDF_l} \tag{12}$$

where

H_{int} is the wheel interaction depth, ft
s_w is the wheel spacing, 6 ft
w_t is the tire patch width, 20 in.
$LLDF_l$ is the live load distribution factor, 1.15
D_i is the inside span of the culvert, in.

$$\text{For } H < H_{\text{int}} \quad A_{LL} = \left(\frac{w_t}{12} + LLDF_l \cdot H + 0.06 \cdot D_i / 12 \right) \cdot \left(\frac{l_l}{12} + LLDF_l \cdot H \right) \tag{13}$$

$$\text{For } H \geq H_{\text{int}} \quad A_{LL} = \left(\frac{w_t}{12} + s_w + LLDF_l \cdot H + 0.06 \cdot D_i / 12 \right) \cdot \left(\frac{l_l}{12} + LLDF_l \cdot H \right) \tag{14}$$

where

H is the culvert depth, ft
w_t is the tire patch width, 20 in.
l_t is the tire patch length, 10 in.
$LLDF_l$ is the AASHTO LRFD live load distribution factor, 1.15

3.1.3 Concrete Pipe Live Load Equations

The proposed live load equations used for concrete pipe design calculations are as presented in Section 3.1.1, except as follows:

$$\text{For } D_i \leq 24in \qquad LLDF_{cp} = 1.15 \tag{15}$$

$$\text{For } 24in < D_i \leq 96in \qquad LLDF_{cp} = 0.00833 \cdot D_i + 0.95 \tag{16}$$

$$\text{For } D_i > 96in \qquad LLDF_{cp} = 1.75 \tag{17}$$

where $LLDF_{cp}$ is the live load distribution factor for concrete pipe

Determine the wheel interaction depth

$$II_{\text{int}} = \frac{s_w - \frac{w_t}{12} - \frac{0.06 D_i}{12}}{LLDF_{cp}} \tag{18}$$

Determine the live load area and pressure

$$\text{For } H < H_{\text{int}} \quad A_{LL} = \left(\frac{w_t}{12} + LLDF_{cp} \cdot H + 0.06 \cdot D_i / 12 \right) \cdot \left(\frac{l_t}{12} + LLDF_{cp} \cdot H \right) \tag{19}$$

$$\text{For } H \geq H_{\text{int}} \quad A_{LL} = \left(\frac{w_t}{12} + s_w + LLDF_{cp} \cdot H + 0.06 \cdot D_i / 12 \right) \cdot \left(\frac{l_t}{12} + LLDF_{cp} \cdot H \right) \tag{20}$$

Determine the governing load length

$$\text{For } H < 0.833 \qquad L_{t.gov} = l_t / 12 \tag{21}$$

$$\text{For } H < 0.833 \qquad L_{t.gov} = \frac{l_t}{12} + LLDF_l \cdot H \tag{22}$$

where

H is the culvert depth, ft
w_t is the tire patch width, 20 in.
l_t is the tire patch length, 10 in.
D_i is the inside span of the culvert, in.
$L_{t.gov}$ is the governing load length in inches

3.1.4 Corrugated Metal Pipe Equations

3.1.4.1 Live Load Equations

The proposed live load equations used for corrugated metal pipe are as presented in Section 3.1.1, except the live load area is as follows.

Determine the wheel interaction depth

$$H_{\text{int}} = \frac{s_w - \frac{w_t}{12} - \frac{0.06 D_i}{12}}{LLDF_l} \tag{23}$$

$$\text{For } H < H_{\text{int}} \quad A_{LL} = \left(\frac{w_t}{12} + LLDF_l \cdot H + 0.06 \cdot \frac{D_i}{12} \right) \cdot \left(\frac{l_t}{12} + LLDF_l \cdot H \right) \tag{24}$$

$$\text{For } H \geq H_{\text{int}} \quad A_{LL} = \left(\frac{w_t}{12} + s_w + LLDF_l \cdot H + 0.06 \cdot \frac{D_i}{12} \right) \cdot \left(\frac{l_t}{12} + LLDF_l \cdot H \right) \tag{25}$$

where
H is the culvert depth, ft
w_t is the tire patch width, 20 in.
l_t is the tire patch length, 10 in.
$LLDF_l$ is the AASHTO LRFD live load distribution factor, 1.15
D_i is the inside span of the culvert, in.
s_w is the wheel spacing, 6 ft

3.1.4.2 Thrust Calculations

For the proposed live load equations, the following live load adjustment is required:

$$F_{1,\text{lim}} = \text{maximum}\left(15/D_i, 1\right) \tag{26}$$

$$F_1 = \text{maximum}\left(\text{F}_{1,\text{lim}}, 0.75 \cdot \left(\frac{D_i/12}{L_t/12 + LLDF_l \cdot H}\right)\right) \tag{27}$$

$$T_t = \frac{\gamma_d \cdot DL + \gamma_l \cdot \left(LL \cdot F_1\right)}{2} \tag{28}$$

3.1.5 Thermoplastic Pipe (Profile Wall) Equations

3.1.5.1 Live Load Equations

The proposed live load equations used for profile wall thermoplastic pipe are as presented in Section 3.1.1, except the live load area is as follows.

Determine the wheel interaction depth

$$H_{\text{int}} = \frac{s_w - \frac{w_t}{12} - \frac{0.06 D_i}{12}}{LLDF_l} \tag{29}$$

$$\text{For } H < H_{\text{int}} \quad A_{LL} = \left(\frac{w_t}{12} + LLDF_l \cdot H + 0.06 \cdot \frac{D_i}{12}\right) \cdot \left(\frac{l_t}{12} + LLDF_l \cdot H\right) \tag{30}$$

$$\text{For } H \geq H_{\text{int}} \quad A_{LL} = \left(\frac{w_t}{12} + s_w + LLDF_l \cdot H + 0.06 \cdot \frac{D_i}{12}\right) \cdot \left(\frac{l_t}{12} + LLDF_l \cdot H\right) \tag{31}$$

where
H is the culvert depth, ft
w_t is the tire patch width, 20 in.
l_t is the tire patch length, 10 in.
$LLDF_l$ is the AASHTO LRFD live load distribution factor, 1.15
D_i is the inside span of the culvert, in.
s_w is the wheel spacing, 6 ft

3.1.5.2 Thrust Calculations

For the proposed live load equations, the following live load adjustments are proposed:

$$F_{1,\text{lim}} = \max\left(15/D_i, 1\right) \tag{32}$$

$$F_1 = \max\left(\text{F}_{1,\text{lim}}, 0.75 \cdot \left(\frac{D_i/12}{L_t/12 + LLDF_l \cdot H}\right)\right) \tag{33}$$

$$F_2 = \frac{0.95}{1 + 0.6 \cdot S_h} \tag{34}$$

$$T_1 = \frac{\gamma_d \cdot DL + \gamma_l \cdot LL \cdot F_1 \cdot F_2}{2} \tag{35}$$

3.1.6 Corrugated Metal Arch Equations

3.1.6.1 Live Load Equations

The proposed live load equations used for corrugated metal arches are as presented in Section 3.1.1, except the live load area is as follows.

Determine the wheel interaction depth

$$H_{\text{int}} = \frac{s_w - \frac{w_t}{12} - 0.06S}{LLDF_l} \tag{36}$$

$$\text{For } H < H_{\text{int}} \quad A_{LL} = \left(\frac{w_t}{12} + LLDF_l \cdot H + 0.06 \cdot S\right) \cdot \left(\frac{l_t}{12} + LLDF_l \cdot H\right) \tag{37}$$

$$\text{For } H \geq H_{\text{int}} \quad A_{LL} = \left(\frac{w_t}{12} + s_w + LLDF_l \cdot H + 0.06 \cdot S\right) \cdot \left(\frac{l_t}{12} + LLDF_l \cdot H\right) \tag{38}$$

where
H is the culvert depth, ft
w_t is the tire patch width, 20 in.
l_t is the tire patch length, 10 in.
S is the culvert span, ft
$LLDF_l$ is the AASHTO LRFD live load distribution factor, 1.15
s_w is the wheel spacing, 6 ft

The service live load is determined from

$$W_L = MPF \cdot \left(1 + IM\right) \cdot W_{LL} \cdot \min\left(S, L_{t,gov}\right) \tag{39}$$

where S is the culvert span, ft, and the other factors are as defined in previous sections.

3.1.6.2 Thrust Calculations

For the proposed live load equations, the following live load adjustments are required:

$$F_{m,arch} = \frac{0.54 \cdot S}{\frac{w_t}{12} + LLDF_l \cdot H + 0.03 \cdot S} \tag{40}$$

$$T_i = \frac{\gamma_d \cdot DL + \gamma_l \cdot LL \cdot F_{m,arch}}{2} \tag{41}$$

3.1.7 Concrete Arch Equations

The proposed live load equations used for concrete arches are as presented in Section 3.1.1, except the live load area is as follows.

Determine the wheel interaction depth

$$H_{\text{int}} = \frac{s_w - \frac{w_t}{12} - 0.06S}{LLDF_l} \tag{42}$$

$$\text{For } H < H_{\text{int}} \quad A_{LL} = \left(\frac{w_t}{12} + LLDF_l \cdot H + 0.06 \cdot S\right) \cdot \left(\frac{l_t}{12} + LLDF_l \cdot H\right) \tag{43}$$

$$\text{For } H \geq H_{\text{int}} \quad A_{LL} = \left(\frac{w_t}{12} + s_w + LLDF_l \cdot H + 0.06 \cdot S\right) \cdot \left(\frac{l_t}{12} + LLDF_l \cdot H\right) \tag{44}$$

where

H is the culvert depth, ft
w_t is the tire patch width, 20 in.
l_t is the tire patch length, 10 in.
S is the culvert span, ft
$LLDF_l$ is the AASHTO LRFD live load distribution factor, 1.15
s_w is the wheel spacing, 6 ft

The service live loads were determined from

$$W_L = MPF \cdot (1 + IM) \cdot W_{LL} \cdot \min(S, L_{t,gov}) \tag{45}$$

where S is the culvert span, ft, and the other factors are as defined in previous sections.

3.2 Recommended Changes to the AASHTO LRFD Bridge Design Specifications

Recommended changes to the 4th Edition *AASHTO LRFD Bridge Design Specifications* are presented in Appendix C. The research team has recommended changes to Sections 3 and 12. Table 3-1 summarizes the changes to each section for the six culvert types.

3.3 Overall Design and Reliability Margin

Section 2.4 described the research team's assessment of the effect of the proposed SDEs on the culvert forces pertinent to design. The results are presented as graphs of design forces from the SDEs versus either Standard or LRFD design forces. These graphs are useful for a detailed assessment of the effect

Table 3-1. Proposed changes to AASHTO LRFD Bridge Design Specifications.

Culvert Type	Section 3 Changes	Section 12 Changes
All types	Eliminate *LLDF* dependence on soil type Effect of fill ignored < 1 ft for round culverts Effect of fill ignored for < 2 ft for flat-top and 3-sided culverts Added equations for rectangular area calculation	N.A.
Concrete Box	Add $0.06 \cdot D_i$ factor (e.g. Eqns (2) & (3))	None
Concrete Pipe	*LLDF* varies from 1.15 to 1.75 Add $0.06 \cdot D_i$ factor Add $L_{t,gov}$ factor	Change live load bedding factor for indirect design to 2.2
Corrugated Metal Pipe	Add $0.06 \cdot D_i$ factor	Eqn (147)–(149)
Thermoplastic Pipe (profile wall)	Add $0.06 \cdot D_i$ factor	Eqn (153)–(155)
Corrugated Metal Arch	Add $0.06 \cdot D_i$ factor	Eqn (161)–(162)
Concrete Arch	Add $0.06 \cdot D_i$ factor	None

Table 3.2. Design for statistics, SDE/Standard and SDE/LRFD ratios.

Structure	Structural Force	Count	Metric	Max.	Min.	Ave.	Stnd Dev.	Coeff. of Variation
Thermoplastic pipe (profile wall)	Peak thrust	80	SDE / Stnd	1.16	0.54	0.996	0.129	0.130
			SDE / LRFD	1.25	0.66	0.939	0.089	0.094
Reinforced concrete pipe	Crown moment	100	SDE / Stnd	1.33	0.20	0.910	0.267	0.294
			SDE / LRFD	1.00	0.78	0.888	0.066	0.074
Reinforced concrete pipe	Crown shear	100	SDE / Stnd	1.24	0.22	0.906	0.229	0.253
			SDE / LRFD	1.08	0.83	0.925	0.052	0.057
Reinforced concrete box	Top middle positive moment	6	SDE / Stnd	1.20	0.96	1.065	0.092	0.086
			SDE / LRFD	0.96	0.81	0.908	0.067	0.073
Reinforced concrete box	Top slab shear	6	SDE / Stnd	1.19	0.96	1.071	0.090	0.084
			SDE / LRFD	0.95	0.81	0.900	0.064	0.071
Corrugated metal pipe	Peak thrust	42	SDE / Stnd	1.48	0.57	1.052	0.196	0.187
			SDE / LRFD	2.29	0.65	1.089	0.340	0.312
Corrugated metal arches	Peak thrust	6	SDE / Stnd	1.48	1.00	1.234	0.208	0.169
			SDE / LRFD	2.14	0.99	1.460	0.499	0.342
Reinforced concrete arches	Peak moment	8	SDE / Stnd	1.50	0.70	0.944	0.260	0.276
			SDE / LRFD	1.14	0.51	0.882	0.213	0.241
Reinforced concrete arches	Peak shear	8	SDE / Stnd	1.35	0.67	0.916	0.260	0.284
			SDE / LRFD	1.13	0.71	0.932	0.156	0.167

of the SDEs and give a general impression of the relative effect of the SDEs on design margin and reliability.

In this section, the research team presents statistics about the ratio of SDE design forces to Standard design forces, and the ratio of SDE to LRFD design forces. Table 3-2 lists the numerical values of the maximum, minimum, average, standard deviation, and coefficient of variation of the design force ratios. The culvert forces listed in the table are those specified in the code and vary according to the culvert type. Some culvert types have two design forces and others have only one.

The maximum, minimum, and average design force ratios are also shown in Figure 3-1. In the figure, the square represents the average ratio and the ends of the vertical bars represent the minimum and maximum ratios. For most design forces, the ratio of SDE to LRFD is between 0.9 and 1.1. Exceptions to these limits are the RCP crown moment at 0.888,

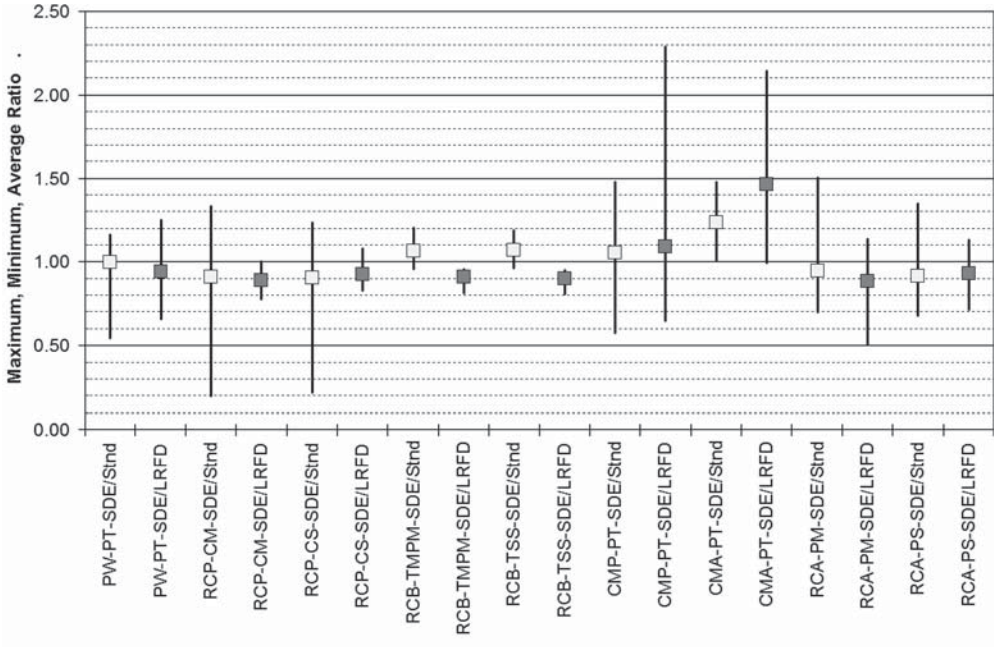

Figure 3.1. Maximum, minimum and average design force ratio.

the corrugated metal arch peak thrust at 1.460, and the reinforced concrete arch peak moment at 0.882.

The range of design force ratios is generally larger for the SDE/Standard ratio. This reflects that the SDEs, like the LRFD design methods, spread the loads from a finite-size wheel patch (typically 20 by 10 inches), rather than a point load.

Figure 3-1 illustrates that, except for a few structure forces, the proposed SDEs do not significantly affect the design margin or reliability on average. However, the relatively large spread in the ratios does mean that there are some combinations of soil type, diameter, and depth where the SDEs are significantly different than the LRFD design forces.

Where there is a significant variation between the proposed SDEs and current practice, the differences are not random—rather the SDEs model behavior not captured in the current standards. For example, in corrugated metal pipe, the ratio gets larger as depth of fill decreases. As noted earlier in this report, this is the result of the high thrust occurring in the crown of these culverts, which occurs because of the low bending stiffness and high axial stiffness.

Based on this study, the current AASHTO load spreading method provides a neutral or conservative approach for all culvert types, except corrugated metal arches. The proposed SDEs are a better fit to the modeling results produced in this study and are generally less conservative than the current AASHTO load-spreading method.

For most reinforced concrete pipe diameters and depths considered, the SDEs generally predict much lower crown moments than the Standard method and moderately lower crown moments than the LRFD method. However, the SDEs are still quite conservative relative to the ACPA Handbook methods that have been used without issue for a substantial number of years.

The research team believes that the proposed SDEs reflect an improvement in the distribution of live load with depth and better culvert designs.

CHAPTER 4

Conclusions

NCHRP Project 15-29, "Design Specifications for Live Load Distribution to Buried Structures," investigated how surface live loads distribute through the soil and load various culvert structures. AASHTO Standard and LRFD Specifications differ in how live loads are spread through fill onto culvert structures. Standard Specifications apply surface point loads and spread loads at the rate of 1.75 times the culvert depth. The LRFD specifications apply live load through a tire footprint of 10 by 20 inches at the surface but attenuate with a lower coefficient (1.00 or 1.15 as a function of soil type) as the depth of fill increases.

This project investigated how live loads spread with depth, as a function of soil and culvert type, using 3D numerical modeling. The numerical investigation included selection of appropriate software and soil models, verification of model predictions, and 3D analysis of about 830 buried culverts, including concrete arches, concrete pipes, concrete boxes, corrugated metal pipe, corrugated metal arches, and thermoplastic pipe (profile wall), to provide a basis for developing SDEs for structural response.

Proposed revisions to AASHTO design specifications were developed. First, the limit states and design methodologies were evaluated and compared for all culvert types included in the AASHTO specifications. Next, numerical values of the limit states from the numerical modeling were compared with the values resulting from the Standard and LRFD Specifications. Finally, proposed SDEs were developed that provided better correlation with modeling results.

For all culvert types, the proposed SDEs included a culvert span-related term in the calculation of the load spread parallel to the culvert axis. Table 3-1 summarizes the proposed changes to each section for the six culvert types. Recommended changes to the AASHTO LRFD Design Specifications are presented in Section 3-2 and Appendix C. The recommended changes are limited to Specification Section 3, where the live load magnitude is specified, and Specification Section 12, where structural responses are calculated.

To understand the effect of the proposed SDEs on culvert designs, the critical structural responses were calculated and compared for Standard, LRFD, and proposed SDEs, for 248 culvert, depth, span, and soil combinations.

For the project, the research team conducted extensive 3D modeling of the transfer of surface live loads to buried culverts. From the results, the research team has proposed SDEs that permit culvert design without modeling. However, many design situations are not addressed by the SDEs. In these situations, 2D and 3D modeling may be used for design.

Guidelines were developed for conducting 2D and 3D modeling. The 2D guidelines provide a means for selecting the surface load intensity to be applied to a 2D model in order to achieve approximately the structural response from a 3D model. Two-dimensional computer models have an inherent limitation when computing the effect of surface live loads. Because the models are 2D, the load spreading that occurs in the longitudinal direction, parallel to the axis of the culvert, cannot be correctly computed. The model represents a vertical slice through the real-world, 3D geometry.

The resulting guideline for the surface pressure to be used for conducting 2D analyses is a two-parameter equation found to provide reasonable results for the structural response of reinforced concrete pipe, thermoplastic (profile wall) pipe, and corrugated metal pipe. The behavior of concrete boxes, concrete arches, and corrugated metal arches was found to be too variable to be adequately captured by these guidelines.

3D guidelines were developed that address software, live load application, representations of the pavement and the soil, model dimensions, element size, symmetry and boundary conditions, representations of the culvert structures, and the soil-culvert interface.

The overall design and reliability margin of the proposed SDEs was assessed by computing statistics about the ratio of SDE design force to Standard design force and the ratio of SDE to LRFD design forces. For most design forces, the ratio of SDE to LRFD is between 0.9 and 1.1. Exceptions to these limits are

the RCP crown moment at 0.888, the corrugated metal arch peak thrust at 1.460, and the reinforced concrete arch peak moment at 0.882.

The range of design force ratios is generally larger for the SDE/Standard ratio. This reflects that the SDEs, like the LRFD design methods, spread the loads from a finite-size wheel patch (typically 20 by 10 inches), rather than a point load.

Except for a few structure forces, the proposed SDEs do not significantly affect the design margin or reliability on average. However, the relatively large spread in the ratios means that there are some combinations of soil type, diameter, and depth where the SDEs are significantly different than the LRFD design forces.

Where there is a significant variation between the proposed SDEs and current practice, the differences are not random—rather the SDEs model behavior not captured in the current standards. For example, in metal pipe, the ratio gets larger as depth of fill decreases. As discussed earlier, this is the result of the high thrust noted in the crown of these pipes which occurs because of the low bending stiffness and high axial stiffness.

The proposed SDEs reflect an improvement in the distribution of live load with depth and better culvert designs.

References

AASHTO (2007). 4th Edition *AASHTO LRFD Bridge Construction Specifications,* AASHTO, Washington, D.C.

ACPA (1998). *Concrete Pipe Design Manual.* ACPA, USA.

ASCE (2000). Standard Practice for Direct Design of Buried Precast Concrete Pipe Using Standard Installations (SIDD). 15–98.

Boussinesq, J. (1885). Application des Potentiels a l'etude de l'equilibre et du movement des solides elastiques, Gauthier-Villars, Paris.

BOXCAR (2000). Version 2.0 for Windows.

Brinkgreve, R. B. J. and Broere, W., Eds. (2004). Plaxis 3D Tunnel Version 2, Plaxis, Netherlands.

Brinkgreve, R. B. J., Ed. (2002). Plaxis 2D Tunnel Version 8, Plaxis, Netherlands.

Duncan, J. M., et al. (1980). "Strength, Stress-Strain and Bulk Modulus Parameters for Finite Element Analysis of Stress and Movements in Soil Masses," *Report No. UCB/GT/80-01,* University of California, Berkeley, Berkeley, CA.

Fernando, N. S. M. and Carter, J. P. (1998). "Elastic Analysis of Buried Pipes under Surface Patch Loadings," *Journal of Geotechnical and Geoenvironmental Engineering,* Vol. 124, No. 8, pp. 720–728.

Heger, F. J., Liepins, A. A., and Selig, E. T. (1985). "SPIDA: Analysis and Design System for Buried Concrete Pipe," Advances in Underground Pipeline Engineering, *Proceedings of the International Conference,* ASCE, pp. 143–154.

Howard, A. K. (1977). "Modulus of Soil Reaction Values for Buried Flexible Pipe," *Journal of the Geotechnical Engineering,* Vol. 103, No. GT1, New York, NY.

Itasca Consulting Group, Inc. (2005), "FLAC3D Fast Lagrangian Analysis of Continua in 3 Dimensions, Version 3."

Jaky, J. (1944). "The Coefficient of Earth Pressure at Rest," *Journal of the Society of Hungarian Architects and Engineers,* Budapest, pp. 355–358 (in Hungarian).

Lade, P. V. (2005). "Overview of Constitutive Models for Soils," *Soil Constitutive Models—Evaluation, Selection, and Calibration,* J. A. Yamamuro and V. N. Kaliakin, Eds., ASCE, Reston, VA, pp. 1–34.

Lin, R. D. (1987). Direct Determination of Bulk Modulus of Partially Saturated Soils, Master Thesis, University of Massachusetts, Amherst, MA.

McGrath, T. J. (1998). "Replacing E′ with the Constrained Modulus in Flexible Pipe Design," Pipelines in the Constructed Environment, *Proceedings of the 1998 Pipeline Division Conference,* ASCE, pp. 28–40.

McGrath, T. J. and Beaver, J. L. (2005). Performance of Thermoplastic Pipe Under Highway Vehicle Loading, Project Report Prepared for Minnesota Department of Transportation, Simpson Gumpertz & Heger Inc., Waltham, MA.

McGrath, T. J., DelloRusso, S. J., and Boynton, J. (2002). "Performance of Thermoplastic Culvert Pipe Under Highway Vehicle Loading," *Pipelines 2002,* G. Kurz, Ed., ASCE.

McGrath, T. J., Liepins, A. A., and Beaver, J. L. (2005). "Live Load Distribution Widths for Concrete Box Culverts," Sixth International Bridge Engineering Conference, Boston, MA.

McGrath. T. J., et al. (2002). *NCHRP Report 473: Recommended Specifications for Large-Span Culverts,* Transportation Research Board, National Research Council, Washington, DC.

Moore, I. D., and Brachman, R. W. (1994). "Three-Dimensional Analyses of Flexible Circular Culverts," *Journal of Geotechnical Engineering,* Vol. 120, No. 10, pp. 1829–1844.

Musser, S. C. (1989). "CANDE-89 User Manual," *FHWA-RD-89-169,* FHWA, McLean, VA.

Pang, S. (1999). "Discussion: Elastic Analysis of Buried Pipes under Surface Patch Loadings by N. S. M. Fernando and J. P. Carter," *Journal of Geotechnical and Geoenvironmental Engineering,* Vol. 125, No. 12, p. 1104.

Poulos, H. G. and Davis, E. H. (1974). *Elasticity Solutions for Soil and Rock Mechanics,* John Wiley & Sons, Inc., New York, NY.

SAP2000 (2000). SAP2000 Plus Version 7.4 Users Manual, Computers and Structures, Inc. Berkeley, CA.

Selig, E. T. (1988). "Soil Parameters for Design of Buried Pipelines," *Pipeline Infrastructure,* B. A. Bennett, Ed., ASCE, New York, NY, pp. 99–116.

Selig, E. T. (1990). "Soil Properties for Plastic Pipe Installations," *Buried Plastic Pipe Technology, STP1093,* G. S. Buczala and M. J. Cassady, Eds., ASTM, Philadelphia, PA, pp. 141–158.

Taleb, B. (2000). Behavior of Large-Span Metal and Reinforced Concrete Culverts under Earth and Live Loadings, Ph.D. Dissertation, University of Massachusetts Amherst, Amherst, MA.

Webb, M. C. (1999). Improved Design and Construction of Large-Span Culverts, Ph.D. Dissertation, University of Massachusetts Amherst, Amherst, MA.

Abbreviations and acronyms used without definitions in TRB publications:

AAAE	American Association of Airport Executives
AASHO	American Association of State Highway Officials
AASHTO	American Association of State Highway and Transportation Officials
ACI–NA	Airports Council International–North America
ACRP	Airport Cooperative Research Program
ADA	Americans with Disabilities Act
APTA	American Public Transportation Association
ASCE	American Society of Civil Engineers
ASME	American Society of Mechanical Engineers
ASTM	American Society for Testing and Materials
ATA	Air Transport Association
ATA	American Trucking Associations
CTAA	Community Transportation Association of America
CTBSSP	Commercial Truck and Bus Safety Synthesis Program
DHS	Department of Homeland Security
DOE	Department of Energy
EPA	Environmental Protection Agency
FAA	Federal Aviation Administration
FHWA	Federal Highway Administration
FMCSA	Federal Motor Carrier Safety Administration
FRA	Federal Railroad Administration
FTA	Federal Transit Administration
IEEE	Institute of Electrical and Electronics Engineers
ISTEA	Intermodal Surface Transportation Efficiency Act of 1991
ITE	Institute of Transportation Engineers
NASA	National Aeronautics and Space Administration
NASAO	National Association of State Aviation Officials
NCFRP	National Cooperative Freight Research Program
NCHRP	National Cooperative Highway Research Program
NHTSA	National Highway Traffic Safety Administration
NTSB	National Transportation Safety Board
SAE	Society of Automotive Engineers
SAFETEA-LU	Safe, Accountable, Flexible, Efficient Transportation Equity Act: A Legacy for Users (2005)
TCRP	Transit Cooperative Research Program
TEA-21	Transportation Equity Act for the 21st Century (1998)
TRB	Transportation Research Board
TSA	Transportation Security Administration
U.S.DOT	United States Department of Transportation